



Effect of quantum well position on the distortion characteristics of transistor laser

S. Piramasubramanian ^{*}, M. Ganesh Madhan ^{*}, V. Radha, S.M.S. Shajithaparveen, G. Nivetha

Department of Electronics Engineering, Madras Institute of Technology Campus, Anna University, Chennai, India



ARTICLE INFO

Keywords:

Transistor laser
Quantum well position
Rate equations
Numerical simulation
Second harmonic distortion (2HD)
Third order intermodulation distortion (IMD3)

ABSTRACT

The effect of quantum well position on the modulation and distortion characteristics of a 1300 nm transistor laser is analyzed in this paper. Standard three level rate equations are numerically solved to study this characteristics. Modulation depth, second order harmonic and third order intermodulation distortion of the transistor laser are evaluated for different quantum well positions for a 900 MHz RF signal modulation. From the DC analysis, it is observed that optical power is maximum, when the quantum well is positioned near base-emitter interface. The threshold current of the device is found to increase with increasing the distance between the quantum well and the base-emitter junction. A maximum modulation depth of 0.81 is predicted, when the quantum well is placed at 10 nm from the base-emitter junction, under RF modulation. The magnitude of harmonic and intermodulation distortion are found to decrease with increasing current and with an increase in quantum well distance from the emitter base junction. A minimum second harmonic distortion magnitude of -25.96 dBc is predicted for quantum well position (230 nm) near to the base-collector interface for 900 MHz modulation frequency at a bias current of $20 I_{bh}$. Similarly, a minimum third order intermodulation distortion of -38.2 dBc is obtained for the same position and similar biasing conditions.

© 2017 Elsevier B.V. All rights reserved.

1. Introduction

RF modulated optical signal transmission through fiber finds many applications in the present communication systems. They include antenna remoting, Cable Television (CATV) and phased array radar. In such schemes, fiber replaces coaxial medium due to its huge bandwidth, low loss and less cost [1–3]. This technology is termed as Radio over Fiber (RoF) which utilizes both long and short range analog optical fiber links. In Fiber-to-the-Home (FTTH) networks, optical fiber is used to transmit video signals and data from the head end to subscribers. Optical fiber is installed between central base station and remote antenna units in the case of mobile cellular applications. Radio over fiber is also found useful for Global Positioning System (GPS) over fiber for indoor applications and distributed antenna system in aircraft cabin [4–9]. RF to RF link efficiency is the parameter that indicates the effectiveness of the RoF systems. Higher modulation depth is required in the optical modulator to increase the overall link efficiency [3]. Fiber loss and photodiode responsivity are other factors that affect the RF to RF link efficiency. Direct modulation of laser diode is preferred in the most of the fiber links than external modulation due to its reduced complexity and less cost. The modulation index is found to be higher

when the laser is biased near to its threshold current in the case of direct modulation. However, biasing the laser diode in this region also produces non linear distortion, when modulated by two or more number of RF tones. Harmonic and intermodulation distortion from the optical source affect the performance of the radio over fiber link. Second harmonic distortion (2HD) analysis is mandatory for the optical source in the case of CATV applications. Fourth and higher order harmonics are not considered in many applications as their magnitudes are quite less. The level of distortion should be less than -50 dBc for analog video signal transmission [7]. Hence, many linearization techniques are used in the laser diode to reduce these distortions. They include predistortion, feed forward and feedback harmonic injection techniques [7].

The Transistor Laser (TL) is a semiconductor device that functions as a normal transistor with an electrical input and generates simultaneous optical and electrical output signals.

The transistor laser was invented by Holonyak and Feng and most of the publications on transistor laser are from the same author group [10–15]. It can be considered as a three port device with electrical input port along with optical and electrical output ports. The transistor laser consists of single or multiple quantum well in its base region

* Corresponding authors.

E-mail addresses: spirama@annauniv.edu (S. Piramasubramanian), mganesh@annauniv.edu (M. Ganesh Madhan).

which produces infrared light by radiative recombination. A reflective cavity in the device leads to lasing action. The quantum well captures the electrons injected in the device and allows it to recombine with positively charged holes in the base region. The device produces photons through stimulated emission process which results in laser beam generation from the cavity. The electrons that are not captured in the quantum well are swept into the collector which produces electrical output [16–19]. As transistor laser is characterized by fast recombination life time, large optical bandwidth, it is envisaged as a potential candidate for analog optical link applications. Low distortion, large dynamic range and minimum noise are the important requirements for optical sources in analog applications. In the literature [17,19], the effect of Quantum Well (QW) position in the base is analyzed for power current characteristics and frequency response characteristics. However their influence in modulation depth and distortion performance has not been previously investigated. The analysis of transistor lasers is carried out by using charge control model [20–22].

In this work, modulation and distortion characteristics of transistor laser are analyzed for different positions of Quantum Well in the base region. The location of quantum well is varied from base-emitter interface to base-collector interface. The position of single quantum well is an important parameter along with quantum well width, that affect the base charge life time [16]. It is well known that the modulation characteristics of any optical source depends on carrier life time. The rate equations which incorporate charge control model of the transistor laser are numerically solved to determine the basic TL characteristics. Based on the same model, we proceed further to investigate the effect of position of the quantum well on the modulation depth, second harmonic and third order intermodulation distortion performance of the TL. Harmonic distortion and modulation analysis are carried out at 900 MHz. Third order intermodulation distortion (IMD3) is calculated for two tone frequencies at 890 MHz and 910 MHz respectively. These frequencies are considered, as they correspond to the carrier frequencies of Global System for Mobile communication (GSM) 900 based cellular communication. The Transistor Laser is assumed to be the optical transmitter for cellular based radio over fiber link.

2. Transistor laser model

The schematic diagram of a transistor laser is shown in Fig. 1(a) [17]. The schematic of energy band diagram of the base region with different quantum well position in the device are shown in Fig. 1(b) and (c). The quantum well placed near to the base-emitter interface and base-collector interface are shown in Fig. 1(b) and 1(c) respectively.

The TL operation in the active region requires base-emitter junction to be forward biased and base-collector junction to be reverse biased. The three level rate equations with charge control model is considered in this work [16,17]

$$\frac{dn(t)}{dt} = \frac{vQ_b(t)}{\tau_{cap}} - \frac{n(t)}{\tau_{qw}} - \frac{v_g g_o}{(n(t) + N_s)(1 + \epsilon_{other}N_p(t))}[n(t) - n_{nom}]N_p(t) \quad (1)$$

$$\frac{dQ_b(t)}{dt} = \frac{I_b(t)}{qV} - \frac{Q_b(t)}{\tau_{rb}} \quad (2)$$

$$\frac{dN_p(t)}{dt} = \frac{\Gamma v_g g_o}{(n(t) + N_s)(1 + \epsilon_{other}N_p(t))}[n(t) - n_{nom}]N_p(t) + \frac{\theta n(t)}{\tau_{qw}} - \frac{N_p(t)}{\tau_p} \quad (3)$$

$$\frac{1}{\tau_{rb}} = \frac{1-v}{\tau_{rbo}} + \frac{v}{\tau_{cap}} \quad (4)$$

Where, $Q_b(t)$ represents the base charge density. $n(t)$ and $N_p(t)$ represent electron density and photon density in the active region of the transistor laser respectively. The base charge captured by the quantum well

Table 1
Model parameters [17].

Parameter	Description	Value
τ_{cap}	Electron capture time in quantum well	1 ps
τ_{esc}	Electron escape time in quantum well	1 ns
τ_{rbo}	Carrier lift time in the base region	1 ns
n_{nom}	Transparency electron density	10^{18} cm^{-3}
τ_p	Lifetime of photon	4.1 ps
N_s	Carrier density-fitting parameter	$0.26 \times 10^{18} \text{ cm}^{-3}$
W_{qw}	Well thickness	5 nm
$d_{barrier}$	Barrier thickness	10 nm
W	Stripe width	2 μm
W_b	Total base width	250 nm
L	Cavity length	250 μm
R	Reflectivity	0.3, 0.9
g_o	Material gain	3600 cm^{-1}
Γ	Optical confinement factor	0.011/well
α_i	Internal loss	5 cm^{-1}
ϵ_{other}	Gain compression factor	$0.5 \times 10^{-17} \text{ cm}^3$
B_{eff}	Recombination coefficient	$1.55 \times 10^{-10} \text{ cm}^{-3} \text{ s}^{-1}$
θ	Spontaneous emission coefficient	10^{-6}
v_g	Group velocity	$0.782 \times 10^8 \text{ m/s}$

is given by $(\frac{vQ_b(t)}{\tau_{cap}})$. The spontaneous recombination rate for electron inside the quantum well is represented by $(\frac{n(t)}{\tau_{qw}})$ and it is implemented by $(B_{eff}n^2)$ in the analysis. The stimulated emission term in the rate equations is $\Omega [n(t) - n_{nom}] N_p(t)$ and the photon loss is given by $(\frac{N_p(t)}{\tau_p})$. The value of base charge bulk life time (τ_{rbo}) is calculated from the parameter $(1/B_{eff} N_b)$, where N_b is low p-doping density. A charge control model is used to describe the dynamics of the minority carrier charge stored in the base. A single quantum well is assumed in the base region of the transistor laser for this analysis. The geometry factor (v) which depends on the relative position of quantum well in the base is given by [16]

$$v = (\frac{W_{qw}}{W_b})(1 - \frac{x_{qw}}{W_b}) \quad (5)$$

v gives the fraction of the base charge captured in the quantum well. Here, W_{qw} is the quantum well width, W_b is base region width, and x_{qw} is the distance from the base-emitter junction to the quantum well.

3. Simulation results

3.1. DC characteristics

In the rate equations (1)–(4), the values of $\frac{dn(t)}{dt}$, $\frac{dQ_b(t)}{dt}$ and $\frac{dN_p(t)}{dt}$ are fixed as zero and the equations are solved for static conditions. A fourth order Runge–Kutta method is used to solve the rate equations in the MATLAB® tool. The parameters used in this numerical analysis are given in the Table 1. The dimensions of our present work are similar to the work of Shirao et al. [17] and exactly similar device structure is used. AlGaInAs/InP material system of 1.3 μm transistor laser is used in our analysis which is similar to the work of Shirao et al. [17].

The steady state solutions of the electron density, base charge and photon densities are obtained for a base current variation between 0 and 15 mA. Further, optical power is evaluated for different quantum well positions in the range of 10 nm to 230 nm from the emitter base junction and plotted in Fig. 2(a). The optical power is found to decrease for a movement of the quantum well position towards base-collector interface. This is due to the fact that more charges are captured in the quantum well when it is near the base-emitter interface. Moreover better recombination occurs, which results in generation of more photons. The effect of position of quantum well in the base region on the threshold current of the device is analyzed. It is observed that the threshold current is found to increase with movement of quantum well position towards base-collector interface and is plotted in Fig. 2(b). A base threshold current of 2.1 mA and 2.4 mA are obtained for the quantum well position $x_{qw} = 10 \text{ nm}$ and 122.5 nm respectively. The

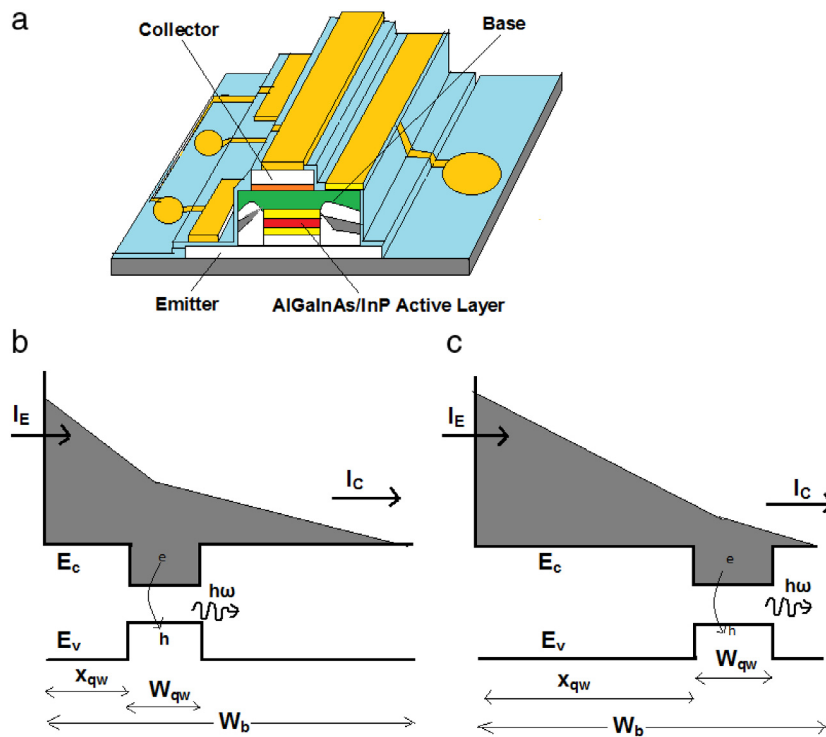


Fig. 1. (a) Schematic diagram of transistor laser [17], (b) position of quantum well in base of Transistor Laser near base–emitter junction and (c) near base–collector junction [16,17].

base threshold current is found to vary from 2.1 to 3.2 mA for quantum well position varying from 10 to 230 nm.

The quantum well position 122.5 nm corresponds to the mid position of the base region in the transistor laser. The predicted threshold base current for this position is found to be match with the report of Shirao et al. [17] and hence validates our simulation. The dimensions in the work of Basu et al. [19] are different from our work. Basu et al. have estimated the values of threshold base current for different quantum well position. The emission wave lengths used in their work are 980 nm, 1000 nm and 1006 nm. In our work, 1.3 μ m transistor laser is used. The increased threshold base current for larger value of quantum well position from emitter base junction is predicted in the work of Basu et al. This increasing trend of threshold base current is also predicted in our work. This variation is in accordance with the mathematical expression for threshold current provided by Zhang et al. [16].

3.2. Effect of quantum well position on the frequency response

The frequency response of the transistor laser is evaluated for various quantum well positions. The rate equations (1)–(4) are solved for base current with AC signal input and the expression is given by

$$I_b = I_{bo} + I_{RF} \sin(\omega t) \quad (6)$$

where, I_{bo} is bias current and I_{RF} is magnitude of RF current. The bias current and RF current are fixed as 7 I_{bth} and 3 mA respectively. The position of the quantum well is fixed as 10, 122.5, 180 and 230 nm. The base current frequency is varied from 100 MHz to 30 GHz. The Magnitude Response (MR) at a frequency is calculated by the ratio of difference between maximum power and minimum power to the power under static (DC) conditions, and shown in Fig. 3(a). The modulation bandwidth of the transistor laser is determined for different quantum well positions and plotted in Fig. 3(b). Modulation bandwidth is found to decrease with movement of quantum well position away from the emitter base interface. As the quantum well is fixed near to the base–emitter interface, the effective minority carrier lifetime in the base region decreases leading to an improvement in bandwidth. Faster

recombination occurs due to reduced lifetime resulting in higher bandwidth. A modulation bandwidth of 3.2 GHz is obtained for the quantum well position $x_{qw} = 10$ nm. The modulation bandwidth is relatively low at lower value of base current as in the case of conventional laser diodes. A modulation bandwidth of 40 GHz is reported in Shirao et al. [17] for two quantum well at a base current of 200 mA and it is reduced to 12 GHz at a base current of 10 mA. In our analysis, single quantum well is considered in the base and its position is varied from 10 nm to 230 nm. However, the base bias current is fixed as 14.7 mA (7 I_{bth} , $x_{qw} = 10$ nm) in this analysis. The selection of base bias current mainly depends on the value of modulation depth. Larger value of modulation bandwidth can be attained at higher base currents at the expense of modulation depth.

The focus of our work is to analyze the effect of quantum well position on modulation depth and distortion characteristics of transistor laser. Optical sources should have larger modulation depth and minimum distortion for analog optical transmission applications. Lower value of modulation bandwidth (2–4 GHz) is predicted in our work due to the choice of base bias current i.e. 4 I_{bth} to 12 I_{bth} . However, larger value of modulation depth is predicted when the bias current is near to the threshold current. Hence, modulation depth and distortion are analyzed at 900 MHz for different quantum well position from emitter base junction to the collector base junction.

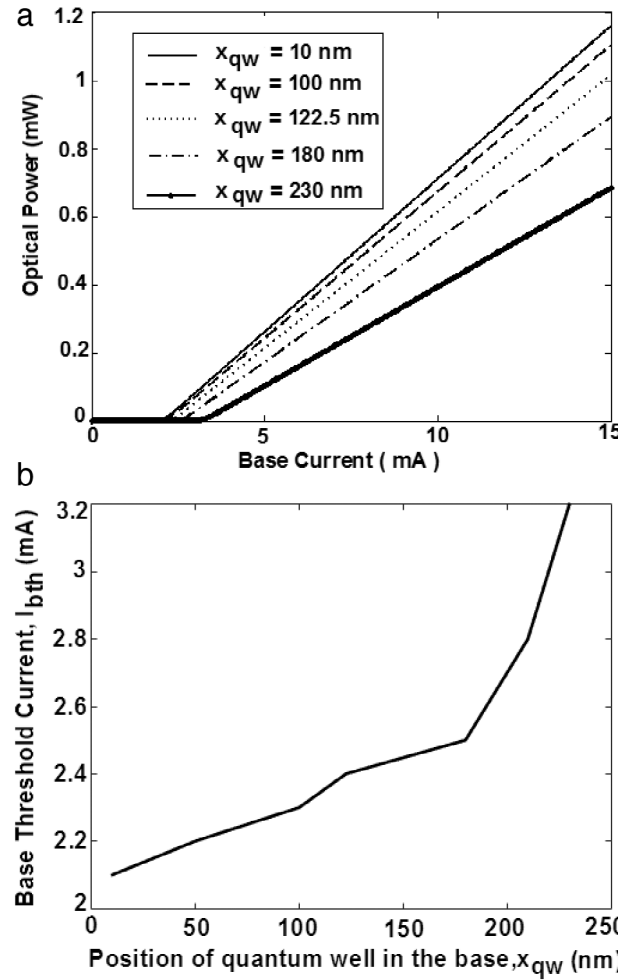
Modulation bandwidth for different bias currents and quantum well position are evaluated and provided in Table 2. The modulation bandwidth is found to increase with increasing bias current. A decrease in modulation bandwidth is predicted as the quantum well position is moved towards the base–collector junction.

If the base current is increased to obtain a larger modulation bandwidth, heat generated will also increase and the device temperature rises. This leads to a change in emission wavelength and threshold current which are undesirable. Heat sinks along with Peltier based thermo electric cooling can be employed as in the case of normal semiconductor laser. The Peltier element is driven by a electronic feedback loop connected to a thermister, which senses the laser temperature.

Table 2

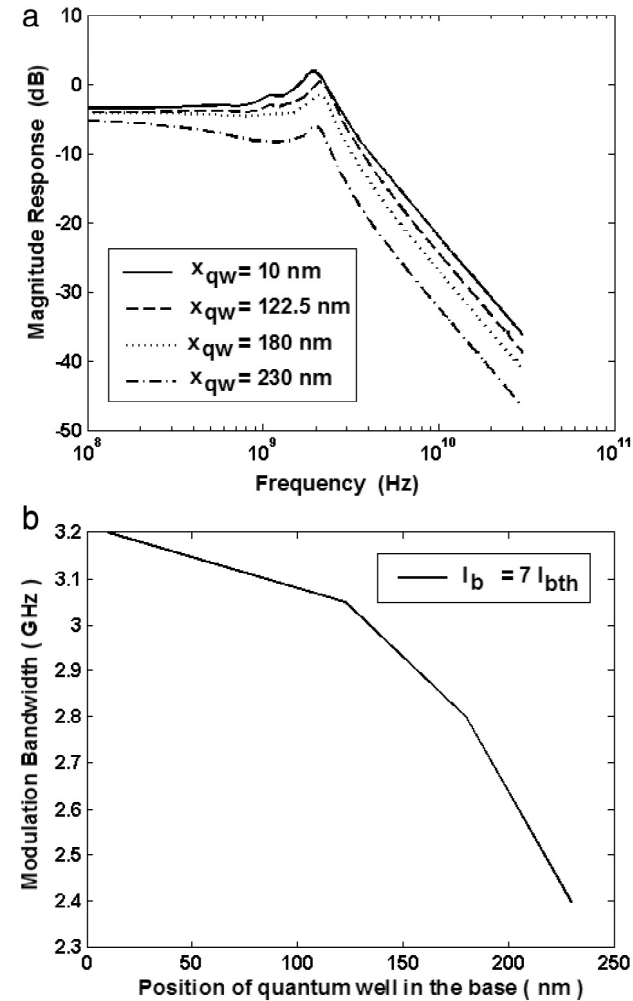
Effect of base current on modulation bandwidth.

Ratio of base current to base threshold current (I_b/I_{bth})	Modulation bandwidth (GHz)				
	$x_{qw} = 10 \text{ nm}$ $I_{bth} = 2.1 \text{ mA}$	$x_{qw} = 100 \text{ nm}$ $I_{bth} = 2.3 \text{ mA}$	$x_{qw} = 122.5 \text{ nm}$ $I_{bth} = 2.4 \text{ mA}$	$x_{qw} = 180 \text{ nm}$ $I_{bth} = 2.5 \text{ mA}$	$x_{qw} = 230 \text{ nm}$ $I_{bth} = 3.2 \text{ mA}$
4	2.3	2.1	2	1.9	1.5
6	2.8	2.7	2.8	2.5	2.1
8	3.4	3.3	3.3	3	2.4
10	3.8	3.7	3.6	3.2	2.7
12	4.2	4.1	4	3.7	3.2

**Fig. 2.** Quantum well position dependent (a) variation of optical power with base current and (b) variation of base threshold current.

3.3. Analysis of modulation depth at 900 MHz

In this analysis, the modulation depth of transistor laser is determined for different positions of quantum well, at 900 MHz RF signal injection. As this frequency band is used for cellular mobile communication [7], this study will help to evaluate the effectiveness of Transistor Laser for optical transmitter in Radio over Fiber based cellular mobile networks. The frequency value is substituted in Eq. (6) and rate equations ((1)–(4)) are solved. The modulation depth is evaluated from optical output power, using the expression ($\frac{P_{\max} - P_{DC}}{P_{DC}}$). Where P_{\max} is maximum optical power and P_{DC} is optical power at the DC bias point. The base bias current is varied from $4 I_{bth}$ to $12 I_{bth}$ and the modulation depth is obtained and plotted in Fig. 4. The magnitude of RF current (I_{RF}) is fixed as 3 mA in this analysis. The modulation depth is found to decrease with increasing base current and position of quantum well. A

**Fig. 3.** Effect of position of quantum well (x_{qw}) on (a) frequency response and (b) modulation bandwidth.

maximum modulation depth of 0.81 is obtained for the 10 nm quantum well position at a bias current of $4 I_{bth}$. Optical signal transmission with higher modulation depth is generally preferred for radio over fiber applications.

4. Distortion analysis

4.1. Second harmonic distortion (2HD) calculation

The direct modulation of laser diode or transistor laser produces harmonic and intermodulation components in the output and leads to distortion. This effect degrades the performance of the system and reduces the signal to noise ratio. Analysis of second harmonic distortion is required for wireless based RoF applications since the source is

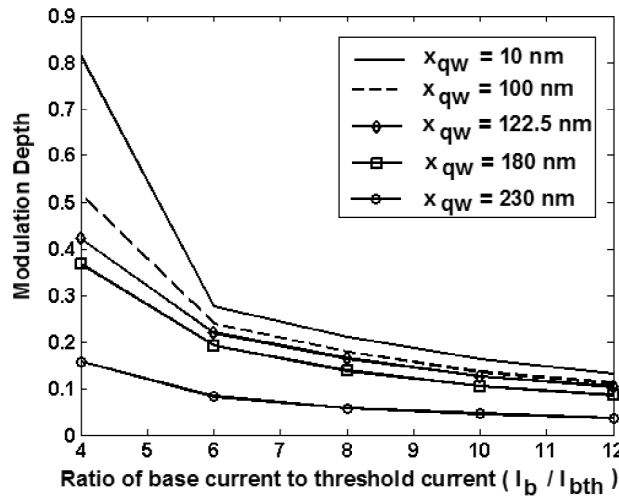


Fig. 4. Variation of modulation depth on quantum well position.

modulated with multiple RF carriers. The second harmonic distortion is calculated as the ratio of magnitude of the fundamental (f) tone to the magnitude of its second harmonic term (2f). In this analysis, the effect of position of quantum well on second harmonic distortion is evaluated for 900 MHz signal. The position of the quantum well is fixed as 10 nm which is near to the base-emitter interface. The base current and RF current are fixed as $4 I_{bth}$ and 3 mA respectively. The spectrum of base current and corresponding optical power are given in Fig. 5(a) and Fig. 5(b) respectively. The spectrum in the laser output shows the fundamental tone at 900 MHz and second harmonic component at 1.8 GHz. The second harmonic component has a significant magnitude of -13.95 dB relative to the fundamental frequency.

The analysis is repeated for various quantum well position and bias currents. The bias current is varied from $4 I_{bth}$ to $12 I_{bth}$ for each quantum well position and the magnitudes of second harmonic distortion are evaluated (Fig. 6). The value of 2HD is maximum at the bias current of $I_b = 4 I_{bth}$ for all the position of the quantum well. This is due to the fact that this bias current is very close to the threshold current of the transistor laser. The second harmonic distortion is found to decrease with increase in the base current. A minimum second harmonic distortion of -25.96 dBc is obtained for the quantum well position 230 nm, at the bias of $12 I_{bth}$. However, the modulation depth is very low at this bias point (Fig. 4).

4.2. Third order intermodulation distortion analysis (IMD3)

The magnitude of IMD3 components for different quantum well positions are analyzed under two tone inputs. The expression for base current with two tones is given by

$$I_b = I_{bo} + I_{RF}[\sin(\omega_1 t) + \sin(\omega_2 t)] \quad (7)$$

where, I_{bo} and I_{RF} are the bias current and magnitude of RF current respectively. The input base current is applied with two tones f_1 ($\omega_1 = 2\pi f_1$) and f_2 ($\omega_2 = 2\pi f_2$) to the transistor laser. For this two tone input, harmonics of fundamental components ($2f_1, 3f_1, \dots, 2f_2, 3f_2 \dots$), second order intermodulation components ($f_1 + f_2, f_1 - f_2$) and the third order intermodulation products ($2f_1 - f_2, 2f_2 - f_1, 2f_1 + f_2, 2f_2 + f_1$) are produced in the output optical power. The third order intermodulation components ($2f_1 - f_2, 2f_2 - f_1$) falls within the operational band and it is difficult to filter it out. Hence, an analysis of intermodulation distortion is required to evaluate the system performance. The Eq. (7) is substituted for $I_b(t)$ in the rate equations (1)–(4) and the solutions are obtained. The input tones at 890 MHz (f_1) and 910 MHz (f_2) are chosen for this calculation. The third order intermodulation terms are 870 MHz

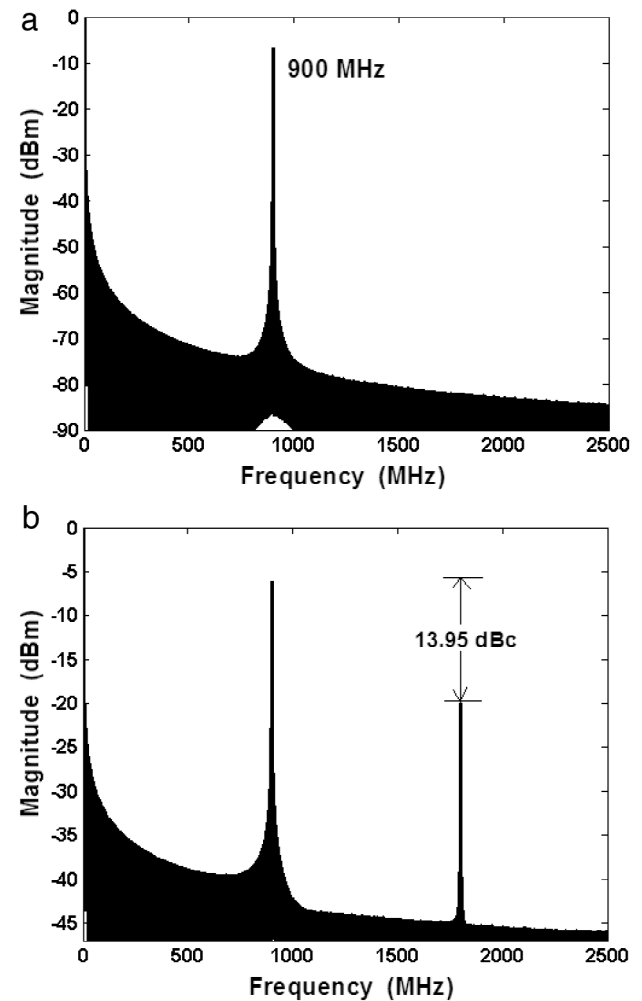


Fig. 5. The spectrum of (a) base current at 900 MHz (b) optical power.

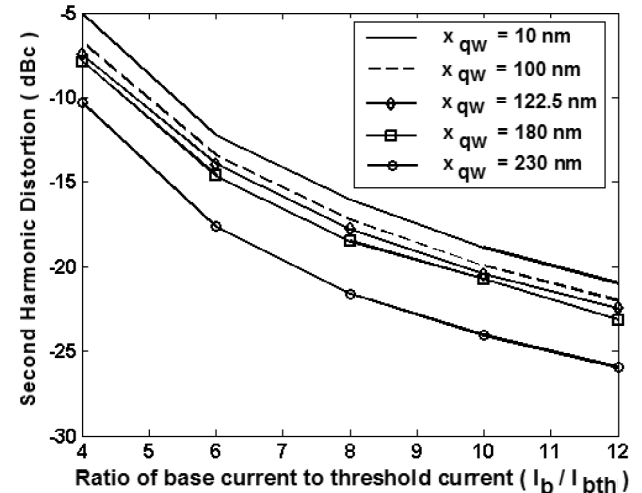


Fig. 6. 2HD variation with base current for different values of x_{qw} .

($2f_1 - f_2$) and 930 MHz ($2f_2 - f_1$) for this input. The spectrum of two tone input current and corresponding optical output power are shown in Fig. 7. A base current of $I_{bo} = 6 I_{bth}$, and position of the quantum well, $x_{qw} = 122.5$ nm are fixed for this case. The magnitude of intermodulation

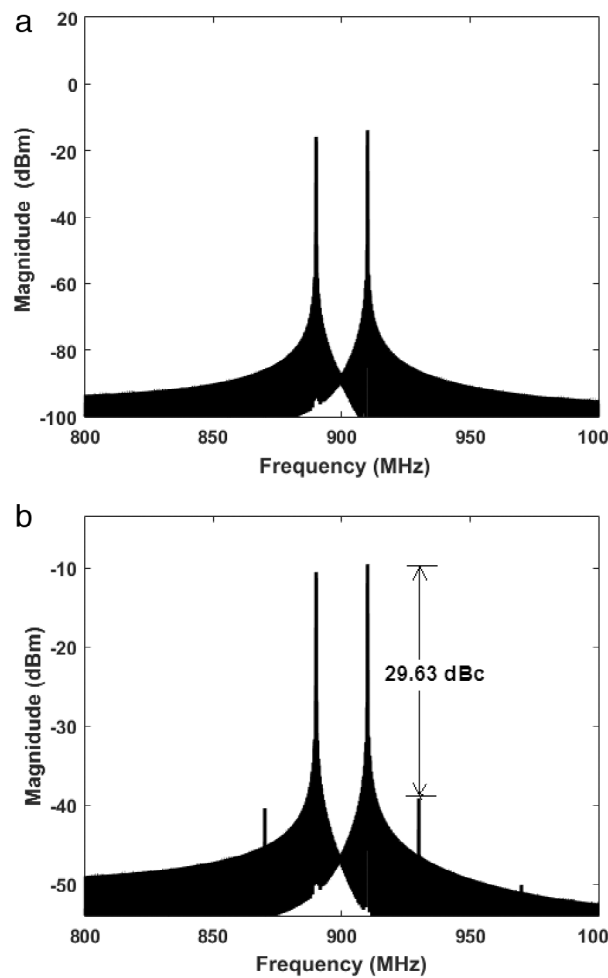


Fig. 7. (a) The spectrum of two tone input current at 890 MHz and 910 MHz (b) optical output with IMD3 components.

product term at 930 MHz ($2f_2 - f_1$) is found to be -29.63 dB with reference to the fundamental tone ($f_2 = 910$ MHz).

The IMD3 components are evaluated for similar fundamental tones at different quantum well positions. The bias current is varied from $4 I_{bth}$ to $12 I_{bth}$ and the calculated IMD3 are indicated in Fig. 8. It is inferred that the magnitude of third order intermodulation distortion products (IMD3) are found to decrease with increase in movement of quantum well position from base-emitter interface. The value of IMD3 is maximum at the bias current of $I_{bo} = 4 I_{bth}$ for all the position of the quantum well. A minimum third order intermodulation distortion of -38.2 dBc is obtained for the quantum well position which is at 230 nm from the emitter interface at a bias of $12 I_{bth}$.

4.3. Effect of RF current magnitude on distortion

The magnitude of fundamental tone and IMD3 components are evaluated for different RF current magnitudes and plotted in Fig. 9. The positions of quantum well (x_{qw}) are kept as 10 nm and 230 nm respectively. For 10 nm position, which is close to the base-emitter interface, the characteristics is shown in Fig. 9(a). The bias current is fixed as $4 I_{bth}$, where I_{bth} is threshold current for corresponding quantum well position. Modulation depth is maximum at this bias point. The two input frequency tones are chosen as 890 MHz and 910 MHz and the harmonic and intermodulation tones appear in the output due to non linearity of the transistor laser. The IMD3 components are 870 MHz and 930 MHz for this input. The magnitude of RF current (I_{RF})

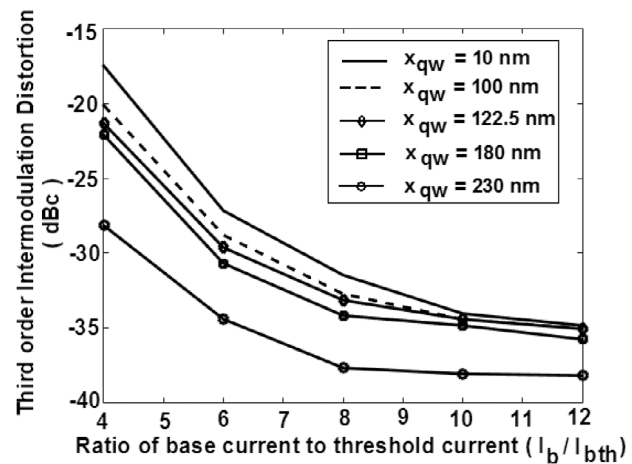


Fig. 8. Variation of IMD3 with base current for different positions of quantum well.

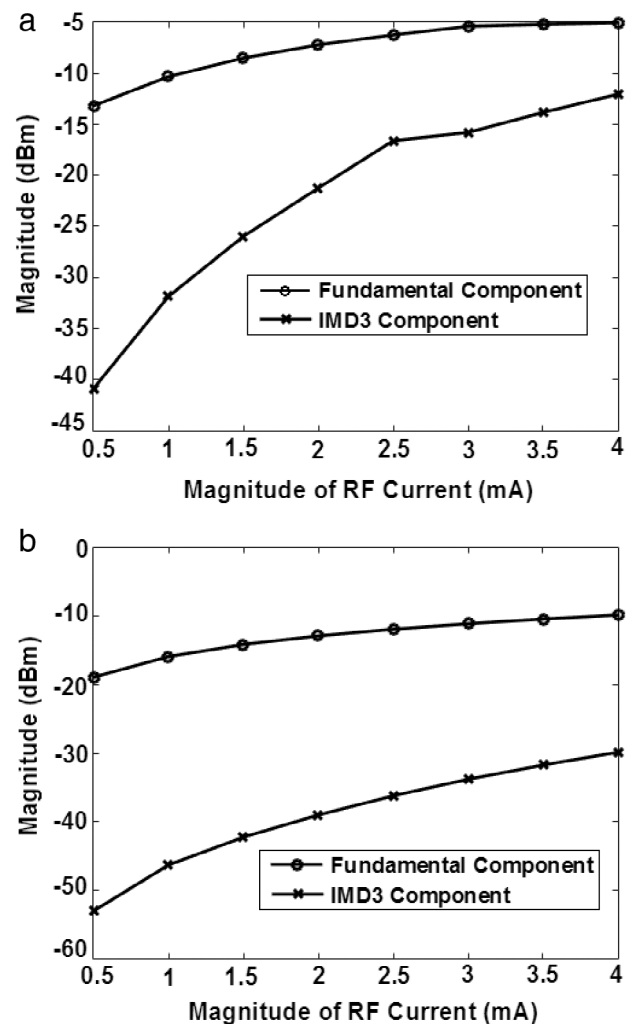


Fig. 9. Variation of magnitude of fundamental tone and IMD3 with different RF current magnitude for (a) $x_{qw} = 10$ nm (b) $x_{qw} = 230$ nm.

is varied from 0.5 mA to 4 mA. The minimum value of RF current depends on received RF power and sensitivity of the receiver. Similarly, the RF current magnitude is limited to 4 mA in this analysis. If the RF current magnitude is increased beyond this value, the magnitude

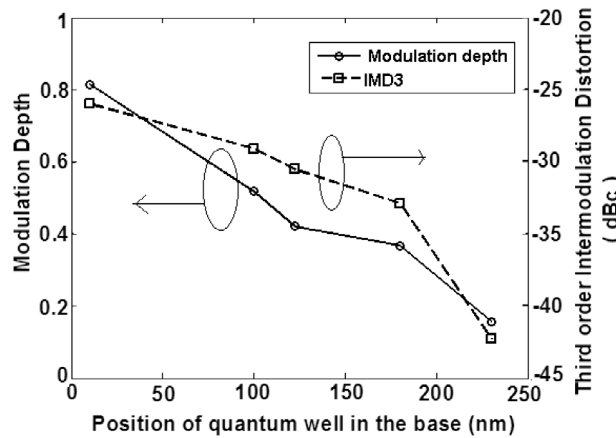


Fig. 10. Variation of modulation depth and IMD3 with different positions of quantum well.

become higher than the I_{bo} which leads to higher intermodulation distortion. The magnitude of IMD3 component is found to increase for increasing RF current magnitude. A minimum magnitude of IMD3 component of -40.87 dBm is obtained for 0.5 mA RF current magnitude. The analysis is repeated for the quantum well position, $x_{qw} = 230$ nm (Fig. 10(b)). The minimum magnitude of IMD3 component is found as -53.07 dBm for 0.5 mA RF current magnitude.

4.4. Effect of position of quantum well on modulation depth and third order intermodulation distortion (IMD3)

Modulation depth and IMD3 variation with different quantum well position (x_{qw}) are plotted as shown in Fig. 10. The position of quantum well is varied from 10 nm to 210 nm. Modulation depth and IMD3 are found to decrease as the quantum well is moved away from base-emitter junction. This is due to the reason that the base threshold current increases if the quantum well is moved toward base-collector junction. Optimum value of modulation depth (0.42) and IMD3 (-21.32 dBc) are obtained for the quantum well position of 122.5 nm (x_{qw}), which is exactly at mid position in the base. However, the maximum modulation depth of 0.81 is obtained for quantum well position $x_{qw} = 10$ nm at the bias point of $I_b = 4 I_{bth}$. The corresponding value IMD3 is -17.46 dBc. This quantum well location can be used for the design of transistor laser for the radio over fiber application with reduced distortion.

5. Conclusion

The DC and AC characteristics of transistor laser are analyzed by solving the rate equations numerically. The power-current characteristics and frequency response are found to be well matched with the literature, which enabled us use the model to investigate the second harmonic distortion and third order intermodulation products. The effect of position of quantum well in the base region on the modulation and distortion performance is also determined. A maximum modulation depth of 0.81 is predicted, when the quantum well is placed at 10 nm

from the base-emitter junction under 900 MHz RF signal modulation, at a current of $4 I_{bth}$. A minimum second harmonic distortion magnitude of -30 dBc is predicted for quantum well positioned near base-collector interface, for $12 I_{bth}$. Similarly, a minimum third order intermodulation distortion of -38.2 dBc is obtained for quantum well near base-collector interface, under similar biasing conditions. Optimum values of modulation depth (0.42) and IMD3 (-21.32 dBc) are obtained when the quantum well is kept at the mid position of the base under 900 MHz signal modulation.

References

- [1] Hamed Al-Rawesshid, Shozo Komaki, Radio Over Fiber Technologies for Mobile Communications Networks, Norwood, MA, 2002.
- [2] Xavier N. Fernando, Radio over Fiber for Wireless Communications: From Fundamentals to Advanced Topics, John Wiley and Sons, United Kingdom, 2014.
- [3] C.H. Cox, E.I. Ackerman, G.E. Betts, J.L. Prince, Limits on the performance of RF over fiber links and their impact on device design, IEEE Trans. Microw. Theory Tech. 54 (2006) 906–920.
- [4] Zhenzhou Tang, Shilong Pan, A full duplex radio over fiber link based on dual polarization Mach-Zhender modulator, IEEE Photon. Technol. Lett. 28 (8) (2016) 852–855.
- [5] Jianyao Chen, Rajeev J. Ram, Roger Helkey, Linearity and third – Order intermodulation distortion in DFB semiconductor Lasers, IEEE J. Quant. Electr. 35 (1999) 1231–1237.
- [6] Jing Wang, Cheng Liu, Junwen Zhang, Ming Zhu, Mu Xu, Feng Lu, Lin Cheng, Gee-Kung Chang, Nonlinear inter-band subcarrier intermodulations of multi-RAT OFDM wireless services in 5G heterogeneous mobile front haul networks, J. Lightwave Technol. 34 (17) (2016) 4089–4102.
- [7] L. Roselli, V. Borgioni, F. Zapparelli, F. Ambrosi, M. Comez, P. Faccin, A. Casini, Analog laser predistortion for multiservice radio-over-fiber systems, J. Lightwave Technol. 21 (5) (2003) 1211–1223.
- [8] S. Piramasubramanian, M. Ganesh Madhan, A novel distortion reduction schemes for multiple quantum well gain lever laser diodes, J. Opt. 15 (2013) 055501.
- [9] S. Piramasubramanian, M. Ganesh Madhan, Simultaneous reduction of IMD3 and IMD5 in bisection laser diode by feedback second harmonic injection, Opt. Commun. 328 (2014) 151–160.
- [10] N. Holonyak Jr., M. Feng, The transistor laser, IEEE Spectr. 43 (2006) 50–55.
- [11] Han Wui Then, Milton Feng, Nick Holonyak Jr., The transistor laser: Theory and experiment, Proc. IEEE 101 (2013) 2271–2298.
- [12] G. Walter, N. Holonyak Jr., M. Feng, R. Chan, Laser operation of a heterojunction bipolar light-emitting transistor, Appl. Phys. Lett. 85 (2004) 4768.
- [13] M. Feng, N. Holonyak Jr., G. Walter, R. Chan, Room temperature continuous wave operation of a heterojunction bipolar transistor laser, Appl. Phys. Lett. 87 (2005) 131103.
- [14] R. Chan, M. Feng, N. Holonyak Jr., G. Walter, Microwave operation and modulation of a transistor laser, Appl. Phys. Lett. 86 (2005) 131114.
- [15] H.W. Then, G. Walter, M. Feng, N. Holonyak Jr., Charge control analysis of transistor laser operation, Appl. Phys. Lett. 91 (2007) 243508.
- [16] Lingxiao Zhang, Jean-Pierre Leburton, Modeling of the transient characteristics of heterojunction bipolar transistor lasers, IEEE J. Quant. Electr. 45 (2009) 359–366.
- [17] Mizuki Shirao, SeungHun Lee, Nobuhiko Nishiyama, Shigehisa Arai, Large signal analysis of a transistor laser, IEEE J. Quant. Electr. 47 (3) (2011) 359–367.
- [18] Behnam Faraji, Wei Shi, David L. Pulfrey, Lukas Chrostowski, Analytical modeling of the transistor laser, IEEE J. Sel. Top. Quantum Electron. 15 (3) (2009) 594–603.
- [19] Rikamanta Basu, Bratati Mukhopadhyay, P.K. Basu, Estimated threshold base current and light power output of a transistor laser with InGaAs quantum well in GaAs base, Semicond. Sci. Technol. 26 (2011) 105014.
- [20] H.W. Then, F. Tan, M. Feng, N. Holonyak Jr., Transistor laser electrical and optical linearity enhancement with collector current feedback, Appl. Phys. Lett. 100 (2012) 221104.
- [21] Stavros Iezekiel, Microwave-photonic links based on transistor-lasers: Small-signal gain analysis, IEEE Photon. Technol. Lett. 26 (2014) 183–186.
- [22] S. Piramasubramanian, M. Ganesh Madhan, Jyothsna Nagella, G. Dhanapriya, Numerical analysis of distortion characteristics of heterojunction bipolar transistor laser, Opt. Commun. 357 (2015) 177–184.

Performance analysis of a digital fiber optic link incorporating gain-levered laser diode transmitter

S. Piramasubramanian  | M. Ganesh Madhan | A. Sindhuja

Department of Electronics Engineering,
Madras Institute of Technology Campus,
Anna University, Chennai, India

Correspondence

S. Piramasubramanian, Department of
Electronics Engineering, Madras Institute
of Technology Campus, Anna University,
Chennai, India.
Email: spirama@annauniv.edu

Abstract

In this paper, digital modulation performance of two-section, multiple quantum well gain-levered laser diode in a fiber optic link is analyzed. This study involves numerical simulation of gain-levered laser diode along with single-mode fiber for evaluating gigabit rate digital transmission. The optical link performance is analyzed by evaluating the eye diagram, extinction ratio, and quality factor for different bit rates, modulation current, and fiber lengths. The results are compared with unlevered or normal laser diode-based fiber optic link with similar operating conditions. A 12-dB improvement in extinction ratio is obtained for gain-levered laser diode when the longer section and shorter section currents are kept as 30 and 0.5 mA, respectively. The Q parameter is found to increase with increasing modulation current in the gain-levered case, and a maximum Q factor of 11 is obtained for a modulation current of 5 mA. The Q value is improved by a factor of 8 and 5 at 1-Gbps and 10-Gbps data rates, respectively, under gain-levered condition, when compared to normal laser diode-based link.

KEYWORDS

extinction ratio, gain-lever effect, numerical simulation, Q factor, rate equations, 2-section laser diode

1 | INTRODUCTION

Optical fiber has already replaced copper-based transmission lines in communication networks because of its attractive characteristics like wide bandwidth, small size, and immunity to electromagnetic interference.^{1,2} Fiber optic cables transport either analog or digital information depending on its applications. The information generated by computers, telephone systems, and data sources are mostly in digital format. Video signals are also converted into digital format, and then it is transmitted through the communication channel in the case of modern Cable Television systems. Further cellular mobile system also utilized digital modulation. High speed Internet access has paved the way for large-scale deployment of transmission in digital formats.²

Semiconductor lasers are ideal optical sources because of their large bandwidth and compatibility with single-mode fiber. They inherently introduce relative intensity noise in the system that influence the performance of any fiber optic link. This noise is due to photons that are generated from spontaneous emission and coupled into lasing mode.³⁻⁹ Coding techniques generally used to represent digital data are return to zero (RZ) and non-return to zero (NRZ) formats; however, NRZ is preferred because of its simple implementation. Further, the NRZ signal requires bandwidth less than that of RZ case.⁷ Digital modulation is realized in optical transmitters under direct and external modulation schemes. However, direct modulation is preferred for data rates less than 10 Gbps because of its low cost and simplicity.²

Information bits coded with NRZ scheme can directly modulate the laser source by varying the injection current proportionally. Pseudorandom nature of the information bits with high bit rate introduce fluctuations in the laser output optical power.⁴ Performance of directly modulated laser diode in the digital fiber link is reported by many researchers in the recent past.³⁻⁹ Dynamics of laser diode are analyzed by Ahmed et al⁵ for gigabit rates. The same author group has also analyzed the influence of transmission bit rate in the fiber optic link.⁴ They also compared the characteristics of laser diode under RZ and NRZ modulation formats. All the literatures available till now have analyzed the performance of digital fiber link, by considering a normal single-section laser diode-based transmitter.³⁻⁹ Pocha et al¹⁰ have envisaged that gain-levered laser diode can be used for digital switching applications. However, gain-levered-based direct modulation and link analysis have not been investigated earlier. In this work, we consider a two-section quantum well laser diode as an optical source, which is operated under gain-levered condition. This transmitter along with single-mode fiber is used to simulate a digital optical link, and its performance is analyzed for the first time.

Two-section laser diode also exhibits optical bistability apart from gain-levered effect, which is reported earlier.^{11,12} Gain-levered effect is generally investigated in two-section laser diode to improve the amplitude modulation efficiency.^{10,13-22} Modulation depth improvement by gain-levered mechanism is demonstrated and theoretically explained by Vahala et al.³ It is well known that signal to noise ratio of any communication link depends on modulation depth.^{1,2} The sublinear nature of optical gain with carrier density present in two-section laser diode is utilized to improve the modulation efficiency. To realize this gain levering effect, the two sections of the laser should have unequal gain constants and carrier lifetimes.¹⁴

The effect of number of quantum wells on gain-levered effect was analyzed by Seltzer et al,¹⁵ and they have also compared the results with conventional laser diode. An improvement in signal to noise ratio is also observed in gain-levered laser diodes by the same group. Amplitude and frequency modulation efficiency improvement by using gain-levered effect in multisection laser diodes was also studied.¹⁰ Both optical and electrical gain lever were demonstrated for different section length ratios and injection currents. Rana et al¹⁷ modified the cavity structure of the laser diode to increase the modulation efficiency. Increase in modulation bandwidth of the device with minimum distortion is achieved in the case of tapered cavity gain-levered laser diode.

Most of the reports in gain-levered laser diode that are published earlier addressed the modulation and distortion characteristics of the device for analog optical fiber link applications.¹⁵⁻¹⁷ Analysis of intermodulation distortion and reduction of third- and fifth-order intermodulation components in two-section gain-levered laser diode were reported.^{19,20} Gain-levered laser diode also finds application in tunable wavelength devices.²¹ Recently, bandwidth enhancement by using optical injection locking in gain-levered laser diode is also reported.²²

In this paper, we have analyzed the performance characteristics of gain-levered laser diode-based fiber optic link under large signal digital modulation. Two-segmented laser diode is modeled using modified rate equations that are numerically solved using MATLAB. The short and long active regions are optically coupled and electrically isolated. The NRZ-coded digital data directly modulate the shorter section current, and a constant DC bias is applied into the longer section. An improvement in extinction ratio (ER) is observed when compared with unlevered laser diode. The output optical power of the laser diode is coupled to a single-mode fiber, and the received data are analyzed.

Standard single-mode fiber is modeled by a parabolic digital filter, which is used to represent the linear propagation in the fiber.^{23,24} This time domain modeling includes the group velocity dispersion and attenuation. The performance of the gain-levered laser diode-based single-mode fiber link is analyzed under different bias, modulation current, and bit rates. Q factor is predicted for the gain-levered laser diode and compared with unlevered laser diode-based fiber link. The effect of fiber lengths are also investigated.

2 | MODELING OF SINGLE-FIBER OPTIC LINK WITH GAIN-LEVERED LASER DIODE

Rate equation model or equivalent circuit model are used to analyze the characteristics of laser diode. Numerical or analytical techniques are normally used to solve the rate equations. The equivalent circuit for laser diode is developed and solved in SPICE model or hardware description languages such as VERLOG-AMS. Symbolically Defined Device model is also used to solve rate equations in high-frequency design software such as Advanced Design System. In equivalent circuit model, the interpretation of rate equation parameter and its equivalent circuit representation is very difficult. However, analytical solution of rate equation is not always possible and also requires some numerical computation.

In general, optical fiber is modeled by its impulse response. Numerical methods are used to find the output of the fiber. Optical receiver is modeled as a low pass filter. Modeling of fiber and implementation is very difficult in equivalent circuit-based models. The accuracy of the numerical technique is better than conventional analytical or circuit model techniques. In optical communication link, integrated simulation of optical source, optical fiber, and optical receiver is required. It is very difficult to integrate all the optical, optoelectronic components and optical fiber in equivalent circuit-based models in single tool. It also requires cosimulation of two different tools. Integrated solution of optical source, optical fiber, and optical receiver can be obtained by numerically solution in MATLAB. Numerical analysis of complete optical fiber link is reported by many researchers recently. However, we have reported the numerical analysis of the performance of gain-levered laser diode-based digital fiber link for the first time. We have solved the rate equation using ode45 routine, which involves fourth-order Runge-Kutta numerical technique.

The block diagram of the fiber optic link is shown in Figure 1. The link includes Pseudo Random Bit Sequence (PRBS) generator, two-segmented laser diode, single-mode fiber, and the detector. The PRBS generator produces random bits, which are coded with the NRZ line coding at a bit rate of several gigabits per second.

The current pulses in NRZ modulation format directly drive the shorter section of the two-section laser diode. Injection current is varied between two current values corresponding to bit 1 and bit 0, respectively. Optical power corresponding to the bit level 1 and bit level 0 current is emitted out from the laser and directly coupled into the single-mode fiber. Linear propagation in standard single-mode fiber is modeled by its impulse response. The detector is modeled as low pass filter, and the output signal from the detector is analyzed.²³

2.1 | Modeling of gain-levered laser diode

Gain-levered phenomenon is used to increase the modulation efficiency in laser diodes with two unequal active regions.¹¹ Gain lever is directly proportional to the ratio of carrier life time and differential gain in both sections.¹⁴ The electrically isolated and optically coupled sections lead to nonuniform carrier densities in the regions. The schematic diagram of a two-section laser diode that reveals the gain-levered effect is shown in Figure 2.

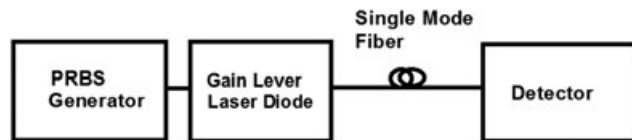


FIGURE 1 Block diagram of the fiber optic link incorporating gain-levered laser diode-based transmitter

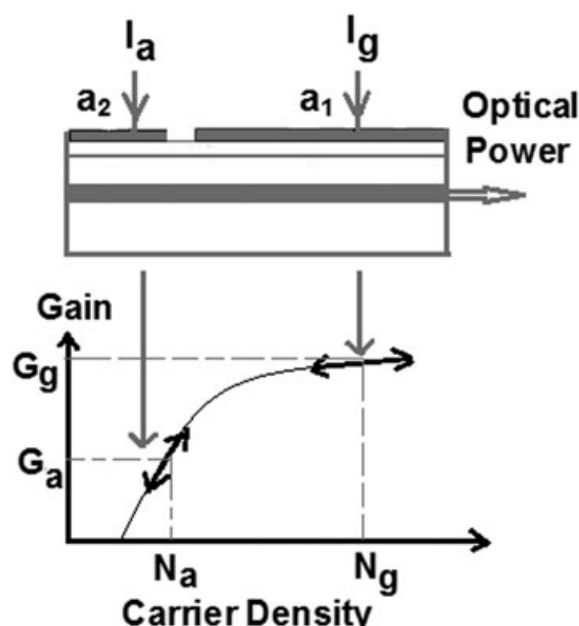


FIGURE 2 Gain-levered laser diode and the sublinear relationship between gain and carrier density¹⁰⁻²⁰

The current “ I_a ” is injected into the shorter section, and current “ I_g ” is provided to the longer section. “ I_m ” is modulation current, and the shorter section is dc biased to a lower gain, when compared to the longer section. Changes in gain of one region will be compensated by equal and opposite changes in the gain of the other region.¹⁴ When shorter region current is reduced, the circulating optical power becomes less, which increases the carrier density in the longer section. A sublinear relationship between gain and the carrier density exists in gain-levered laser, which in turn increases the modulation efficiency.^{10,13-17}

The rate equations of a laser diode govern the interaction of photons and electrons in the active region thereby modeling the electrical and optical performance of the device. The relationship between optical output power and drive current can be determined using rate equation. The modified rate equation for the two-segmented laser diode is given as¹²

$$\frac{dN_g}{dt} = \frac{I_g}{a_1 q V} - BN_g^2 - v_g g_g (N_g - N_{og}) S(1 - \epsilon S) - \frac{N_g}{\tau_{nr}}, \quad (1)$$

$$\frac{dN_a}{dt} = \frac{I_a}{a_2 q V} - BN_a^2 - v_g g_a (N_a - N_{oa}) S(1 - \epsilon S) - \frac{N_a}{\tau_{nr}}, \quad (2)$$

$$\frac{dS}{dt} = -\frac{S}{\tau_p} + [a_1 v_g g_g (N_g - N_{og}) + a_2 v_g g_g (N_a - N_{oa})] \Gamma S(1 - \epsilon S) + \Gamma \beta (a_1 B N_g^2 + a_2 B N_a^2). \quad (3)$$

The parameters and values used in this simulation correspond to a device realized by Uenohara et al,¹² where $N_a(t)$ and $N_g(t)$ are the carrier densities in the shorter and longer section, respectively. $S(t)$ represents the photon density in the cavity and a_1 and a_2 denote the volume ratio of longer section and shorter section, respectively. I_a and I_g represent currents in shorter section and longer section, respectively. N_{oa} and N_{og} are the carrier densities in the shorter and longer section at transparency. Group velocity, electron charge, gain compression factor, and spontaneous emission factor are represented by v_g , q , ϵ , and β , respectively. Γ represents optical confinement factor, and the output power is calculated from the photon density using formula¹¹

$$P(t) = \eta \left(\frac{hc}{\lambda} \right) \left(\frac{V}{\Gamma} \right) \left(\frac{S(t)}{\tau_p} \right), \quad (4)$$

where c , h , V , η , and λ represent velocity of light, Planck's constant, volume of the active region, internal quantum efficiency, and wavelength, respectively.

2.2 | Single-mode fiber model

The optical power output is coupled into the single-mode fiber and detected at the other end. The fiber is modeled by its impulse response that includes group velocity dispersion and attenuation. The impulse response of the fiber is given by²³

$$h(t) = (1 + i)(4\pi\beta_2 L)^{-1/2} \exp\left(\frac{-it^2}{2\beta_2 L}\right), \quad (5)$$

$$D = -\frac{2\pi c \beta_2}{\lambda_o^2}, \quad (6)$$

where D is the group velocity dispersion. The electric field ($E(t)$) at the input of the fiber is proportional to the optical power coupled into the fiber. The electric field is given by²³

$$E(t) = \sqrt{P(t)} \exp[j\phi(t)]. \quad (7)$$

The optical power at the output of the fiber is calculated by the convolution of electric field at the input of the fiber with impulse response of the fiber.²¹ The output optical power after the fiber is given by

$$Po(t) = A |E(t) \otimes h(t)|^2, \quad (8)$$

where $P_o(t)$ is the optical power after the fiber and “A” is the fiber attenuation. The impulse response $h(t)$ is truncated and smoothed by a window function,²¹ and the window function is

$$h_w(t) = 0.54 + 0.46 \cos\left(\pi\left|\frac{t}{T_{\max}}\right|^3\right). \quad (9)$$

The power output at the end of the fiber is given by²¹

$$P_{out}(kTs) = A \left| \sum_{n=0}^{N-1} a(n) E[(k-n)T_s] \right|^2, \quad (10)$$

where E_{in} , A , L , and N represent the electric field envelop function, attenuation, length of the fiber, and number of filter coefficients, respectively.

3 | NUMERICAL SIMULATIONS AND RESULTS

3.1 | Static characteristics

The rate equations are numerically solved to study the characteristics of the device. Fourth-order Runge-Kutta method is used to solve the equations in MATLAB. The parameters for two-segmented laser diode are taken from previous studies^{12,23} and provided in Table 1.

Carrier densities in longer section (N_g) and shorter section (N_a), photon density (S), and optical power are evaluated from the solution of rate equations. Optical power variation with injection currents are shown in Figure 3, for both gain-levered and unlevered conditions. To obtain the characteristics for the unlevered condition, both the current terminals are shorted together and equal current is given to both regions ($I_g = I_a$).^{10,13-16} To validate our simulation results, the

TABLE 1 Parameters used for 2-section laser diode and single-mode fiber^{12,23}

Parameter	Description	Value
λ	Wavelength	1.3 μm
V	Total volume of active region of laser diode	$48.52 \times 10^{-12} \text{ cm}^3$
q	Charge of the electron	$1.603 \times 10^{-19} \text{ C}$
B	Effective recombination coefficient	$1 \times 10^{-10} \text{ cm}^3 \text{ s}^{-1}$
τ_{nr}	Nonradiative recombination time	1 ns
τ_p	Photon lifetime	1.87 ps
g_a	Gain constant-shorter section	$80 \times 10^{-16} \text{ cm}^2$
g_g	Gain constant-longer section	$2 \times 10^{-16} \text{ cm}^2$
N_{oa}	Transparency carrier density-shorter section	$1.25 \times 10^{18} \text{ cm}^{-3}$
N_{og}	Transparency carrier density-longer section	$1.25 \times 10^{18} \text{ cm}^{-3}$
a_1	Section length ratio-longer section	0.97
a_2	Section length ratio-shorter section	0.03
β	Spontaneous emission factor optical	1×10^{-5}
Γ	Confinement factor	0.15
ε	Gain compression factor	$2 \times 10^{-17} \text{ cm}^3$
v_g	Group velocity	$0.85714 \times 10^{10} \text{ cms}^{-1}$
η	Internal quantum efficiency	0.1
L	Length of the fiber	1 km
D	Dispersion parameter	1 ps/nm Km
A	Fiber attenuation	0.4 dB/km

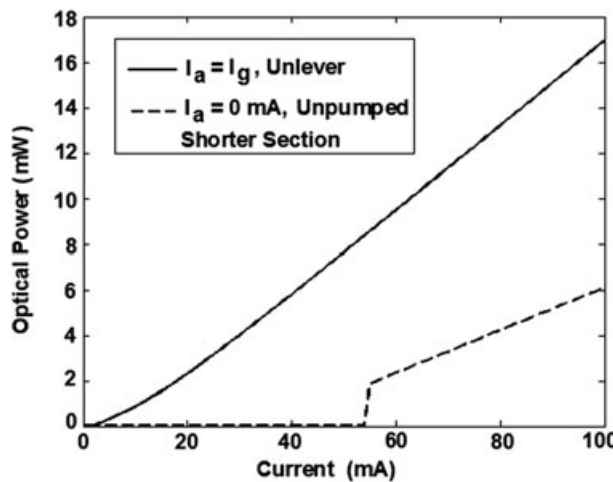


FIGURE 3 Static characteristics of two-section laser diode and unlevered laser diode

optical power variation with longer section current is calculated for unpumped shorter section ($I_a = 0$). For this analysis, the longer section current is varied from 0 to 100 mA, and optical power is calculated. The longer section threshold current is found to be 54 mA, which is exactly similar to the experimental results of Uneohara et al.¹² This analysis validates our simulation of bisection laser diode. The analysis is repeated for unlevered condition, where threshold current of the device is found to be 1.2 mA.

The variation of optical power with shorter section current is shown in Figure 4. The longer section of the laser diode is DC biased with fixed values of 20, 30, 40, and 50 mA, respectively. The optical power is found to increase with shorter section current. A maximum power of 6.5 mW is predicted for the longer and shorter section currents of 50 and 40 mA, respectively. The shorter section threshold current (I_{ath}) is evaluated for different longer section currents in the range of 10 to 54 mA and plotted in Figure 5. The shorter section threshold current is found to reduce with increase in longer section current. At a longer section current value of 54 mA, the shorter section threshold current (I_{ath}) reduces to zero. This is due to the fact that the longer section current is greater than the threshold current of the device at this condition. This result also coincides with the value of longer section threshold current for unpumped ($I_a = 0$) shorter section case (Figure 3).

The ER of a directly modulated digital fiber link mainly depends on the slope efficiency of the laser diode. Hence, an analysis of slope efficiency with bias current is performed, where the longer section currents (I_g) are fixed as 20, 30, and 40 mA. The shorter section current is varied up to 8 times of the shorter section threshold current ($8 I_{ath}$), and the slope efficiency (mW/mA) is plotted as shown in Figure 6. The slope efficiency is found to decrease with increasing shorter

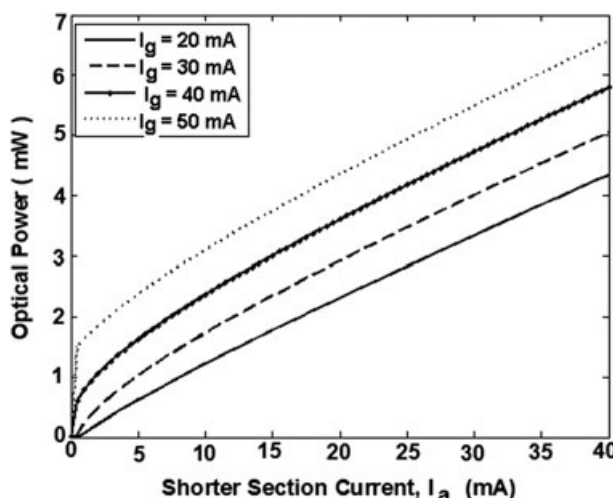


FIGURE 4 Static characteristics of two-section laser diode under different longer section current injection

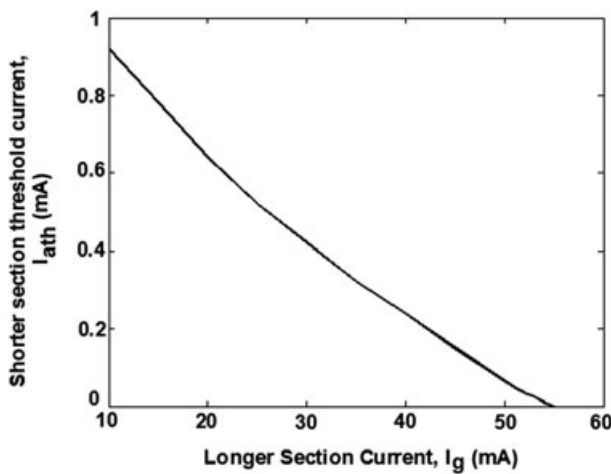


FIGURE 5 Shorter section threshold current variation with longer section current

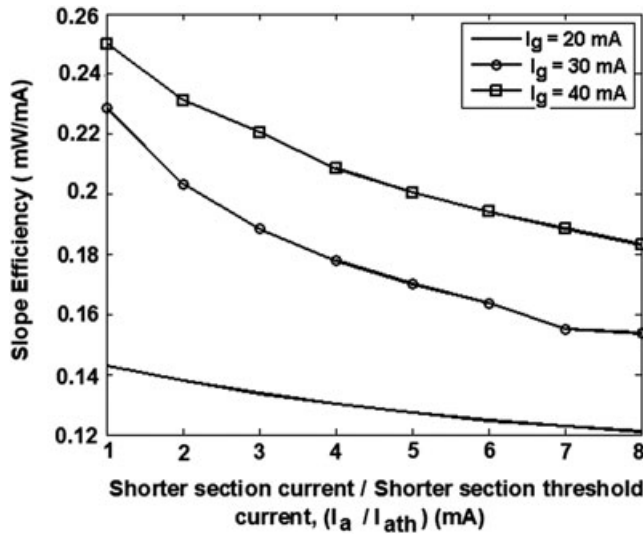


FIGURE 6 Variation of slope efficiency with shorter section current

section current. A maximum slope efficiency (0.25 mW/mA) is obtained for the longer and shorter section currents of $I_g = 40$ mA and $I_a = I_{ath}$, respectively.

3.2 | Frequency response of the two-section laser diode

The frequency response of the gain-levered laser diode is evaluated for fixed longer and shorter section bias currents. The magnitude of optical power is calculated for different frequencies as the ratio of $P(j\omega)$ and P_{dc} . The longer section currents are fixed as 20, 30, and 40 mA for this analysis along with a shorter section current of 15 I_{ath} , where I_{ath} is shorter section threshold current. An AC signal is injected into the shorter section, and a constant bias is provided to the longer section of the laser diode. The shorter section current is $I_a = I_{adc} + I_{RF} \sin(\omega t)$, where I_{adc} and I_{RF} are the magnitude of DC and RF currents, respectively. The magnitude of RF current is kept as 2 mA (I_{RF}), and the shorter section DC currents (I_{adc}) are fixed as 9.75, 6.3, and 3.75 mA (15 I_{ath}). For the longer section, the currents are (I_g) 20, 30, and 40 mA, respectively. The shorter section threshold current is obtained from DC analysis provided in previous section (Figure 5). The frequency of AC signal is varied from 100 KHz to 70 GHz, and the magnitude response is plotted as shown in Figure 7A. A maximum resonant frequency of 17-GHz and 3-dB modulation bandwidth of 32 GHz is obtained for the bias currents of $I_g = 20$ and $I_a = 9.75$ mA.

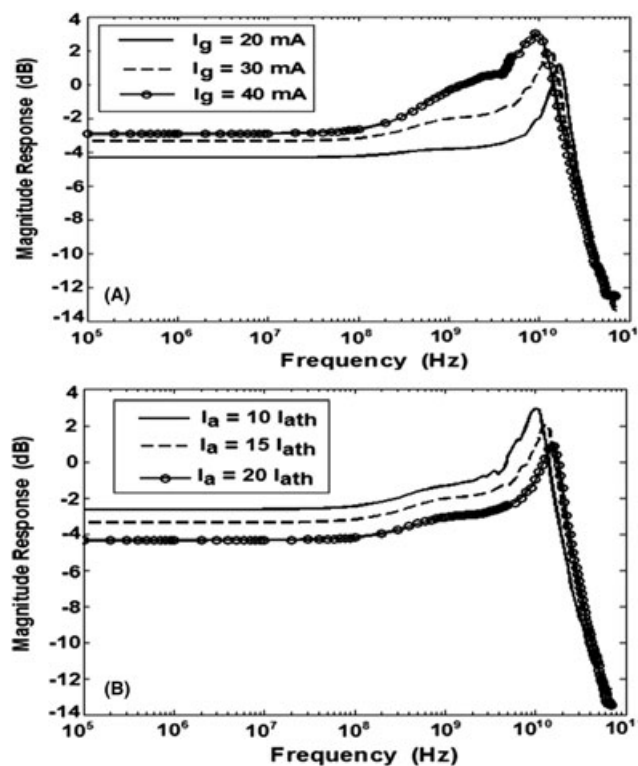


FIGURE 7 Frequency response of two-section laser diode for A, different longer section currents ($I_a = 15 I_{\text{ath}}$) and B, shorter section currents ($I_g = 30 \text{ mA}$)

The analysis is repeated for the fixed longer section bias current (I_g), and the magnitude response is plotted (Figure 7B). The shorter section currents (I_{adc}) are fixed as 10, 15, and $20 I_{\text{ath}}$, respectively. The resonant frequency and modulation bandwidth are found to increase with increasing shorter section current, which is similar to the behavior of normal laser diodes. A 3-dB modulation bandwidth of 23, 28, and 32 GHz is obtained for the shorter section bias currents of 10, 15, and $20 I_{\text{ath}}$, respectively. From this analysis, a longer section current of 30 mA is chosen for digital modulation as it provides a modulation bandwidth of 23 GHz at a shorter section current of $15 I_{\text{ath}}$.

3.3 | Two-section laser diode under digital modulation and analysis of extinction ratio

The performance of the gain-levered laser diode is first analyzed under gigabit rate direct modulation by evaluating the ER. This is required to investigate the link under different fiber lengths and bit rates. The ER of the optical pulse is defined as the ratio of power level corresponding to the bit 1 to the power level corresponding to the bit 0.

$$ER = 10 \log \left(\frac{P_1}{P_0} \right), \quad (11)$$

where P_1 and P_0 are the power at the levels 1 and 0. It is important to achieve a good ER for the best link performance. In normal lasers, there exists a trade-off between the ER and modulation bandwidth.¹ The effect of a poor ER will be manifested in the form of power penalty at the receiver.³

In gain-levered laser diode, the shorter section is injected with a DC bias current along with modulation current ($I_a + I_m$). The modulation current represents randomly generated NRZ-coded digital data. To use gain-levered effect, longer section is given with constant DC bias, which is fixed as 30 mA in this case. The shorter section current is fixed as 2 mA for level 0 and the 6 mA for level 1. The PRBS data sequence is kept as 1110011001, for this study. The shorter section current input and corresponding optical output are shown in Figure 8A,B, respectively. The maximum and minimum output optical powers are obtained as $P_1 = 1.341 \text{ mW}$ and $P_2 = 0.4801 \text{ mW}$ for the above-mentioned biasing conditions. The ER is calculated from the above Equation 11 and found to be 4.46 dB.

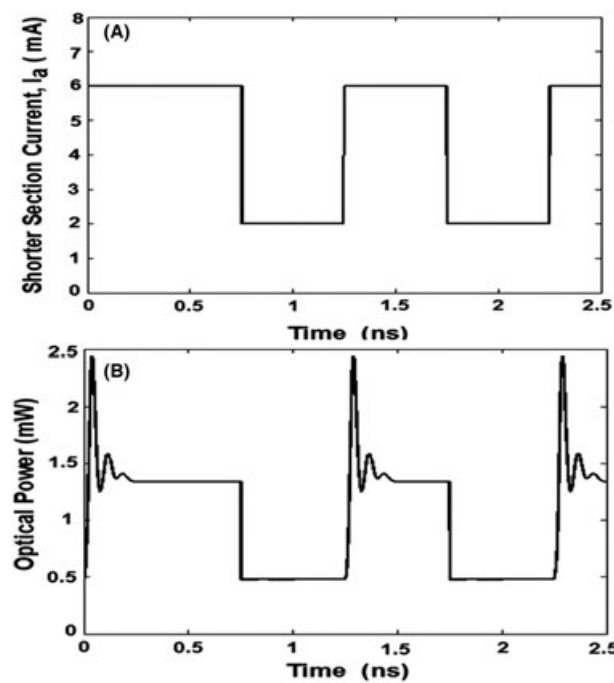


FIGURE 8 A, Shorter section current pulses for a data sequences “1110011001” ($I_g = 30$ mA); B, output optical power

In unlevered laser diode, the longer section and shorter section current are shorted together, and the same current is injected to both the sections ($I_g = I_a$). A current of 16 mA ($(30 + 2$ mA)/2) is given for bit 0, and the current of 18 mA ($(30 + 6$ mA)/2) is given for bit 1 to compare the results with gain-levered condition.¹¹⁻¹⁵ These bias currents are equal to that of bias currents given under gain-levered condition. The generated random NRZ data is “1110011001” as in the gain-levered case. The input current and corresponding optical power are shown in Figure 9A,B, respectively. The calculated ER is 0.6395 dB for the unlevered condition.

The difference between the ER for gain-levered and unlevered condition is calculated. The ER of gain-levered laser diode is 3.82 dB higher than unlevered case. This result shows that the gain-levered laser diode provides larger ER than

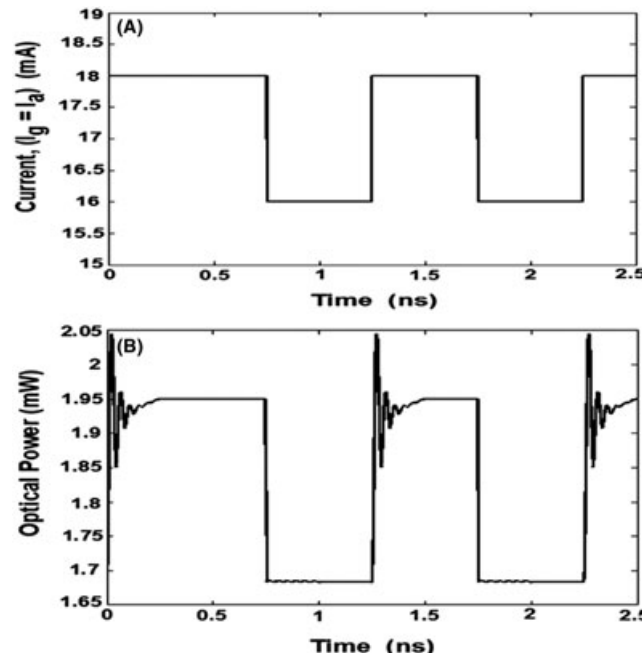


FIGURE 9 A, Injected current of 16 and 18 mA corresponding to 1 and 0; B, the output optical power

conventional laser diode under similar operating conditions. This analysis is repeated for other bias currents, and ER is evaluated. The variation of ER with shorter section and longer section currents is shown in Figure 10. The shorter section current (I_a) is varied from 0.5 to 6 mA (shown in x-axis at the top of Figure 10), and the longer section current (I_g) is fixed as 30 mA for this analysis. The total current injected into the device is 30.5 mA ($I_a + I_g = 0.5 + 30$ mA). The magnitude of NRZ pulse is fixed as 4 mA in this case, and maximum ER of 13.5 dB is obtained for the shorter section current of 0.5 mA. The ER is found to reduce for increasing shorter section current. The analysis is repeated for unlevered laser diode for comparison, and the current ($I_a = I_g$) is varied from 15.25 to 18 mA (given in bottom x-axis of Figure 10). The total current applied to the laser diode is varied from 30.5 mA ($I_a + I_g$) to 36 mA ($I_a + I_g$), which is equal to the total injected current under unlevered condition. The ER is also found to reduce for increasing applied current. Maximum ER improvement is predicted when the shorter section current is close to the threshold current of the device.

Similar analysis is performed for other longer section currents, and the improvement in the ER is evaluated. The longer section currents are fixed as 30, 40, and 50 mA, respectively, and the result is shown in Figure 11. The improvement in ER is the ER difference between gain-levered and unlevered laser cases. The improvement in ER is maximum for 30 mA and found to decrease with increasing longer section currents. This result is due to the fact that the optical power at a shorter section current (I_a) is found to be higher for the longer section currents of 40 and 50 mA, when compared to

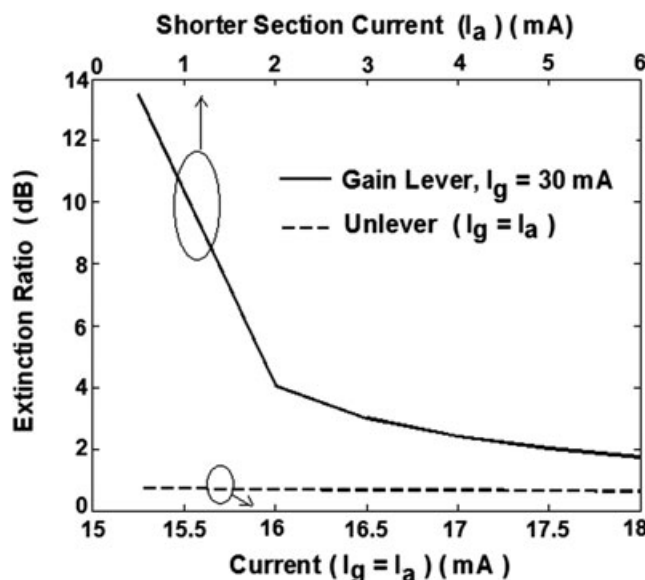


FIGURE 10 Extinction ratio variation with bias current for gain-levered and unlevered laser conditions

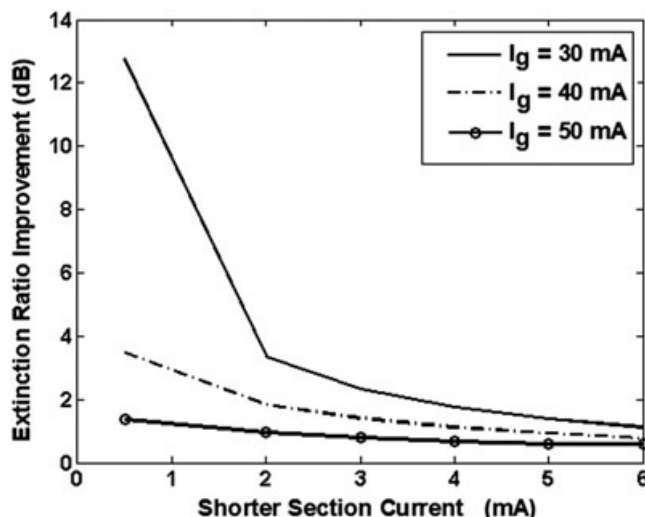


FIGURE 11 Extinction ratio improvement with shorter section current

the 20 mA (Figure 4). This characteristic of the device leads to the lower ER for higher current injection at the longer section.

The NRZ digital data is transmitted through the single-mode fiber link, which is modeled by its impulse response that incorporates group velocity dispersion and attenuation. Since laser diode wavelength is 1.3 μm , the group velocity dispersion and fiber attenuation are considered as 1 ps per km-nm and 0.4 dB per km, respectively. The length of the fiber is kept as 1 km. The power output at the end of the fiber is obtained for the gain-levered and unlevered laser diode-based transmitters and shown in Figure 12A,B, respectively. It is observed that the ER is higher for the fiber link, which is based on gain-levered laser diode than that of unlevered laser diode transmitter.

From the above results, it is predicted that gain-levered diode-based transmitter exhibits better performance than conventional laser diode because of higher ER. Further, the pulse current amplitude required to provide output power modulation is less compared to unlevered case. However, DC current required at the longer section is higher than the shorter section to achieve higher ER.

3.4 | Analysis of eye diagram and Q factor

3.4.1 | Effect of bit rate on Q factor and eye diagram

The transmission performance of gain-levered and unlevered laser diode-based single-mode fiber link is examined in detail by evaluating Q factor and eye diagram. Q factor is defined as the ratio of difference between the power corresponding to bit 1 and the power corresponding to bit 0 to the sum of standard deviation at the level of bit1 and bit 0.

$$Q = \frac{P_1 - P_0}{\sigma_1 + \sigma_0}, \quad (12)$$

where P_1 and P_0 denote the mean power at the bit 1 and bit 0, respectively, and σ_1 and σ_0 represent the corresponding standard deviations for bit 0 at the bit 1. The difference between power ($P_1 - P_0$) determines the height of the eye opening in the received signal.

For the gain-levered laser diode, longer section is provided with a current of 30 mA, and the shorter section is given 4.5 and 0.5 mA for bit 1 and bit 0, respectively. The input data rate is fixed as 1, 2, and 4 Gbps, and the eye diagrams at the receiver are analyzed for a fiber length of 1 km. The eye diagrams corresponding to the received signals are shown in

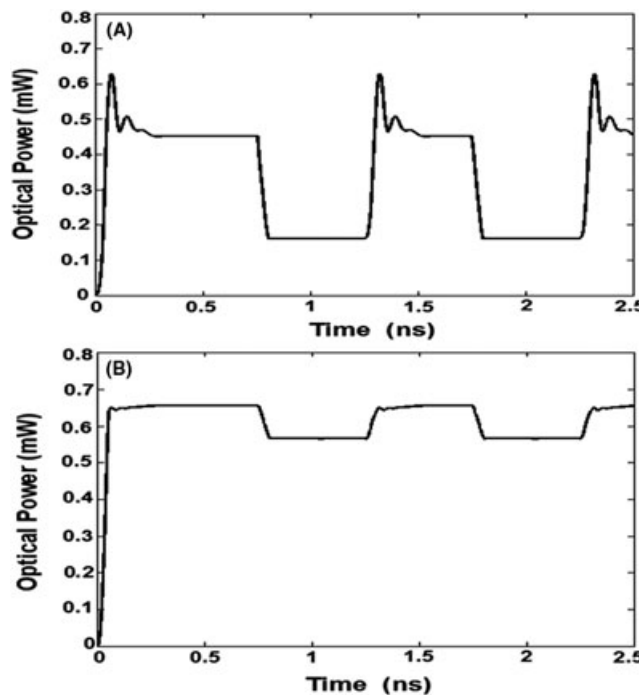


FIGURE 12 Output power at the end of the fiber A, for the gain-levered laser diode, $I_a = 2$ mA and $I_g = 30$ mA, and B, for unlevered laser diode, $I_a = I_g = 16$ mA

Figure 13A-C, respectively. The result shows that the distortion increases as the number of bits transmitted per second is increased, leading to reduced eye opening. These results coincide with theory.³⁻⁷

For the unlevered laser diode, an equal current is provided to both regions. The current pulse of magnitudes 15.25 and 17.25 mA is given for bit 0 and bit 1, respectively. The same data rate (1, 2, and 4 Gbps) and fiber length are used for transmission, and eye diagram is plotted in Figure 14A-C. From the results, it is understood that eye opening of unlevered laser diode is small when compared to the gain-levered laser diode. The difference between the power level 1 and the power level 0 is also less, when compared to gain-levered laser diode. The distortion in the output is found to increase for increasing transmission bit rate as in gain-levered case. The eye opening also follows the same result. There is no distortion in the eye diagram for 1 Gbps, and the eye closure becomes significant for the data rates beyond 2 Gbps. Modulation efficiency is also found to decrease with increasing bit rate.

Q factor and bit error rate are calculated from the eye diagram for gain-levered and unlevered laser diode and plotted. These results are shown in Figure 15A,B, respectively. The transmission bit rate is varied from 1 to 10 Gbps. The operating conditions like bias current and modulation current are fixed as in the case of previous analysis. As the number of bits per second is increased, the distortion increases and the eye tends to close, leading to a decrease *Q* factor. The results of the unlevered laser diode and gain-levered laser diode are compared. It is found that *Q* factor at any bit rate is higher for gain-levered laser diode when compared to the unlevered case. This results due to the fact that the gain-levered laser diode exhibits higher ER than unlever condition. The bit error rate is found to increase with increase in bit rate (Figure 15B). This result agrees well with the performance of conventional laser diode in the fiber link with increasing transmission bit rate.³

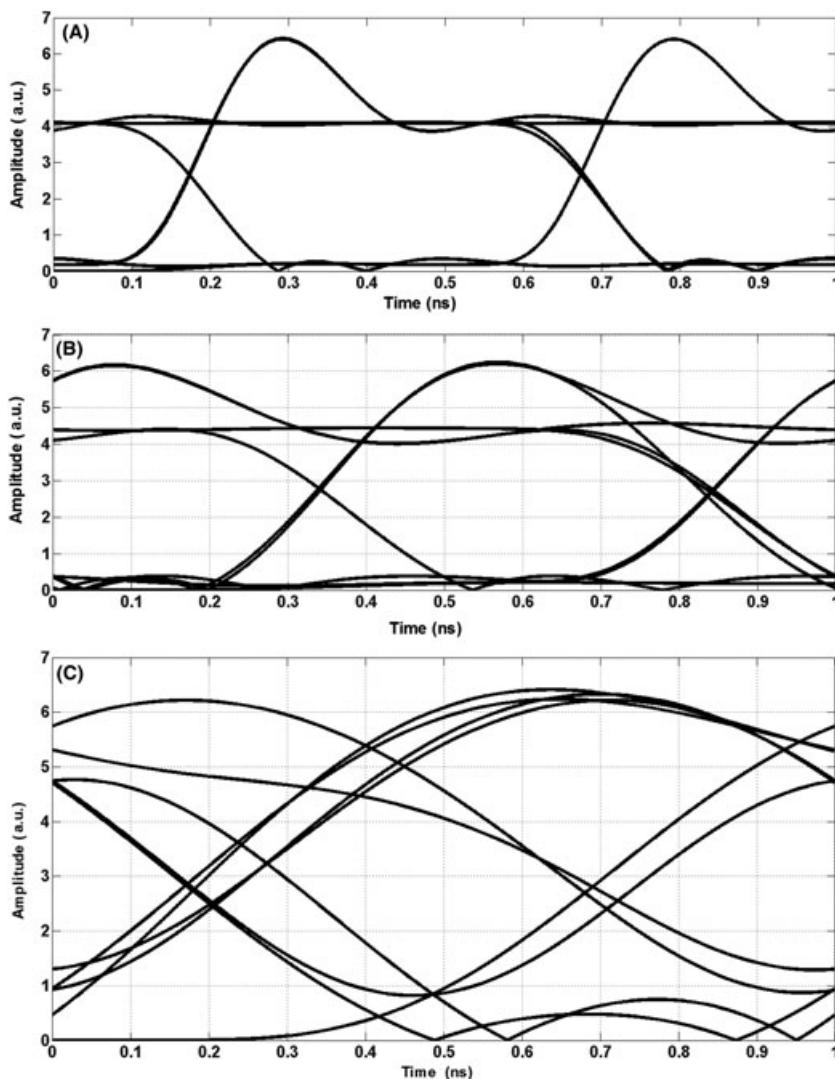


FIGURE 13 Eye diagram at the receiver of the link with gain-levered laser diode-based transmitter. A, 1 Gbps; B, 2 Gbps; and C, 4 Gbps

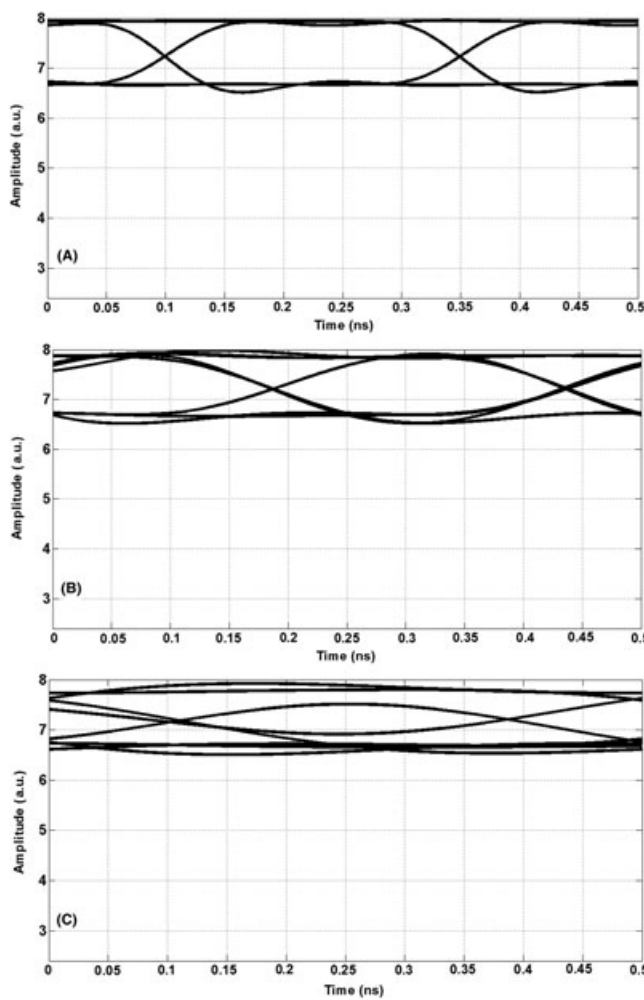


FIGURE 14 Eye diagram at the receiver for unlevered laser diode transmitter with the data rate of A, 1 Gbps; B, 2 Gbps; and C, 4 Gbps

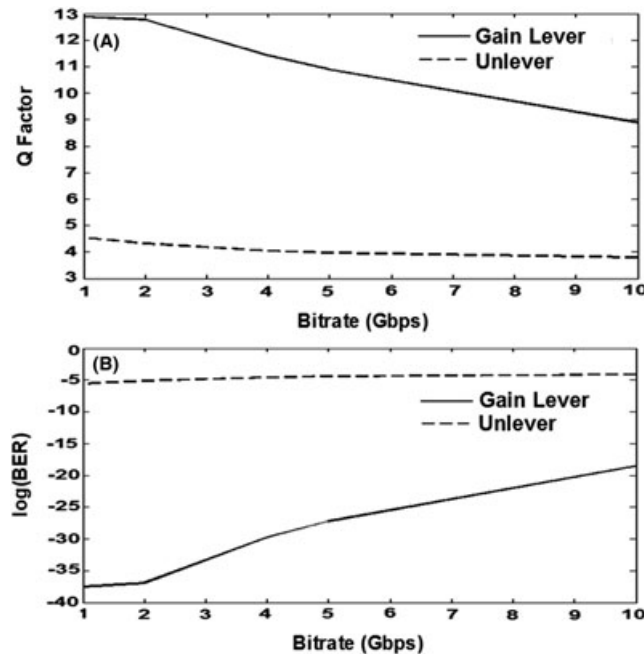


FIGURE 15 A, The variation of Q factor with transmitted data rate; B, bit error rate variation with transmitted bit rate

3.4.2 | Effect of shorter section bias current on eye diagram and Q factor

Eye diagrams are obtained by varying the shorter section DC bias current at a fixed modulation current and bit rate. The larger section current is kept constant at 30 mA for gain-levered laser diode and the length of the fiber is fixed as 1 km. The shorter section current (I_a) is kept as 0.2, 0.5, and 2 mA along with a constant modulation current of 4 mA. The corresponding output eye diagrams after the receiver are shown in Figure 16A-C, respectively. The shorter section current with NRZ data is varied from 0.2 to 4.2 mA, and the corresponding eye diagram is shown in Figure 16A. The bias current in the shorter section is less than the threshold current of this section ($I_{ath} = 0.4$ mA for $I_g = 30$ mA). As the DC bias current is increased, the difference between the power corresponding to bit 1 and bit 0 also increases, leading to an improvement in eye opening.

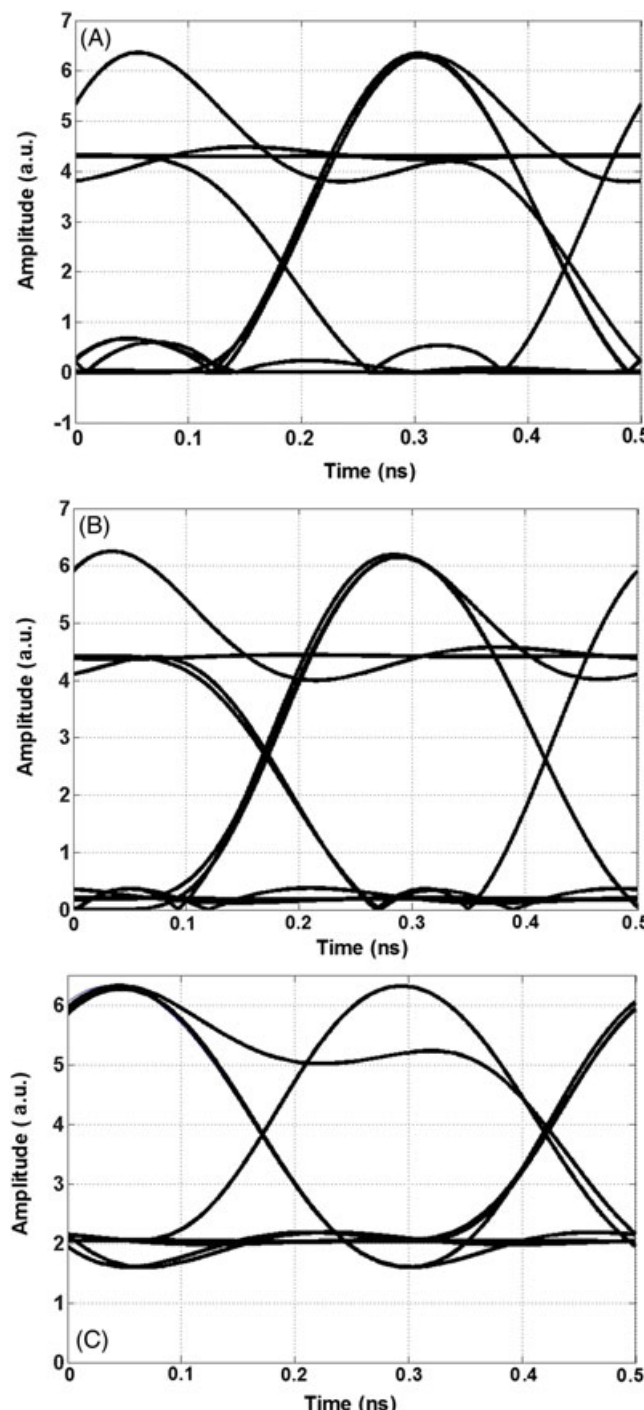


FIGURE 16 Eye diagram for the bias current of A, 0.2 mA; B, 0.5 mA; and C, 2 mA

The eye diagram calculation is repeated for unlevered laser diode for the same current as given in the case of gain-levered laser diode. Eye opening for the bias currents of 15.2, 15.25, and 16 mA in the case of unlevered laser diode is illustrated in Figure 17A-C. Eye opening is found to be greater for gain-levered laser diode when compared to the unlevered condition.

Q factor is calculated from the eye diagram by varying the shorter section bias current with constant modulation current (Figure 18A). The bit error rate ($\log(\text{BER})$) is calculated from *Q* factor and plotted in Figure 18B. The transmission bit rate and length of the fiber are held constant. The shorter section current is varied from 0.4 to 5 mA, and the longer section current is fixed as 30 mA. This scale is given at the top x-axis of Figure 18. The magnitude of modulation current, fiber length, and bit rate is fixed as 4 mA, 1 km, and 2 Gbps, respectively. The predicted *Q* factor is 6.5 and corresponding bit error rate is 10^{-10} for a shorter section current of 0.2 mA. The *Q* factor is found to increase till the shorter section current reaches to 2 mA and decreases beyond. This indicates that there is an increase in the *Q* factor near the threshold current. The analysis is repeated for unlevered laser diode where the current in both of the sections is varied from 15 to 17.5 mA ($I_g = I_a$). This current is equal to the total current applied for the gain-levered laser diode. The *Q* factor is found

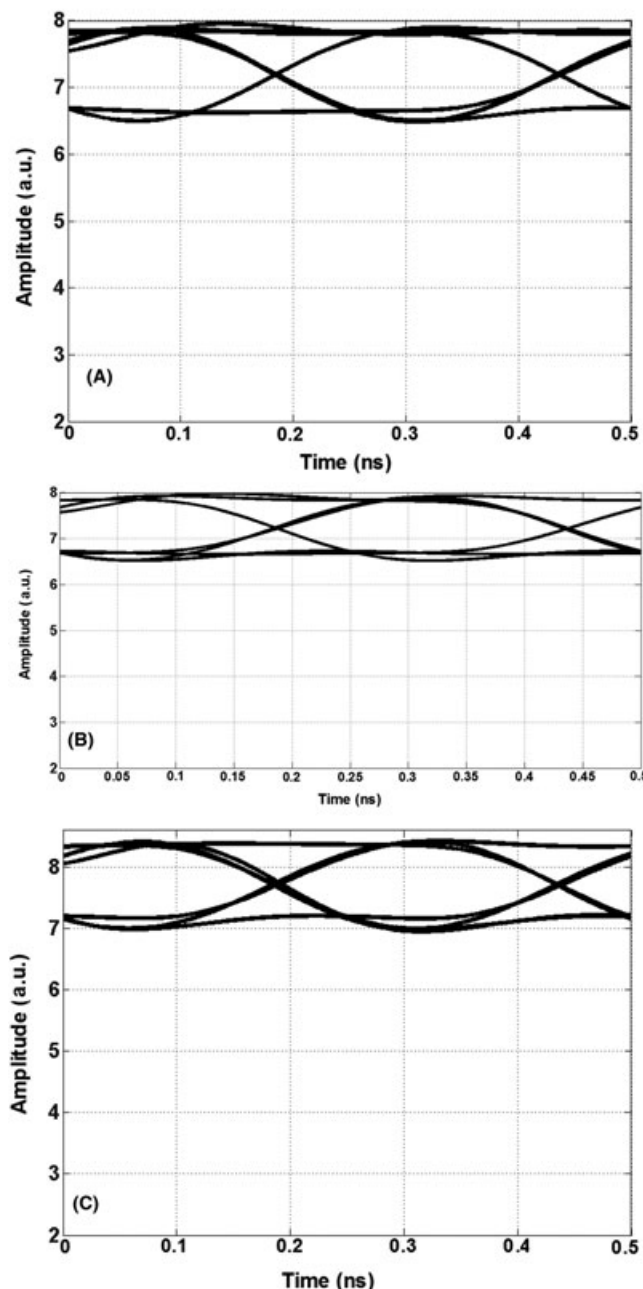


FIGURE 17 Eye diagram for the bias current of A, 15.2 mA; B, 15.25 mA; and C, 16 mA

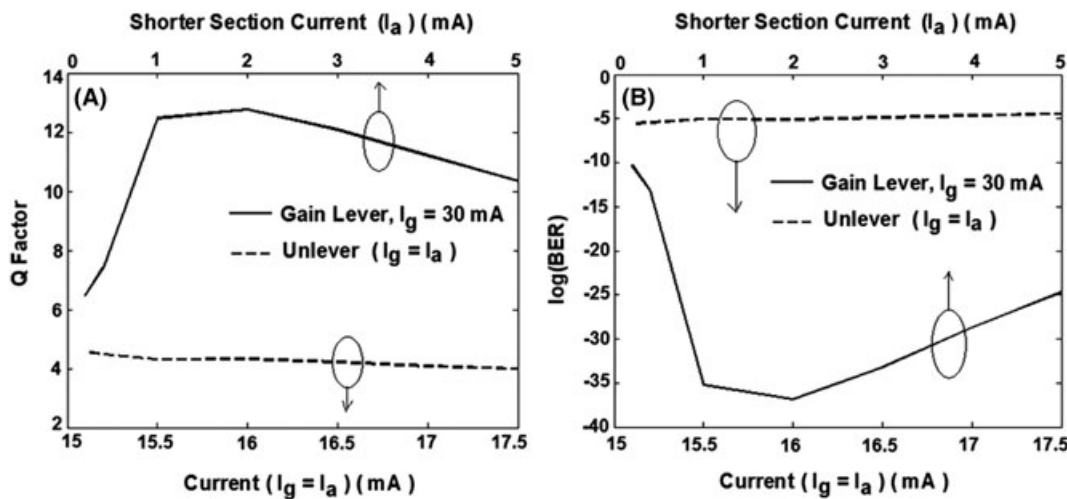


FIGURE 18 A, Variation of Q factor and B, bit error rate with current

to decrease for increasing bias current and is also low corresponding to unlevered condition. The performance of gain-levered diode indicates its suitability for optical transmitter in the digital fiber link.

The variation in Q factor and bit error rate with different modulation current magnitude of the NRZ pulse is evaluated and plotted. The longer and shorter section bias currents are fixed as 30 and 2 mA, respectively. Fiber length and transmission bit rate are fixed as constants for this analysis. The modulation current is varied from 0.5 to $5 I_{ath}$. This result is shown in Figure 19, which indicates an increase in Q factor and decrease in bit error rate with increasing modulation current. The value of Q factor is found to increase with increasing modulation current. A maximum Q factor of 11 and minimum bit error rate of 10^{-28} are obtained for a modulation current of $5 I_{ath}$. However, the value of the Q factor can be further improved by increasing the modulation current beyond $5 I_{ath}$. But the increase in modulation current increases the intensity of bit level "1." The difference between the photon population for bit level 0 and 1 is also high along with increased chirp in the device.⁷ Hence, the modulation current is limited to $5 I_{ath}$ in our analysis.

The performance of optical link with the effect of fiber length in the range of 1 to 80 km is investigated. The transmission bit rate, shorter section and longer section current, and magnitude of modulation current are held as constant in this simulation. The effect of fiber length on the height of the eye opening is calculated for both gain-levered and unlevered laser diode-based links and compared (Figure 20). The eye height is found to decrease with increasing fiber length as expected. The eye height for gain-levered laser diode-based fiber link is 2 times higher than the unlevered laser diode-based fiber link at 10 km. It is inferred that the gain-levered laser diode-based fiber link display better performance than that of conventional laser link under high bit rate digital modulation.

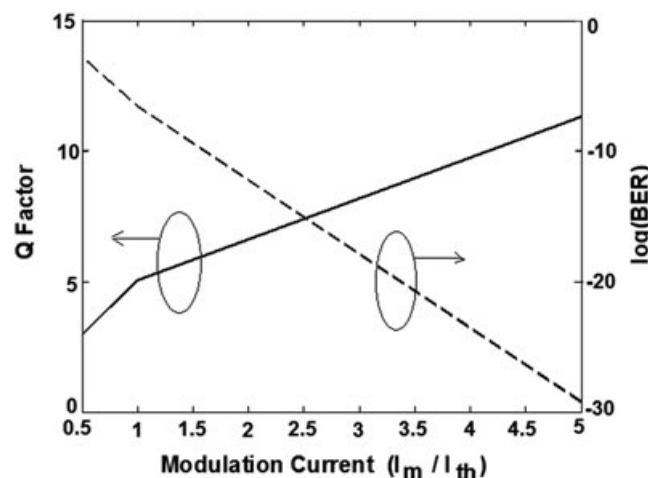


FIGURE 19 Variation of Q factor and bit error rate with modulation current

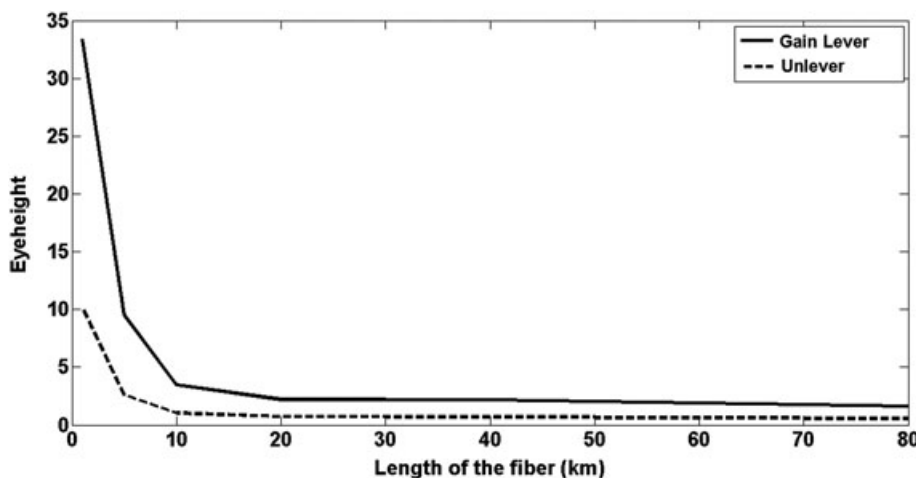


FIGURE 20 Eye height variation with length of the fiber

4 | CONCLUSION

The performance of single-mode fiber link incorporating 1.3- μm gain-levered laser diode-based transmitter is analyzed under high bit rate NRZ digital modulation. The gain-levered laser diode is modeled by rate equations and single-mode fiber is analyzed by its transfer function. The performance of gain-levered laser diode is evaluated in terms of slope efficiency, ER, eye diagram, and Q factor, and the results are compared with unlevered laser diode. The bias current, modulation current, bit rate, and fiber length are varied to analyze the performance of the fiber link. An improvement in ER of 12 dB is obtained for gain-levered laser diode with the longer section and currents of 30 and 0.5 mA, respectively. The Q factor of the received signal decreases with the increase in bit rate and is found to increase with increasing modulation current. A maximum Q factor of 11 is obtained for a modulation current of 5 mA in the gain-levered laser diode. An improvement in Q factor of 8 and 5 at 1 and 10 Gbps is obtained for gain-levered laser diode when compared to normal laser diode. The numerical simulation predicts that gain-levered laser diode-based fiber optic link performs better than unlevered laser diode in terms of pulse current magnitude, data rate, and Q factor.

ORCID

S. Piramasubramanian <http://orcid.org/0000-0002-3645-6697>

REFERENCES

1. Kaiser G. *Optical Fiber Communications*. New Delhi: Tata McGraw-Hill; 2008.
2. Agrawal GP. *Fiber-Optic Communications Systems*. New York: Wiley; 2010.
3. Ahmed MF. Influence of transmission bit rate on performance of optical fiber communication systems with direct modulation of laser diodes. *J Phys D Appl Phys*. 2009;42:185104(18):185104.
4. Mahmoud SWZ. Influence of gain suppression on static and dynamic characteristics of laser diodes under digital modulation. *Egypt J Solids*. 2007;30(2):237-251.
5. ahmed M, Yamada M, Mahmoud SWZ. Analysis of semiconductor laser dynamics under gigabit rate modulation. *J Appl Phys*. 2007;101(3):033119.
6. Ahmed M, Yamada M. Effect of intensity noise of semiconductor lasers on the digital modulation characteristics and the bit error rate of optical communication. *J Appl Phys*. 2008;104(1):013104.
7. Ahmed M, Mahmoud SWZ, Mahmoud AA. Comparative study on modulation dynamic characteristics of laser diodes using RZ and NRZ bit formats. *Int J Numer Model*. 2014;27:138-152.
8. Alshahriel A, Mahmoud SWZ. Multimode modeling of digital modulation in nearly single-mode semiconductor lasers. *Phys Wave Phenom*. 2016;24(2):114-123.
9. Balasubramanian K, Ganesh Madhan M. Simulation of thermal effects in laser diode and its impact on high speed fiber optic link. *J High Speed Networks*. 2010;17(4):175-184.

10. Pocha MD, Goddard LL, Bond TC, et al. Electrical and optical gain lever effects in InGaAs double quantum-well diode lasers. *IEEE J Quantum Electron.* 2007;43(10):860-868.
11. Ganesh Madhan M, Vaya PR, Gunasekaran N. Effect of source and load resistance on the performance of Bistable lasers. *IEEE Photon Technol Lett.* 2000;12(4):380-382.
12. Uenohara H, Takahashi R, Kawamura Y, Iwamura H. Static and dynamic response of multiple-quantum-well voltage-controlled bistable laser diodes. *IEEE J Quantum Electron.* 1996;32(5):873-883.
13. Vahala KJ, Newkirk MA, Chen TR. The optical gain lever: a novel gain mechanism in the direct modulation of quantum well semiconductor lasers. *Appl Phys Lett.* 1989;54(25):2506-2508.
14. Moore N, Lau KY. Ultrahigh efficiency microwave signal transmission using tandem-contact single quantum well GaAlAs lasers. *Appl Phys Lett.* 1989;55(10):936-938.
15. Seltzer CP, Westbrook LD, Wickes HJ. The gain-lever effect in InGaAsP/InP multiple quantum well lasers. *J Lightwave Technol.* 1995;13(2):283-289.
16. Westbrook LD, Seltzer CP. Reduced intermodulation-free dynamic range in gain-lever lasers. *Electron Lett.* 1993;29(5):488-489.
17. Rana F, Manolatou C, Schubert MF. Tapered cavities for high-modulation- efficiency and low-distortion semiconductor lasers. *IEEE J Quantum Electron.* 2007;43(11):1083-1087.
18. Naderi NA, Li Y, Dziak C, Xin YC, Kovanis V, Lester LF. Quantum dot gain-lever diode. Proc. IEEE LEOS Annual Meeting, Montreal, QC, Canada, 2006; 52-53.
19. Piramasubramanian S, Ganesh Madhan M. A novel distortion reduction scheme for multiple quantum well gain lever laser diodes. *J Opt.* 2013;15(5):055501.
20. Piramasubramanian S, Ganesh Madhan M. Simultaneous reduction of IMD3 and IMD5 in bisection laser diode by feedback second harmonic injection. *Optics Comm.* 2014;328:151-160.
21. Thomas R, Briglin D, Krysa AB, Smowton PM. Mechanism for enhanced wavelength tuning in gain-levered InP quantum dot lasers. *IET Optoelectron.* 2015;62:1-4.
22. Sarraute J-M, Schires K, LaRochelle S, Grillot F. Enhancement of the modulation dynamics of an optically injection-locked semiconductor laser using gain lever. *IEEE J Selected Topics Quantum Electron.* 2015;21(6): 1801408.
23. Vuorinen K, Gaffiot F, Jacquemod G. Modeling single-mode lasers and standard single-mode fibers using a hardware description language. *IEEE Photon Technol Lett.* 1997;9(6):824-826.
24. Fernando XN, Sesay AB. Adaptive asymmetric linearization of radio over fiber links for wireless access. *IEEE Trans Vehicular Technol.* 2002;51(6):1576-1586.

How to cite this article: Piramasubramanian S, Ganesh Madhan M, Sindhuja A. Performance analysis of a digital fiber optic link incorporating gain-levered laser diode transmitter. *Int J Numer Model.* 2018;e2321. <https://doi.org/10.1002/jnm.2321>

Numerical analysis of extinction ratio improvement in gain lever laser diode

S. PIRAMASUBRAMANIAN*, M. GANESH MADHAN

Department of Electronics Engineering, Madras Institute of Technology Campus, Anna University, Chennai, India, 600 044

In this paper, extinction ratio improvement is predicted in 1.3 μm, bisection multiple quantum well laser diode employing gain lever effect. Two section laser diode is modeled by rate equations and numerically solved by fourth order Runge - Kutta method. The optical power variation with longer and shorter section currents are analyzed. Slope efficiency is evaluated for different shorter section currents at constant current injection in the longer section of the bisection laser diode. Higher slope efficiency of the gain lever case than unlever condition is utilized for extinction ratio improvement in the bisection laser diode. The effect of shorter section current on extinction ratio is analyzed. Extinction ratio is calculated for gain lever and unlever conditions for various shorter section currents. For a longer section biased of 35 mA, an extinction ratio improvement of 10.53 dB is obtained for an electrical pulse injection of 4 mA amplitude biased at $2I_{\text{ath}}$ at the shorter section.

(Received October 29, 2015; accepted June 7, 2017)

Keywords: Bi section MQW laser, Gain lever effect, Extinction ratio, Optical switching, Rate equations, Numerical simulation

1. Introduction

Large extinction ratio is one of the important requirement for optical transmitters in high speed digital optical links and regenerators, to improve the link performance [1] - [5]. Extinction ratio improvement in laser diodes subsequently enhances the eye opening, leads to better BER characteristics in directly modulated optical link [5]. Two section laser diode can exhibit optical bistability, gain lever and self pulsation phenomenon [6] - [10]. Gain lever effect, is a mechanism investigated to improve the modulation efficiency in two or multiple section laser diodes [11]-[15]. Gain lever effect was analyzed by Vahala et al. [9] in two section quantum well laser. The detailed rate equation analysis of gain lever single quantum well GaAlAs laser diode was provided by Moore et al [10]. Gain lever effect in bulk and multiple quantum well laser was demonstrated by Seltzer et al [11]. For a laser diode, to exhibit gain lever effect, the active region has to be divided in to two unequal sections. RF current is given to the shorter section of laser diode and the larger section is dc biased at high gain level [11] - [15]. Gain lever phenomenon results due to the non linear transfer characteristic of laser diode. In this work, gain lever effect in bisection laser diode is utilized for extinction ratio enhancement, by providing electrical pulse instead of RF current.

2. Rate equation model for gain lever effect

Gain lever is a measure of slope efficiency improvement in the laser diode. The slope efficiency of

two section laser diode is higher than the slope efficiency of unlevered laser diode [12]. The structure of two section laser diode is provided in Fig. 1. However detailed description of device structure can be obtained in ref [7]. The longer (a_1) and shorter (a_2) sections are electrically isolated and optically connected. Electrical pulse along with bias current (I_a) is applied to the shorter section, dc current (I_g) is applied to longer section. At lasing threshold, total optical gain overcomes the cavity loss. An increase in gain in one section of the laser diode allows equal decrease in gain in other section [9]. When current in shorter section I_a decreases, circulating optical power decreases, which results in increase of carrier density N_g in other section. The relation between optical gain and carrier density is sub linear [9]. Hence a small amount of increase in carrier density N_g results in AM efficiency enhancement in such multi section laser diodes [9] - [15]. Current pulses representing digital data is given to the shorter section (a_2) of laser diode and the larger section (a_1) is DC biased at high gain level (Fig. 1).

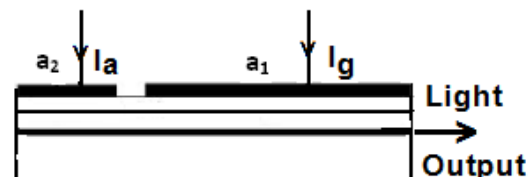


Fig. 1. Bi section gain lever laser diode

The gain lever laser diode is modelled by using rate equations as given below [8,9]

$$\frac{dN_g}{dt} = \frac{I_g}{a_1 q V} - BN_g^2 - v_{gg}(N_g - N_{og})S(1 - \epsilon S) - \frac{N_g}{\tau_{nr}} \quad (1)$$

$$\frac{dN_a}{dt} = \frac{I_a}{a_2 q V} - BN_a^2 - v_{gg} g_a (N_a - N_{oa}) S (1 - e^{-S}) - \frac{N_a}{\tau_{nr}} \quad (2)$$

$$\frac{dS}{dt} = -\frac{S}{\tau_p} + [a_1 v_{gg} g_g (N_g - N_{og}) + a_2 v_{gg} g_a (N_a - N_{oa})] \Gamma S (1 - e^{-S}) + \Gamma \beta B (a_1 N_g^2 + a_2 N_a^2) \quad (3)$$

Where ' N_g ', ' N_a ' are carrier densities in section length a_1 and a_2 , respectively. The total photon density is 'S' and the total volume of active region is denoted as 'V'. Optical power output is calculated from photon density by the following equation

$$P = \frac{chV\eta S}{\Gamma \tau_p \lambda} \quad (4)$$

The extinction ratio is defined as the ratio of power required to transmit '1' bit (P_1) to the power required to transmit '0' bit (P_0) [1]. The extinction ratio (ER) is

$$ER(dB) = 10 \log\left(\frac{P_1}{P_0}\right) \quad (5)$$

3. Simulation results

The rate equations (1) - (3) are numerically solved by using fourth order Runge-Kutta method to obtain its static characteristics in MATLAB®. All the parameters used in this simulation are similar to that of ref [7]. For static conditions, left hand side of equations (1),(2) and (3) are made equal to zero and the solutions are obtained for carrier densities and photon density, with respect to applied injection currents in the respective sections.

The optical power is calculated by the equation (4) with fixed shorter section current of 3 mA and unpumped conditions ($I_a = 0$). The longer section current is varied from 0 to 150 mA and optical power variation is shown in Fig. 2. The longer section threshold current of 54 mA is obtained when the shorter section is not injected with any current. This result matches well with the experimental result of Uenohara et al [7] and verifies our simulation results for the same device structure used in our analysis.

The calculation for power with shorter section current varied from 0 to 15mA at constant longer section bias of 15 mA, 25 mA, 35 mA and 45 mA is shown in Fig. 3. The longer section current should be higher than the shorter section current to exhibit gain lever effect. The longer section currents are assumed in the range of 15 mA to 45 mA, which satisfies this condition. However, any set of current values ($I_g > I_a$) may be chosen for this analysis. The optical power variation for shorter section current indicates slope efficiency increment for increase in longer section current. The optical power is found to increase with increase in longer section current. A decrease in threshold current is predicted for increase in longer section current.

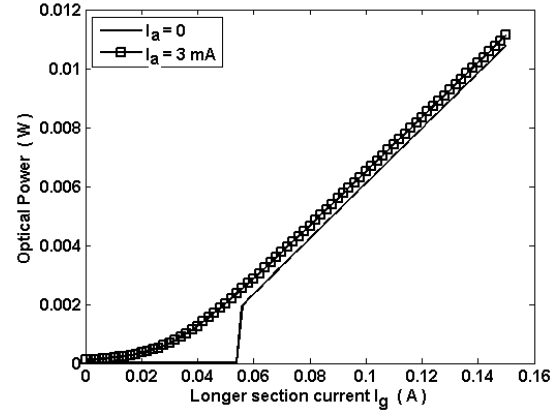


Fig. 2. Optical power variation with longer section current

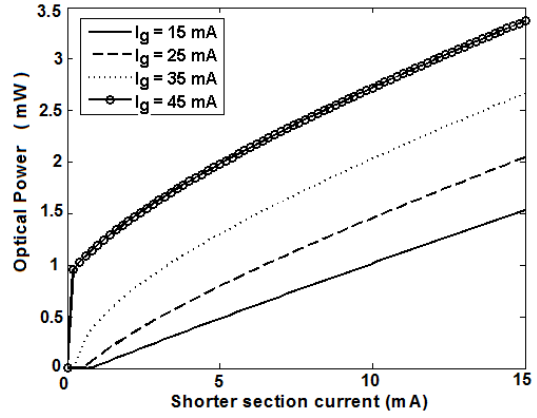


Fig. 3. Optical power variation with shorter section current

The optical power variation with shorter section current is plotted for 35 mA longer section current (I_g) to evaluate the slope efficiency (Fig. 4a). A threshold current of 0.4 mA is obtained in this case. The calculations are repeated for unlever laser diode where both of the sections are shorted together ($I_g = I_a$). The slope efficiency is evaluated and plotted as shown in Fig. 4b. The shorter section bias current is varied from $2I_{ath}$ to $10I_{ath}$ for a 4 mA pulse. A maximum slope efficiency of 0.22 (mW / mA) is obtained for gain lever case at a bias of $2I_{ath}$. The slope efficiency is found to reduce for increase in bias current. The slope efficiency is 0.08 (mW / mA) for unlever case under same bias conditions. A similar trend is observed for other bias currents too. It is evident that the slope efficiency of bisection laser diode is higher than the normal laser (unlever) diode.

The electrical pulse input and corresponding optical outputs are shown in Fig. 5, for gain lever condition. The electrical pulse is biased at 0.8 mA ($2I_{ath}$) with 4 mA amplitude. The longer section is biased with 35 mA constant current. The output optical power is switched from 0.11 mW to 1.37 mW. The extinction ratio is calculated by using equation (5) and 11.11 dB is obtained under this condition.

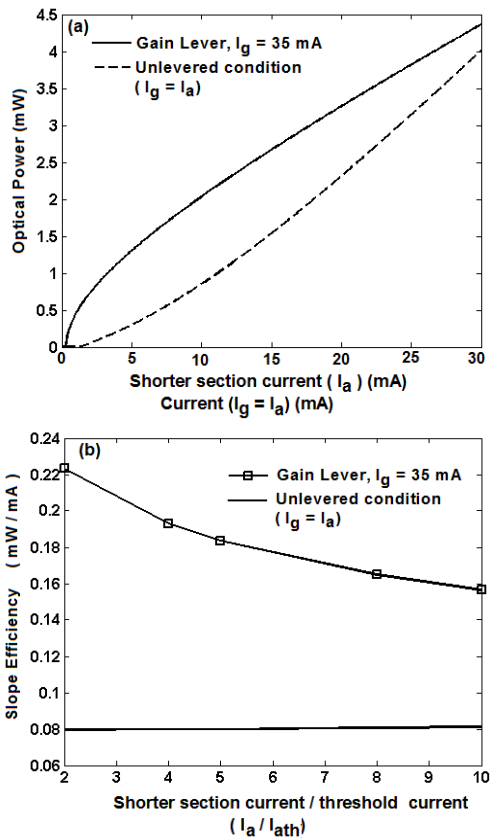


Fig. 4. (a) Static characteristics of gain lever ($I_g = 35$ mA) and unlevered laser diode ($I_a = I_g$). (b) slope efficiency variation with current

The analysis is repeated for unlever case (Fig. 6). The extinction ratio improvement (dB) is calculated as the difference between the extinction ratio of laser diode under gain lever condition to the extinction ratio of the device under normal unlever mode. The characteristics of bisection laser diode under unlever condition is analyzed by shorting both of the electrodes [9] - [12]. In the simulation, equal currents are provided to the both the sections ($I_g = I_a$) to get the similar results. Hence, both the sections are biased at 17.9 mA with 2 mA magnitude ($I_g = I_a$) (Fig. 6). This is equal to the 4 mA pulse (I_a , 0.8 mA to 4.8 mA) provided to the shorter section and 35 mA (I_g) current injection at the longer section.

The optical power output is switched from 1.99 mW to 2.27 mW under unlever case and extinction ratio is 0.572 dB. A 10.53 dB improvement in extinction ratio is predicted under this case. The average transmitted power is high in this condition. Hence it is predicted that the gain lever laser diode can exhibit higher extinction ratio than the conventional laser diode with low average transmitted power.

The analysis is repeated for other value of shorter section currents and extinction ratio are evaluated for gain lever and unlever laser diode (Fig. 7). The extinction ratio is found to decreases for increase in bias current. This value is almost constant for unlever laser

diode. It is observed that the extinction ratio is higher for gain lever than unlever condition.

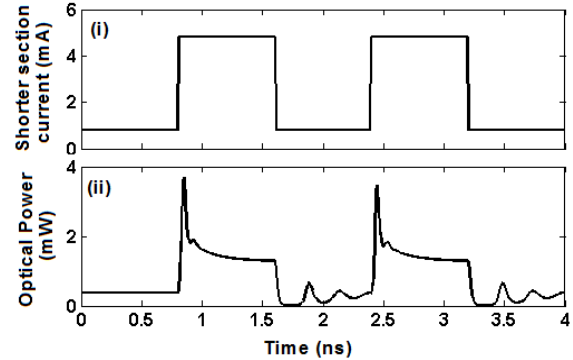


Fig. 5. (i) input electrical pulse for gain lever laser diode
(ii)output optical power. The longer section current $I_g = 35$ mA

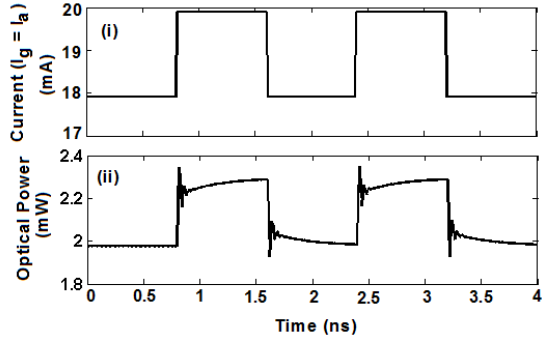


Fig. 6. (i) input electrical pulse for unlever laser diode
(ii)output optical power

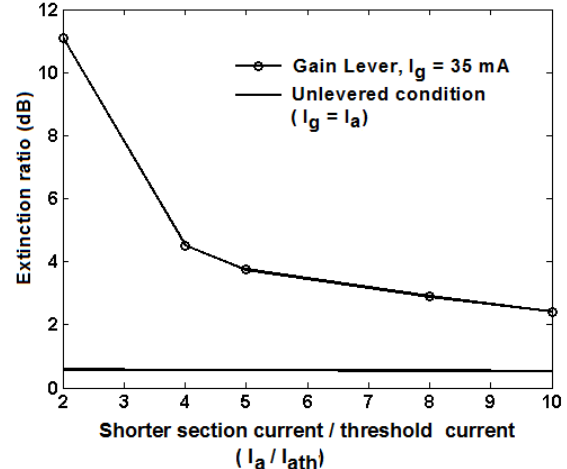


Fig. 7. Extinction ratio variation with shorter section current

The improvement in extinction ratio is plotted in Fig. 8a under various shorter section currents. The extinction ratio improvement is calculated with respect to unlevered laser diode, where both the electrodes are shorted together ($I_g = I_a$).

The extinction ratio is found to reduce for increase in shorter section bias current. The extinction ratio improvement for different longer section currents are evaluated and plotted (Fig. 8b). The longer section current is varied from 5 mA to 35 mA for this analysis. The shorter section current is fixed as twice of shorter section threshold current ($2I_{\text{ath}}$). The extinction ratio is found to increase for increase in longer section bias current. The analysis is repeated for the shorter section currents of $4 I_{\text{ath}}$ and $5 I_{\text{ath}}$ respectively. A maximum extinction ratio of 10.53 dB is obtained when the longer section is biased at 35 mA. It is predicted that gain lever effect can be utilized to improve the extinction ratio in bisection laser diodes.

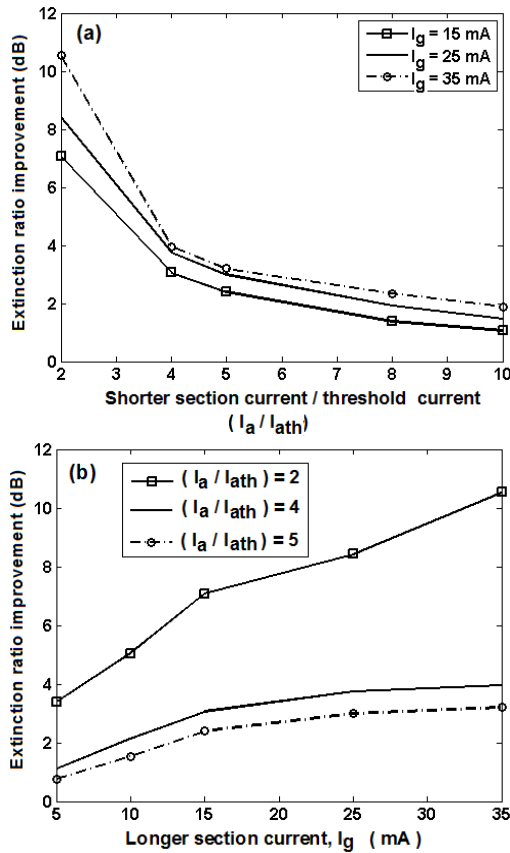


Fig. 8. Extinction ratio improvement with a) shorter section current and b) longer section current

4. Conclusions

In this work, extinction ratio improvement is predicted in $1.3 \mu\text{m}$, bisection multiple quantum well laser diode employing gain lever effect. The rate equations are numerically solved in this simulation.

The effect of shorter section current on extinction ratio is analyzed. An extinction ratio improvement of 10.53 dB is obtained for an electrical pulse injection of 4 mA amplitude biased at $2I_{\text{ath}}$ to the shorter section, for a longer section bias of 35 mA. It is predicted that gain lever laser diode is found useful for high speed optical communication, optical switching and optical signal processing applications.

References

- [1] Carmina del Río Campos, Paloma R. Horche, Alfredo Martín Minguez, Optics Communications **283**(15), 3058 (2010).
- [2] Mingshan Zhao, Geert Morthier, Roel Baets, IEEE Photonics Technology Letters **14**(7), 992 (2002).
- [3] Chun-Hyung Cho, Jongseong Kim, Hyuk-Kee Sung, Journal of the Korean Physical Society **69**(5), 745 (2016).
- [4] Toshiya Sato, Naoto Yoshimoto, IEEE Journal of Lightwave Technology **25**(6), 1474 (2007).
- [5] Zhaoyang Hu, Marcelo Davanco, Daniel J. Blumenthal, IEEE Photonics Technology Letters **15**, 1419 (2003).
- [6] M. Ganesh Madhan, P. R.Vaya, N. Gunasekaran, IEEE Photonics Technology Letters **11**(6), 644 (1999).
- [7] Hiroyuki Uenohara, Ryo Takahashi, Yuichi Kawamura, Hidetoshi Iwamura, IEEE Journal of Quantum Electronics **32**(5), 873 (1996).
- [8] M. Ganesh Madhan, P. R.Vaya, N. Gunasekaran, IEEE Photonics Technology Letters **12**(4), 380 (2000).
- [9] K. J. Vahala, M. A. Newkirk, Applied Physics Letters **54**(25), 2506 (1989).
- [10] N. Moore, K. Y. Lau, Applied Physics Letters **55**(10), 936 (1989).
- [11] C. P. Seltzer, L. D. Westbrook, H. J. Wicks, IEEE Journal of Lightwave Technology **13**(2), 283 (1995).
- [12] M. D. Pocha, L. L. Goddard, T. C. Bond, R. J. Nikolic, S. P. Vernon, J. S. Kallman, E. M. Behymer, IEEE Journal of Quantum Electronics **43**(10), 860 (2007).
- [13] Robert Thomas, Daniel Briglin, Andrey B. Krysa, Peter Michael Smowton, IET Optoelectronics, **62**, 1 (2015).
- [14] Jean-Maxime Sarraute, Kevin Schires, Sophie LaRochelle, Frederic Grillot, IEEE Journal of Selected Topics in Quantum Electronics **21**(6), 1801408 (2015).
- [15] David A. Murrell, Ravi Raghunathan, Luke F. Lester, IEEE Photonics Technology Letters **27**(13), 1441 (2015).

*Corresponding author: spsnanthan@gmail.com



Numerical analysis of distortion characteristics of heterojunction bipolar transistor laser

S. Piramasubramanian*, M. Ganesh Madhan*, Jyothsna Nagella, G. Dhanapriya

Department of Electronics Engineering, Madras Institute of Technology Campus, Anna University, Chennai, India



ARTICLE INFO

Article history:

Received 29 June 2015

Received in revised form

25 August 2015

Accepted 30 August 2015

Available online 15 September 2015

Keywords:

Transistor laser

Second harmonic distortion (2HD)

Third order intermodulation distortion (IMD3)

Numerical simulation
rate equations

ABSTRACT

Numerical analysis of harmonic and third order intermodulation distortion of transistor laser is presented in this paper. The three level rate equations are numerically solved to determine the modulation and distortion characteristics. DC and AC analysis on the device are carried out to determine its power-current and frequency response characteristics. Further, the effects of quantum well recombination time and electron capture time in the quantum well, on the modulation depth and distortion characteristics are examined. It is observed that the threshold current density of the device decreases with increasing electron lifetime, which coincides with earlier findings. Also, the magnitude of harmonic distortion and intermodulation products are found to reduce with increasing current density and with a reduction of spontaneous emission recombination lifetime. However, an increase of electron capture time improves the distortion performance. A maximum modulation depth of 18.42 dB is obtained for 50 ps spontaneous emission life time and 1 ps electron capture time, for 2.4 GHz frequency at a current density of $2J_{th}$. A minimum second harmonic distortion magnitude of -66.8 dBc is predicted for 50 ps spontaneous emission life time and 1 ps electron capture time for 2.4 GHz frequency, at a current density of $7J_{th}$. Similarly, a minimum third order intermodulation distortion of -83.93 dBc is obtained for 150 ps spontaneous emission life time and 5 ps electron capture time under similar biasing conditions.

© 2015 Elsevier B.V. All rights reserved.

1. Introduction

The transistor laser is a heterojunction bipolar transistor (using different materials for the base and emitter regions) that employs multiple quantum wells in its base region that causes emissions of infrared light [1–12]. The inclusion of quantum wells in the active region (base) increases the efficiency of light generation. A reflective cavity formed in the base region provides the necessary condition for lasing. The quantum well in the base region captures electrons that would normally be sent out through the collector output. These electrons then undergo a process of radiative recombination, during which electrons and positively charged holes recombine in the base and photons are released through stimulated emission thereby generating coherent light. Since, the device possess transistor features with laser output, it has high potential for optical switching and communication applications. The transistor laser was reported by Holonyak and Feng in 2006 [1]. Since then a number of works have been reported on the modulation performance and bandwidth [2,3]. Parallel to the development of

devices, mathematical models for the analysis of transistor lasers have also been reported. As, the transistor laser is basically a three terminal bipolar transistor, the theories well known for transistor analysis, have been introduced for this device also. The charge control model for transistor lasers is quite popular and used for analysis. As the transistor laser has multiple quantum wells in the base region, detailed models for carrier transport in quantum well are also introduced for this device [4]. Hence, any model for transistor laser incorporates quantum well effects, generation-recombination mechanism in the active region and charge control effects. From, the literature, it is observed that a number of authors have reported on the static and dynamic characteristics of transistor laser [4–6]. However, distortion analyses have not been extensively carried out. Only the report of Then et al. [3] investigates about the distortion reduction in transistor lasers, by using the collector current feedback. In their paper, third order intermodulation components are suppressed by the electrical signal available in the collector which is fed back in to the base. However, their analysis has not included the quantum well effects such as electron capture time and spontaneous emission life time in quantum wells. A reduction of 18.2 dB in the electrical output and 8.4 dB in optical output are reported for IMD3 components [3]. Zang et al. [4] have investigated the effect of electron capture time on the modulation response of the device. The charging process of

* Corresponding authors.

E-mail addresses: spirama@annauniv.edu (S. Piramasubramanian),
mganesh@annauniv.edu (M. Ganesh Madhan).

base-emitter (BE) junction capacitance, base diffusion capacitance and base stimulated recombination time are found to be the main sources of nonlinearity in the transistor laser [3]. Hence, an analysis on the impact of spontaneous emission lifetime (τ_{qw}) and electron capture time (τ_{cap}) in quantum well on nonlinear distortion in transistor laser becomes important.

It is well known that for analog signal transmission in Radio over Fiber (RoF) applications, linearity and modulation response are important for laser device [13–20]. The performance of RoF link mainly depends on modulation process, fiber and photo detector. The non linearity of laser diode is a key parameter in direct modulation, that determines the overall performance of the link along with gain, noise figure and dynamic range. The dynamic range of the analog optical link cannot be enhanced, even by adding amplifiers before and after RoF link [13].

Third order intermodulation distortion (IMD3) of the laser diode or optical modulator determines the Spurious Free Dynamic Range (SFDR) of the fiber link. Hence, IMD3 of the laser diode is reduced by schemes such as feed forward, feedback and pre distortion circuits. The SFDR upto 120 dB Hz^{2/3} have been reported earlier for directly modulated link [13]. This value of dynamic range is obtained for operating frequencies lesser than the relaxation oscillation frequency of the laser diode [17]. The SFDR value reduces when the operating frequency is close to the resonant frequency.

In this paper, we have numerically solved the rate equations pertaining to the transistor laser [4] and obtained the power characteristics and frequency response as a first step. The results are found to match with the literature, thereby validating our approach. Based on the same model, we proceed further to investigate the effect of capture time and spontaneous emission recombination time on the modulation depth, second harmonic and third order inter modulation distortion performance of the device. The effect of injected carrier density on the distortion performance is also determined. A comparison of the performance of the distortion characteristics of laser diode and transistor laser is provided as a Table 1.

This analysis predicts an IMD3 value of -83.9 dBc for a particular value of τ_{qw} , τ_{cap} , which is better than previous report [3]. Further it is slightly better than the report of Yabre et al. [19] for diode laser. Hence, it is concluded that the present analysis provide conditions for better IMD3 performance.

Also the modulation bandwidth of the transistor laser is

reported as 13.5 GHz in experiment and 44 GHz in theory [4]. The value of modulation bandwidth of transistor laser is similar to that of diode laser, and hence has potential to replace diode laser in many analog applications. The IMD3 reduction in transistor laser can also be realized by collector current feedback [3] which is not possible in conventional laser diodes and this also reduces the complexity of the system.

2. Transistor laser model

The schematic of the transistor laser and the carrier injection process in the quantum well base region is illustrated in Fig. 1.

The currents are similar to that of a simple transistor and the base current is responsible for light generation in the device. The operation of the device requires base-emitter junction to be forward biased and collector junction to be reverse biased.

We have used rate used the rate equation model which is similar to the work of Zhang et al. [4]. The model incorporates charge control effects and similar to the carrier transport effect for quantum well laser diodes [4]. In their approach, characteristics of transistor laser is analyzed by varying the spontaneous recombination time in the quantum well (τ_{qw}) and electron capture time (τ_{cap}). We have adopted the same model in our analysis to find the effect of life time on nonlinear distortion.

The spontaneous recombination time (τ_{qw}) and stimulated emission life time determine the threshold current of the device. The value of the life times τ_{qw} and electron capture time τ_{cap} depend on QW geometry factor, which is depend on QW position and width in the base of the transistor laser [4]. In a quantum well, electron capture time (τ_{cap}) increases with effective barrier height and carrier density of confined states. In narrow quantum well laser diode, smaller effective barrier height provides higher value of electron capture time. This time constant also depends on the quantum well thickness. Threshold carrier density and gain compression coefficient are found to increase for increase in capture time. The rate equations with charge control model is used for the analysis of transistor laser [4].

$$\frac{dn(t)}{dt} = \frac{\nu Q_b(t)}{\tau_{\text{cap}}} - \frac{n(t)}{\tau_{\text{qw}}} - \Omega[n(t) - n_{\text{nom}}]N_p(t) \quad (1)$$

Table 1
Comparison of third order intermodulation distortion (IMD3) in laser diode and laser transistor.

Authors	Features	Remarks
Laser Diode		
Yabre et al. [19]	Second and third order intermodulation(IMD3) are investigated in injection locked semiconductor laser diode. The IMD3 magnitudes of -80 dBc at 500 MHz, -60 dBc at 1 GHz and -50 dBc at 2 GHz are reported	Additional laser diode is required for injection locking scheme
Yan-Tae Moon et al. [20]	Intermodulation distortion is reduced in Distributed Feedback laser diode by using predistortion circuit. IMD3 is reduced to -60 dBc for the two tone input of 2.2 GHz and 2.201 GHz	Predistortion circuit is to be included in the system and it limits the operating bandwidth
Cox et al. [13]	Limits of analog optical system is analyzed for directly modulated optical link. The spur free dynamic range decreases if the operating frequency is close to the resonance frequency of the laser diode	Electronic linearization is required to reduce second harmonic distortion in directly modulated CATV system
Way et al. [16]	Dynamic range requirement for GSM microcell and picocells are analyzed	Dynamic range of 40–55 dB is required for picocell and 80–90 dB is required for microcell applications
Transistor Laser		
Then et al. [3]	IMD3 is reduced in transistor laser with collector current feedback. The two tone frequencies are 20 MHz and 20.05 MHz	IMD3 of -58.3 dBc is obtained in electrical output and -48.7 dBc is obtained in optical output with collector current feedback.
In this report	Second harmonic distortion and third order intermodulation distortion are analyzed for different spontaneous recombination time and electron capture time in QW of the base of the transistor laser	IMD3 of -83.9 dBc is predicted for the 150 ps spontaneous emission life time and 5 ps electron capture time.

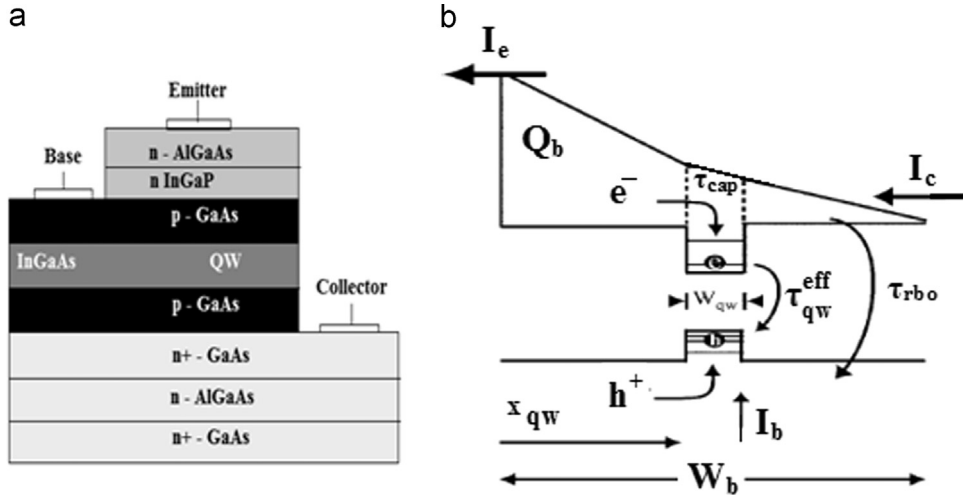


Fig. 1. Transistor laser (a) structure (b) charge control model [4].

$$\frac{dQ_b(t)}{dt} = \frac{J(t)}{q} - \frac{Q_b(t)}{\tau_{rb}} \quad (2)$$

$$\frac{dN_p(t)}{dt} = \Omega[n(t) - n_{nom}]N_p(t) + \frac{\theta n(t)}{\tau_{qw}} - \frac{N_p(t)}{\tau_p} \quad (3)$$

$$\frac{1}{\tau_{rb}} = \frac{1 - \nu}{\tau_{rb0}} + \frac{\nu}{\tau_{cap}} \quad (4)$$

where, $n(t)$ represents the carrier density, $\frac{\nu Q_b(t)}{\tau_{cap}}$ denotes the base charge captured by the quantum well and $\frac{n(t)}{\tau_{qw}}$ represents electron spontaneous recombination rate inside the quantum well. $\Omega[n(t) - n_{nom}]N_p(t)$ denotes the stimulated emission term. A linear variation of gain with carrier density is assumed for the analysis. The equation for base charge is related to the injected carrier density through the term $\frac{\nu Q_b(t)}{\tau_{cap}}$. The factor θ represents the fraction of spontaneous emission that is coupled to the cavity mode and photon loss is given by $\frac{N_p(t)}{\tau_p}$. A charge control model is used to describe the dynamics of the minority carrier charge stored in the base.

3. Simulation results

3.1. DC characteristics

The rate Eqs. (1)–(3) are numerically solved for static conditions by setting $\frac{dn(t)}{dt} = 0$, $\frac{dQ_b(t)}{dt} = 0$ and $\frac{dN_p(t)}{dt} = 0$. A fourth order Runge–Kutta method is used to obtain the steady state solution of the electron, base charge and photon densities with respect to the injected base current density. This technique is sufficient for the analysis of rate equations. Zhang et al. have used similar method to solve the rate equations for the transistor laser [4]. All the parameters used in the analysis are provided in Table 2.

The analysis is repeated for different values of electron recombination time (τ_{qw}) and plotted in Fig. 2a. The electron capture time in the QW is fixed as 1 ps for this analysis. The results indicate photon density variations similar to that of conventional semiconductor lasers. Threshold current densities of 5000 (A/cm²) and 200 (A/cm²) are obtained for recombination times of 50 ps

Table 2
Model parameters and their values [4].

Parameter	Description	Value
ν	Quantum well geometry factor	0.05
τ_{cap}	Electron capture time in quantum well	1–5 ps
τ_{qw}	Recombination lifetime via spontaneous emission in quantum well	50–1000 ps
τ_{st}	Recombination lifetime via stimulated emission in quantum well	Variable, sec
τ_p	Photon lifetime	3.5 ps
Ω	Differential gain factor	0.5 cm ² /s
n_{nom}	Transparency electron density	10 ¹² cm ⁻²
θ	Fraction of spontaneous emission	Variable, Unit less
τ_{rb0}	Base charge bulk lifetime	150 ps
N	Electron density	Variable, cm ⁻²
N_p	Photon density	Variable, cm ⁻²
N_{p0}	Steady state photon density	Variable, cm ⁻²
Q_b	Base charge density	Variable, cm ⁻²
J	Current density	Variable, A cm ⁻²
J_{th}	Threshold current density	kAcm ⁻²

and 1000 ps respectively. As recombination time increases, the device starts lasing at lower current density itself.

Similar analysis is repeated for different values of electron capture time (τ_{cap}) for fixed value of electron recombination time ($\tau_{qw}=150$ ps) (Fig. 2b). Threshold current densities of 1890 (A/cm²) and 2500 (A/cm²) are obtained for electron capture times of 1 ps and 5 ps respectively. These results coincide with the findings of Zang et al. [4], thereby validating our simulation.

3.2. Large signal AC analysis

The frequency response of the transistor laser is analyzed by varying the base current frequency. The magnitude response (MR) is calculated by finding the difference between the maximum and minimum value of time varying photon density. In Fig. 3, the frequency response of the transistor laser is analyzed for different spontaneous emission time in the QW (τ_{qw}). The value of τ_{qw} is varied from 50 ps to 1000 ps. The base current density $J(t) = J_0 + J_{th} \sin(\omega t)$, is applied into the rate equations, where J_{th} is threshold current density. The dc term in the equation J_0 is fixed as $2J_{th}$. Threshold current densities (J_{th}) of 5000 (A/cm²) and 200 (A/cm²) are obtained for recombination times of 50 ps and

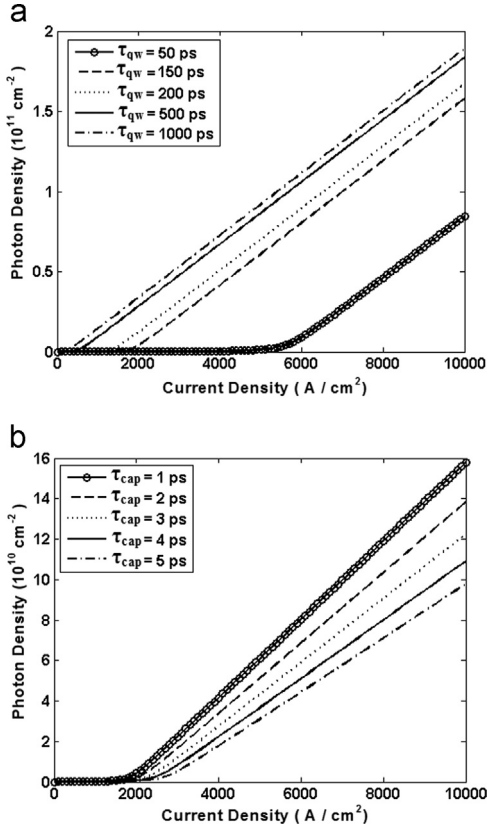


Fig. 2. Dependence of photon density on the base current density under (a) spontaneous emission time in QW. (b) electron capture time in QW.

1000 ps respectively. The frequency is varied from 100 MHz to 50 GHz.

The predicted resonant frequencies for $\tau_{\text{qw}} = 50$ ps and 1000 ps are 15 GHz and 2.5 GHz respectively. For $\tau_{\text{qw}} = 50$ ps, the magnitude response is nearly flat before rolling off at higher frequencies due to its higher threshold current density than 1000 ps. The threshold current density is low for 1000 ps spontaneous recombination time in the device. Hence, a different kind of frequency response is observed for this case. The 3 dB modulation bandwidth of the laser diode is inversely proportional to the life time. The predicted bandwidth is less than 10 GHz for $\tau_{\text{qw}} = 1000$ ps and $\tau_{\text{cap}} = 1$ ps. These results are in accordance with the reports of Zang et al. [4], and verify our simulation. Hence we proceed further to use the same model for investigating the distortion performance of the device, which is explained in the subsequent sections.

3.3. Analysis of modulation depth at 2.4 GHz

Transistor laser can be used an optical source in analog optical links due to its large bandwidth [4]. Modulation depth is an

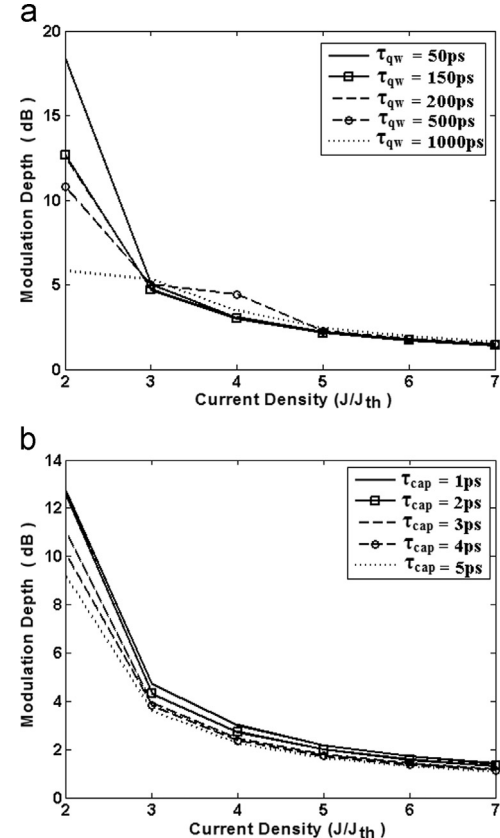


Fig. 4. Modulation depth dependence on current density (a) effect of τ_{qw} (b) effect of τ_{cap} .

important parameter for optical modulators which determines the overall link gain and signal to noise ratio in such links [13]. In this analysis, the modulation depth of transistor laser is determined with the effect of bias current density, spontaneous recombination life time and electron capture time, at 2.4 GHz RF signal injection. The choice of 2.4 GHz frequency is based on ISM and WLAN applications. Hence we investigate the performance of transistor laser for radio over fiber scheme for 2.4 GHz RF transport applications.

Modulation depth is evaluated from the maximum and minimum value of photon density under RF signal input. The base current density, $J(t) = J_0 + J_{\text{th}} \sin(\omega t)$ is substituted in the rate equation and the output photon density is evaluated. The DC component of current density (J_0) is varied from $2 J_{\text{th}}$ to $7 J_{\text{th}}$ and the modulation depth is evaluated and plotted in Fig. 4a. The electron capture time (τ_{cap}) is fixed as 1 ps for this analysis. The modulation depth is found to decrease for increase in current density and spontaneous emission life time. A maximum modulation depth of 18.42 dB is obtained for the spontaneous emission

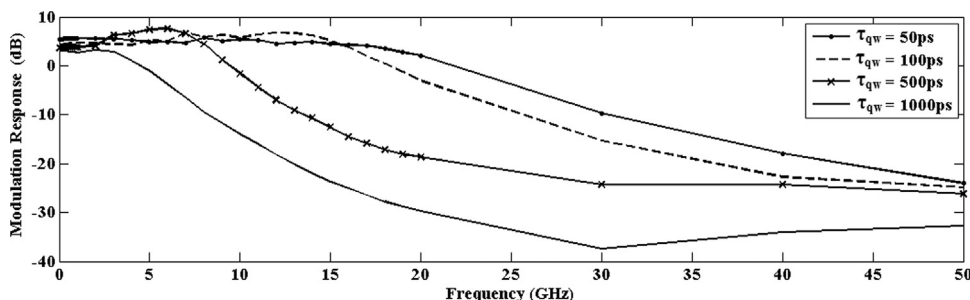


Fig. 3. Magnitude Response (MR) of Transistor Laser for different lifetimes (τ_{qw}).

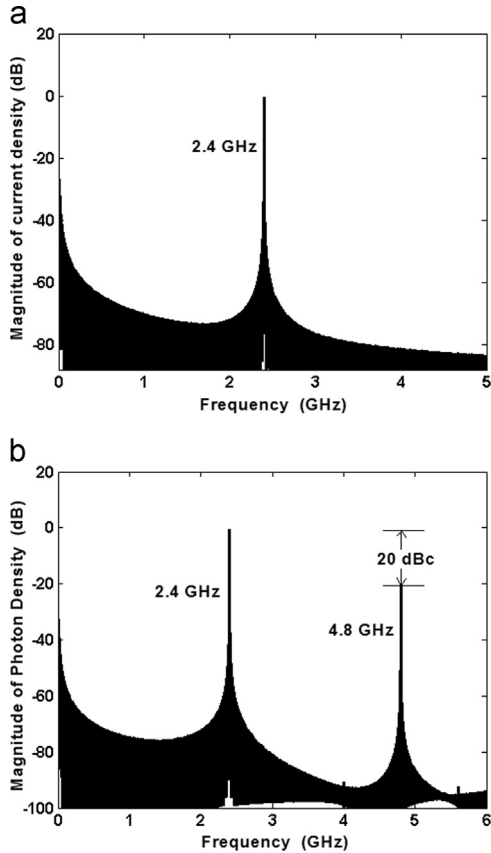


Fig. 5. The spectrum of (a) input current density and (b) photon density. ($\tau_{\text{qw}} = 150 \text{ ps}$ and $\tau_{\text{cap}} = 1 \text{ ps}$).

life time and current density of 50 ps and 10,000 (A/cm^2) or $2 J_{\text{th}}$, respectively. The value of modulation depth is less than 3 dB for the current densities beyond $4 J_{\text{th}}$.

Similar analysis is repeated for different electron capture time and it is illustrated in Fig. 4b. Spontaneous emission life time is fixed as 150 ps for this analysis. The modulation depth is found to decrease for increase in current density and electron capture time. A maximum modulation depth of 12.68 dB is obtained for 1 ps electron capture time.

4. Distortion analysis

4.1. Second harmonic distortion calculation (2HD)

In this analysis, the input base current density is varied at a frequency of 2.4 GHz and the second harmonic components in the

output optical signal are analyzed. The 2.4 GHz RF signal biased at $2J_{\text{th}}$. The rate equations are dynamically solved by using fourth order Runge–Kutta method and 1048576 point Fast Fourier Transform (FFT) is used to calculate the spectrum.

The spectrum of current density and photon density are given in Fig. 5a and b respectively. The spontaneous recombination time (τ_{qw}) and electron capture time (τ_{cap}) are fixed as 150 ps and 1 ps respectively for this analysis. The spectrum in the laser output shows the fundamental tone at 2.4 GHz and second harmonic component at 4.8 GHz. The second harmonic component has a significant magnitude of -20 dB relative to the fundamental frequency.

The magnitude of second harmonic of photon density with respect to the primary (2.4 GHz) is determined for various current density values from $2J_{\text{th}}$ to $7J_{\text{th}}$ and plotted in Fig. 6. It is inferred that as the input current density increases beyond the threshold current density, second harmonic distortion decreases. Further, the 2HD is found to increase with increasing τ_{qw} . This is due to the fact that larger values of τ_{qw} results in lower threshold (Fig. 3) and 2 HD becomes significant at current densities below and close to threshold.

The second harmonic distortion analysis is repeated for different electron capture time in quantum well (τ_{cap}) at various base current density values from $2 J_{\text{th}}$ to $7 J_{\text{th}}$ with $\tau_{\text{qw}} = 150 \text{ ps}$. The variation is plotted in Fig. 7, which also shows a trend similar to Fig. 6. However, it is observed that lower values of capture time leads to increased distortion. This can be explained by the threshold current variation with capture time.

4.2. Third order intermodulation distortion analysis (IMD3)

The analysis of IMD3 components are important for non linear active devices when two or more tones are applied as input. The IMD3 components fall in the main signal band and it is very difficult to remove this undesired component [3,13]. The base current density $J(t) = J_0 + J_{\text{th}} [\sin(\omega_1 t) + \sin(\omega_2 t)]$, is applied into the rate equations. Where J_{th} is threshold current density. The input current density is provided to the base region in the form of two tones at 2.25 GHz (f_1) and 2.35 GHz (f_2) and the third order intermodulation products ($2f_1 - f_2$, $2f_2 - f_1$) are evaluated in the optical output. The spectrum of two tone current density and corresponding output photon density are shown in Fig. 8. The current density is varied from $2J_{\text{th}}$ to $6J_{\text{th}}$ and corresponding spectrum is shown in Fig. 8a. The spectrum of the output photon density is illustrated in Fig. 8b. The magnitude of intermodulation product terms at 2.15 GHz ($2f_1 - f_2$) and 2.45 GHz ($2f_2 - f_1$) are found to be -68.87 dBc with reference to the fundamental tones.

The magnitude of third order intermodulation distortion (IMD3) is evaluated for two tone modulation for different spontaneous emission recombination times in the QW in the base. The spontaneous recombination time in the QW in the base is varied

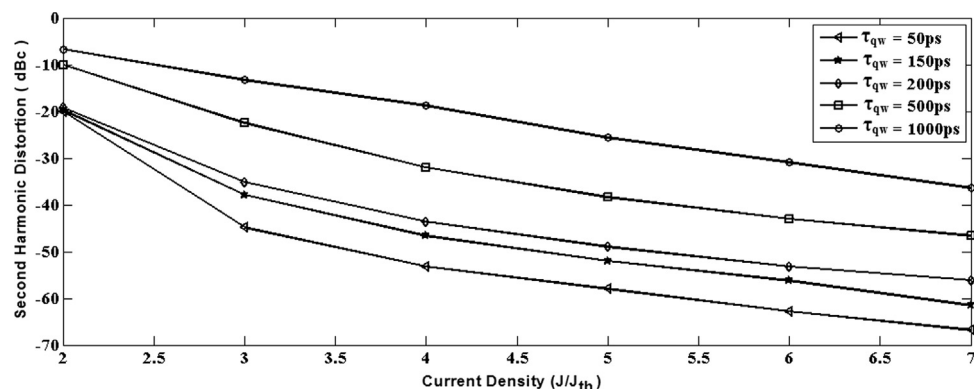


Fig. 6. 2HD variation with base current density J for different values of τ_{qw} with $\tau_{\text{cap}} = 1 \text{ ps}$.

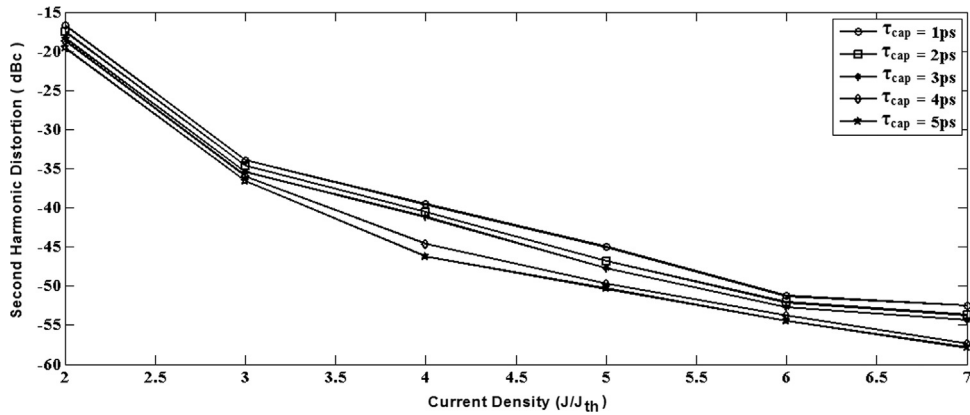


Fig. 7. 2HD variation with base current density J at $\tau_{qw}=150$ ps.

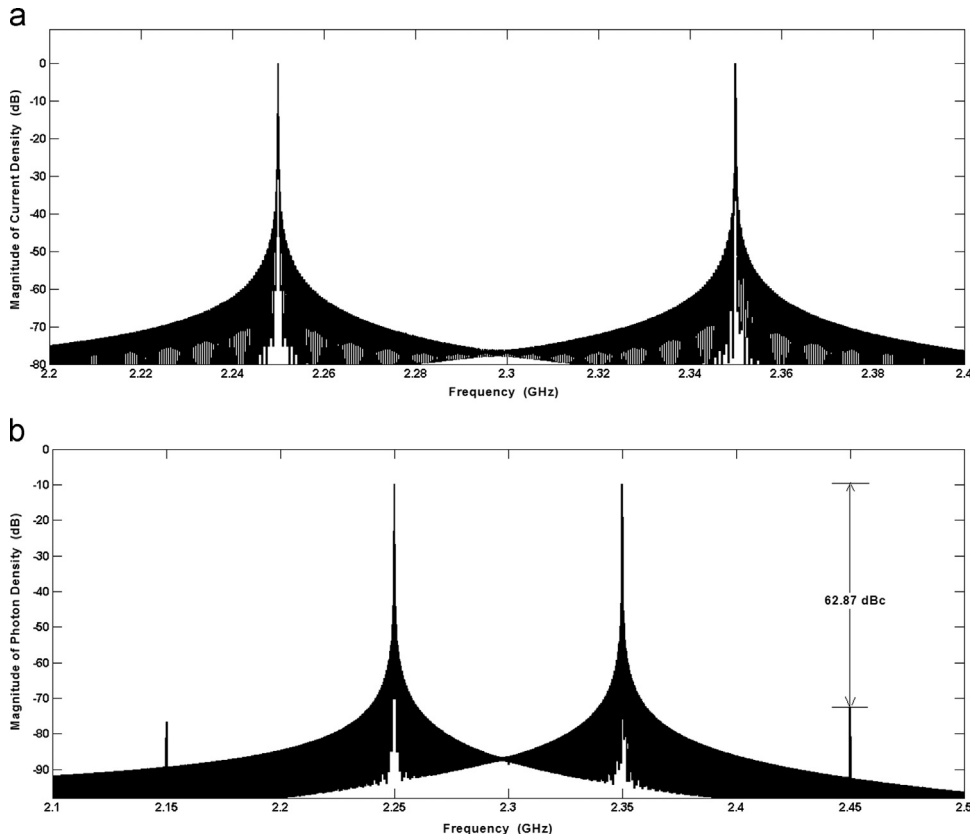


Fig. 8. The spectrum of (a) two tone input current density at 2.25 GHz and 2.35 GHz (b) photon density. ($\tau_{qw}=150$ ps and $\tau_{cap}=1$ ps).

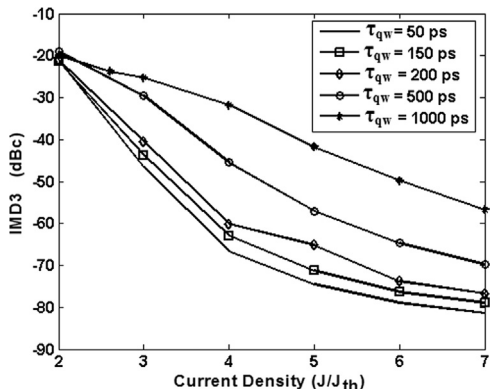


Fig. 9. IMD3 variation with base current density for different values of τ_{qw} and $\tau_{cap}=1$ ps.

from 50 ps to 1000 ps. Threshold current densities (J_{th}) of 5000 (A/cm^2) and 200 (A/cm^2) are obtained for recombination times of 50 ps and 1000 ps respectively. The two tone frequencies are fixed as $f_1=2.25$ GHz and $f_2=2.35$ GHz in this simulation along with threshold current density values from $2J_{th}$ to $7J_{th}$.

From Fig. 9, it is inferred that when the input current density increase beyond the threshold current density, third order intermodulation distortion decreases as in the case of 2HD.

The predicted magnitude of third order intermodulation distortion (IMD3) for $\tau_{qw}=1000$ ps, is high due it's threshold current density when compared to other value of τ_{qw} . The dc current density is fixed as $400 \text{ A}/\text{cm}^2 (2J_{th})$ and the amplitude of two tones are $200 \text{ A}/\text{cm}^2$ for this case. Hence the magnitude of IMD3 is found as higher than other value of spontaneous recombination time.

The analysis is repeated for similar operating conditions, but for different quantum well capture times. Simulations predict a

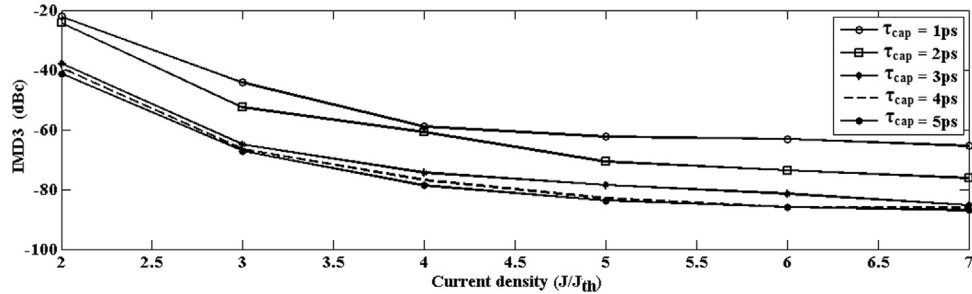


Fig. 10. IMD3 variation with base current density for different values of τ_{cap} and $\tau_{\text{QW}} = 150$ ps.

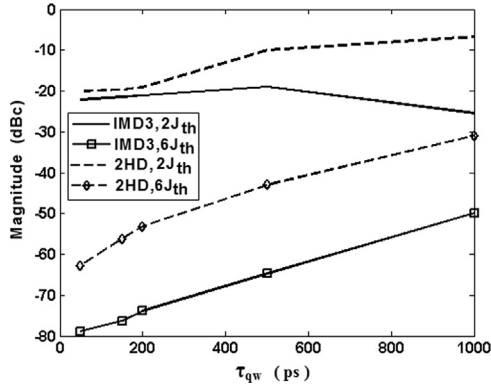


Fig. 11. Magnitude of 2HD and IMD3 variation with spontaneous emission time in the QW.

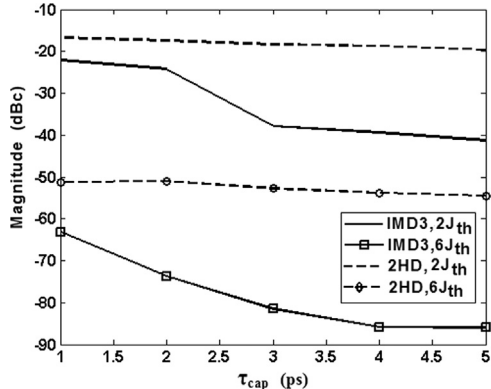


Fig. 12. Magnitude of 2HD and IMD3 variation with electron capture time in the QW.

decrease in IMD3, for higher values of τ_{cap} . Fig. 10 illustrates the behavior.

Spurious Free Dynamic Range (SFDR) of the analog optical link is directly proportional to the IMD performance of the device. The dynamic range can be improved by reducing the IMD. In general, lesser value of 3rd-order IMD always improves the SFDR of the link. The IMD3 requirement for MQW DFB laser diode is -60 dBc for optical CATV applications. A third order IMD value of -84 dBc is better than many of the reports in the literatures and also close to the IMD value of distortion less modulation in diode laser.

4.3. Overall effect of spontaneous emission time and electron capture time in quantum well on distortion

The effect of spontaneous emission time in the QW on the magnitude of second harmonic distortion and third order intermodulation distortion are determined from the previous analysis

and plotted in Fig. 11. The electron capture time in the quantum well is fixed as 1 ps for this analysis. The base current density are chosen as $2J_{\text{th}}$ and $6J_{\text{th}}$ for comparison. The RF signal at 2.4 GHz are provided for single tone analysis and 2.25 GHz (f_1) and 2.35 GHz (f_2) are used for IMD3 analysis. The magnitude of 2HD and IMD3 components are found to increase with spontaneous emission time in the QW (τ_{QW}). This effect is mainly due the decrease of threshold base current density (J_{th}) with increase in spontaneous emission time in the QW. The threshold base current densities are 5000 A/cm^2 and 200 A/cm^2 for QW spontaneous emission time of 50 ps and 1000 ps respectively. Minimum predicted values of 2HD and IMD3 are -62.82 dBc and -78.9 dBc respectively, for 50 ps QW spontaneous emission time at a bias level of $6J_{\text{th}}$.

Similar analysis are repeated for different electron capture time in the QW (τ_{cap}) for fixed value of QW spontaneous emission time (150 ps). The magnitude of 2HD and IMD3 components are found as decrease with increasing electron capture time (Fig. 12). The threshold base current density (J_{th}) increases with electron capture time QW of the transistor laser. The threshold base current densities are 1890 A/cm^2 and 2500 A/cm^2 for electron capture time of 1 ps and 5 ps respectively. Minimum values of 2HD and IMD3 are -54.46 dBc and -85.95 dBc respectively, predicted for 5 ps (τ_{cap}) at a bias of $6J_{\text{th}}$.

5. Conclusion

The static and dynamic characteristics of transistor laser are evaluated by solving the rate equations numerically. The power characteristics and frequency response are found to match well with the literature, which enabled us to use the model for investigation of second harmonic distortion and third order intermodulation products. The effect of recombination time and capture time in the quantum well on the modulation and distortion performance are also determined. A maximum modulation depth of 18.42 dB is obtained for 50 ps spontaneous emission life time and 1 ps electron capture time, for 2.4 GHz frequency at a current density of $2J_{\text{th}}$. A minimum second harmonic distortion magnitude of -66.8 dBc is predicted for 50 ps spontaneous emission life time and 1 ps electron capture time in the quantum well at 2.4 GHz for $7J_{\text{th}}$. Similarly, a minimum third order intermodulation distortion of -83.93 dBc is obtained for 150 ps spontaneous emission life time and 5 ps electron capture time in the quantum well, under similar biasing conditions. It is inferred that larger values of electron capture time and smaller values of spontaneous lifetime leads to better distortion characteristics in the transistor laser.

References

- [1] N. Holonyak Jr., M. Feng, The transistor laser, IEEE Spectr. 43 (2006) 50–55.
- [2] Han Wu.I. Then, Milton Feng, Nick Holonyak Jr., The transistor laser: theory and experiment, Proc. IEEE 101 (2013) 2271–2298.

- [3] H.W. Then, F. Tan, M. Feng, N. Holonyak Jr, Transistor laser optical and electrical linearity enhancement with collector current feedback, *Appl. Phys. Lett.* 100 (2012) 21104.
- [4] Lingxiao Zhang, Jean-Pierre Leburton, Modeling of the transient characteristics of heterojunction bipolar transistor lasers, *IEEE J. Quantum Electron.* 45 (2009) 359–366.
- [5] Shirao Mizuki, SeungHun Lee, Nobuhiko Nishiyama, Shigehisa Arai, Large signal analysis of transistor laser, *IEEE J. Quantum Electron.* 47 (3) (2011) 359–367.
- [6] Behnam Faraji, Wei Shi, David L. Pulfrey, Lukas Chrostowski, Analytical modeling of transistor laser, *IEEE J. Sel. Top. Quantum Electron.* 15 (3) (2009) 594–603.
- [7] M. Feng, N. Holonyak Jr., H.W. Then, G. Walter, Charge control analysis of transistor laser operation, *Appl. Phys. Lett.* 91 (2007) 053501.
- [8] R. Chan, M. Feng, N. Holonyak Jr., G. Walter, Microwave operation and modulation of a transistor laser, *Appl. Phys. Lett.* 86 (2005) 131114.
- [9] H.W. Then, G. Walter, M. Feng, N. Holonyak Jr., Collector characteristics and the differential optical gain of a quantum-well transistor laser, *Appl. Phys. Lett.* 91 (2007) 243508.
- [10] G. Walter, N. Holonyak Jr., M. Feng, R. Chan, Laser operation of a heterojunction bipolar light-emitting transistor, *Appl. Phys. Lett.* 85 (2004) 4768.
- [11] M. Feng, N. Holonyak Jr., G. Walter, R. Chan, Room temperature continuous wave operation of a heterojunction bipolar transistor laser, *Appl. Phys. Lett.* 87 (2005) 131103.
- [12] Stavros lezekiel, Microwave photonic links based on transistor lasers: small signal gain analysis, *IEEE Photon. Technol. Lett.* 26 (2014) 183–186.
- [13] C.H. Cox, E.I. Ackerman, G.E. Betts, J.L. Prince, Limits on the Performance of RF-over-fiber links and their Impact on device design, *IEEE Trans. Microw. Theory Tech.* 54 (2006) 906–920.
- [14] Hazaveh Kamyar, Xavier Fernando, Adaptive modeling of laser diode non-linearity with memory, in: Proceedings of the Canadian Conference on Electrical and Computer Engineering (CCECE'2003), Montreal, Canada 2003, May 5–7.
- [15] Xavier Fernando, Abu Sesay, Characteristics of directly modulated RoF links for wireless access, in: Proceedings of the Canadian Conference on Electrical and Computer Engineering (CCECE'2004), Niagara Falls, Canada vol. 4, 2004, pp. 2167–2170.
- [16] W.I. Way, Optical fiber based microcellular systems: An overview, *IEICE Trans. Commun.* E76-B (1993) 1091–1102 , no.9.
- [17] Jianyao Chen, Rajeev J. Ram, Roger Helkey, Linearity and third order inter-modulation distortion in DFB semiconductor lasers, *IEEE J. Quantum Electron.* 35 (1999) 1231–1237.
- [18] S. Piramasubramanian, M.Ganesh Madhan, Simultaneous reduction of IMD3 and IMD5 in bisection laser diode by feedback second harmonic injection, *Opt. Commun.* 328 (2014) 151–160.
- [19] Gnatabour'e Yabre, Jean Le Bihan, Reduction of nonlinear distortion in directly modulated semiconductor lasers by coherent light injection, *IEEE J. Quantum Electron.* 33 (1997) 1132–1140.
- [20] Yon-Tae Moon, Woon-Kyung Choi, Young-Wan Choi, A broadband linearization method using a novel opto-electrical predistorter for radio over fiber systems, *Microw. Opt. Technol. Lett.* 52 (2010) 1638–1640.



Analysis of the effect of optical confinement factor on the distortion performance of gain lever laser diode

S. Piramasubramanian*, M. Ganesh Madhan

Department of Electronics Engineering, Madras Institute of Technology campus, Anna University, Chennai 600044, India

ARTICLE INFO

Article history:

Received 20 August 2014

Accepted 24 August 2015

Keywords:

Gain lever laser diode
Optical confinement factor
Third order intermodulation distortion (IMD3)
Fifth order intermodulation distortion (IMD5)
Rate equations

ABSTRACT

The effect of optical confinement factor on gain lever and intermodulation distortion are analyzed in two section gain lever laser diode, under 900 MHz, 1.8 GHz and 2.4 GHz RF signal injection. Rate equations are solved numerically to find the gain lever and distortion characteristics. A section length ratio of 97/03 is considered for the device and the optical confinement factor is varied from 0.05 to 0.25. The effect of optical confinement factor on threshold current, gain lever and intermodulation distortion are analyzed. The threshold current of the laser diode is found to reduce with increase in optical confinement factor as in the case of simple laser diodes. A maximum gain lever of 13.85 dB is obtained at 2.4 GHz for an optical confinement factor of 0.25. The magnitudes of IMD3 and IMD5 are predicted as -35.54 dBc and -37.97 dBc, respectively, at 900 MHz for an optical confinement factor of 0.05.

© 2015 Elsevier GmbH. All rights reserved.

1. Introduction

Optical fiber link replaces coaxial cables in today's communication networks. The advantages of optical fibers include large bandwidth, comparatively less cost, free from electromagnetic interference, etc. Analog optical links are finding applications in phased array antenna, CATV, antenna remoting and micro/pico cell mobile communication networks [1,2]. This approach leads to reduction of equipments as well as system complexity. In these applications, optical carrier is either directly or externally modulated by RF signal. Directly modulated optical links are preferred as they are characterized by low cost and less complexity. The performance of these RF transmission over fiber links is evaluated based on the Spurious Free Dynamic Range (SFDR), which depends on the overall link signal to noise ratio (SNR). However, link SNR is directly proportional to the square of the optical modulation depth. At the same time, the link efficiency degrades due to the distortion in the optical transmitters. Hence, improving the modulation depth and the reduction of distortion in the laser diode has become important, especially for directly modulated optical transmitters. Recently, various techniques are proposed to increase the optical modulation depth and to reduce the effect of distortion [2].

Optical bistability and self pulsation are observed in the two section laser diode structures [3–6]. Improvement in optical modulation depth is also observed in such devices due to gain lever effect [7–15]. The inherent nonlinearity of the two section gain lever laser diode also produces harmonic and intermodulation distortion. Hence, efficient operation of gain lever laser diode for RoF applications requires distortion reduction schemes to be incorporated. The effect of nonlinearity on harmonic distortion in Fabry – Perot and Distributed Feedback Laser diodes is investigated by Mortier et al. [16]. The characteristics of intermodulation distortion in DFB laser diodes are analyzed by Chen et al. [17]. In optical transmitters, conventional linearization techniques include predistortion, feedforward and feedback harmonic injection schemes [18–22]. A tapered cavity structure for bisection gain lever laser diodes for distortion reduction and improvement in gain lever was proposed by Rana et al. [13]. However, this approach requires a complex device structure. From the literature, it is observed that intermodulation distortion analysis in bisection laser diode remains sparse. Further, it is well known that the device parameters play an important role in the modulation behavior of laser diodes [23]. Earlier, we proposed a novel distortion reduction scheme in gain lever laser diode based on feedback harmonic injection technique. RF signals are extracted from longer section of the laser diode and used for IMD3 reduction [14]. The third and fifth order intermodulation components are simultaneously reduced by our proposed technique [15]. The distortion reduction circuit is used externally in the above technique to reduce the intermodulation components.

* Corresponding author. Tel.: +91 44 22516104.

E-mail addresses: spirama@annauniv.edu, spsnanthan@gmail.com (S. Piramasubramanian), mganesh@annauniv.edu (M. Ganesh Madhan).

In this paper, we investigate the gain lever and distortion performance in a standard bisection laser cavity with variation in optical confinement factor (Γ). A $1.3\text{ }\mu\text{m}$ InGaAs/InGaAsP, multiple quantum well gain lever laser diode is considered for the present study. Optical confinement factor varies due to variation in laser diode structures. The analysis is carried out by solving the rate equations for a bisection laser diode. Fourth order Runge – Kutta method is used for this numerical simulation in MATLAB software.

2. Gain lever effect in two section laser diode

Gain lever effect has been realized in two section bulk and MQW laser diodes in order to improve the optical modulation depth (amplitude modulation efficiency), leading to an improvement in RF link efficiency [7,8]. A two section laser diode with longer (a_1) and shorter (a_2) active regions is shown in Fig. 1a. These two parts of the active regions are electrically isolated and have a common optical cavity. In the shorter section of the laser diode, bias current (I_a) and RF signal are injected. The longer section of the laser diode is injected with a constant DC current. The longer section is biased to have higher carrier density than the shorter section. The total optical gain overcomes the loss of the cavity at lasing threshold. An increase in gain in one section of the laser diode allows equal decrease in gain in other section [11]. When current in shorter section I_a decreases, circulating optical power decreases, which results in increase of carrier density N_g , in other section. A sublinear relation between optical gain and carrier density is obtained. Hence a small amount of increase in carrier density N_g , results in modulation depth improvement in such multi section laser diodes [8–12]. The two sections of laser diode are shorted together as shown in Fig. 1b for the analysis of unlever case. An improvement in optical modulation depth (AM efficiency) is obtained with respect to the unlevered laser diode.

The carrier density (N_g, N_a) variation with respect to time in the longer section and shorter section of the laser diode are given as (dN_g/dt) and (dN_a/dt) , respectively. The photon density (S) in the laser diode is assumed to be uniform along the cavity. The rate equations for longer and shorter section carrier densities and photon density are given as [3–6,14],

$$\frac{dN_g}{dt} = \frac{I_g}{a_1 q V} - \frac{N_g}{\tau_g} - v_g g_g (N_g - N_{og}) S (1 - e^{-S}) - \frac{N_g}{\tau_{nr}} \quad (1)$$

$$\frac{dN_a}{dt} = \frac{I_a}{a_2 q V} - \frac{N_a}{\tau_a} - v_g g_a (N_a - N_{oa}) S (1 - e^{-S}) - \frac{N_a}{\tau_{nr}} \quad (2)$$

$$\begin{aligned} \frac{dS}{dt} = & -\frac{S}{\tau_p} + [a_1 v_g g_g (N_g - N_{og}) + a_2 v_g g_a (N_a - N_{oa})] \Gamma S (1 - e^{-S}) \\ & + \Gamma \beta \left(\frac{a_1 N_g}{\tau_g} + \frac{a_2 N_a}{\tau_a} \right) \end{aligned} \quad (3)$$

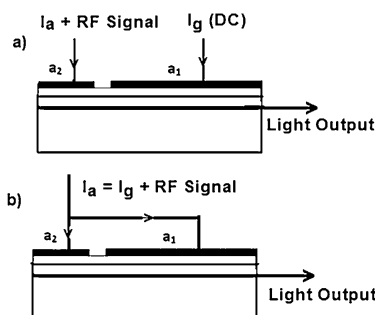


Fig. 1. Two section laser diode with (a) gain lever effect and (b) both sections are shorted together (unlever).

$$\tau_g = \frac{1}{(B N_g)}, \tau_a = \frac{1}{(B N_a)} \quad (4)$$

The total volume of the active region is ' V ' and charge of the electron is ' q '. The transparency carrier densities in longer and shorter sections of the laser diode are ' N_{og} ' and ' N_{oa} ', respectively. The carrier life time in longer and shorter sections are ' τ_g ' and ' τ_a ', respectively. ' τ_p ' is photon life time in the cavity and ' Γ ' is optical confinement factor. The non radiative recombination time is ' τ_{nr} ' and ' v_g ' is group velocity. The gain constants for longer and shorter sections of the laser diode are given as ' g_g ' and ' g_a ', respectively. The effective recombination coefficient and gain compression factor are denoted as ' B ' and ' ϵ ', respectively. $g_g (N_g - N_{og}) (1 - e^{-S})$ represents the optical gain in longer section. The gain in shorter section is given by $g_a (N_a - N_{oa}) (1 - e^{-S})$ [3]. Eq. (5) is used to calculate the optical power from the device.

$$P = \left(\frac{hc}{\lambda} \right) \left(\frac{\eta VS}{\Gamma \tau_p} \right) \quad (5)$$

where, ' η ' is internal quantum efficiency, ' h ' is Planck's constant and ' c ' is light velocity.

Gain lever is defined as the ratio of slope efficiency of two section laser diode when both the sections are separately excited, to the slope efficiency of the laser diode when both the sections are shorted ($I_a = I_g$). The gain lever (GL) is evaluated from the following equation:

$$GL = \frac{\left(\frac{P_2}{P_1} \right) (I_g = \text{const})}{\left(\frac{P_2}{P_1} \right) (I_g = I_a, \text{shorted})} \quad (6)$$

The two section laser diode introduces gain lever when both the sections have different gain constants, section lengths and carrier life time.

The optical confinement factor can be varied by changing the active layer thickness. Olesen et al. [24] proposed a modified device structure by integrating three MQW sections with different waveguide dimensions and optical confinement factors, using selective MOVPE re growth method. An improved gain lever and FM efficiency is reported in that work. Epitaxial re growth technology can also be used for realising different optical confinement factors [24].

3. Static characteristics of two section laser diode

Optical power is evaluated by solving rate Eqs. (1)–(5), using fourth order Runge – Kutta method. A longer section to shorter section length ratio of (97/03) is used for the analysis. Gain constant for shorter (g_a) and longer sections (g_g) are fixed as $80 \times 10^{-16}\text{ cm}^2$ and $2 \times 10^{-16}\text{ cm}^2$, respectively. The transparency carrier densities (N_{oa}, N_{og}) in both the sections are fixed as $1.25 \times 10^{18}\text{ cm}^{-3}$. All the parameters used in the rate equations are similar to that of reported by Uenohara et al. [3]. For this simulation, an internal quantum efficiency of 0.1 is used.

The optical power variation with longer section current are evaluated and plotted in the Fig. 2. No current is applied to the shorter section ($I_a = 0$). The optical confinement factor is fixed as 0.15. The longer section threshold current is obtained for unpumped short section. The longer section current is increased from 0 to 100 mA and decreased to 0 mA subsequently, to plot the bistable characteristics. This characteristics is found to exactly coincide with results of Uenohara et al. [3], thereby validating our simulation methodology.

The effect of optical confinement factor on longer section current is analyzed in this section. Here the longer section current is varied from 0 to 200 mA and optical power is plotted (Fig. 3). The shorter section current is kept zero ($I_a = 0$, unpumped), and

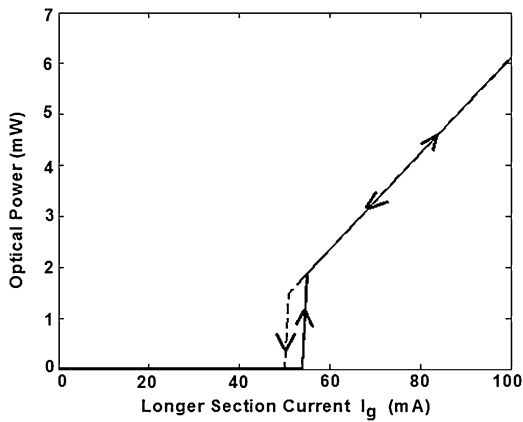


Fig. 2. Static characteristics of the bisection laser diode ($I_a = 0$, $\Gamma = 0.15$).

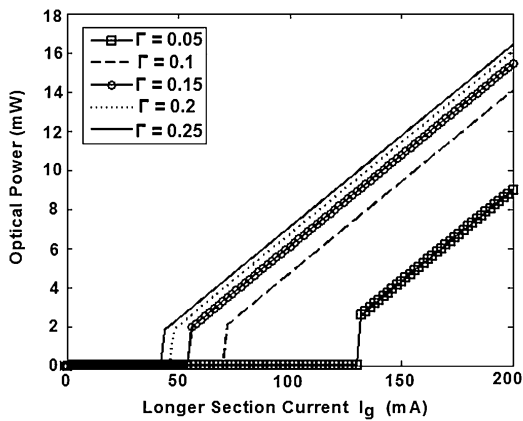


Fig. 3. Optical power variation with longer section current and optical confinement factor ($I_a = 0$).

functions as an absorber medium. The optical confinement factor is fixed as 0.05, 0.1, 0.15, 0.2 and 0.25 in this analysis. The threshold current is found to reduce when optical confinement factor increased from 0.05 to 0.25. A threshold current of 52 mA is obtained when optical confinement factor for both the sections are 0.15. This result agrees with the experimental results of Uenohara et al. [3] and hence validates our approach.

The shorter section current (I_a) is varied from 0 to 20 mA and corresponding optical power is calculated. Longer section current is fixed as 20 mA and optical confinement factor is varied from 0.05 to 0.25. The shorter section threshold current is found to be 2.2 mA, 1 mA, 0.7 mA, 0.65 mA and 0.55 mA for optical confinement factor of 0.05, 0.1, 0.15, 0.2 and 0.25, respectively. The shorter section threshold current is found to reduce and the slope efficiency is found to increase with increasing optical confinement factor. This behavior is illustrated in Fig. 4.

The effect of optical confinement factor and longer section current on the device characteristics is evaluated. In this analysis, the shorter section current (I_a) is varied from 0 to 20 mA in steps of 5 mA and optical confinement factor is varied for each current. Longer section current fixed as 30 mA and optical confinement factor is varied from 0.05 to 0.25. The shorter section threshold current is found to reduce with increasing optical confinement factor and the slope efficiency is found to increase. This behavior is found in Fig. 5.

The analysis is repeated for the longer section current of 30 mA. A similar behavior as Fig. 4 is observed. However, the slope is found to increase for higher value of optical confinement factor. This behavior is depicted in Fig. 5. Further increase in longer section

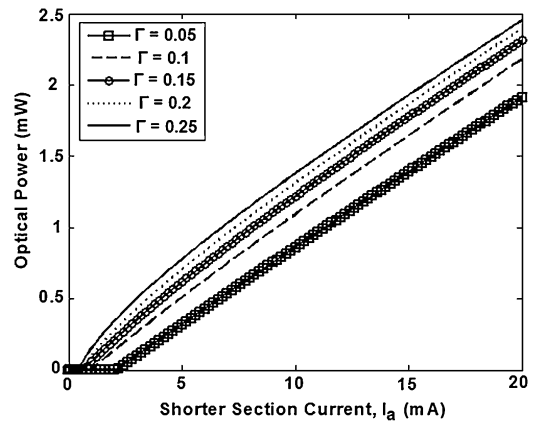


Fig. 4. Optical power variation with shorter section current ($I_g = 20$ mA).

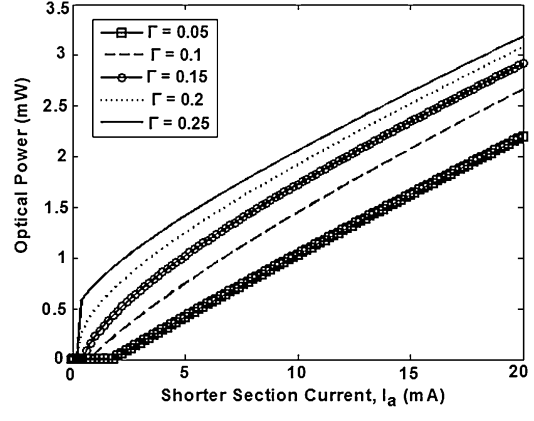


Fig. 5. Optical power variation with shorter section current ($I_g = 30$ mA).

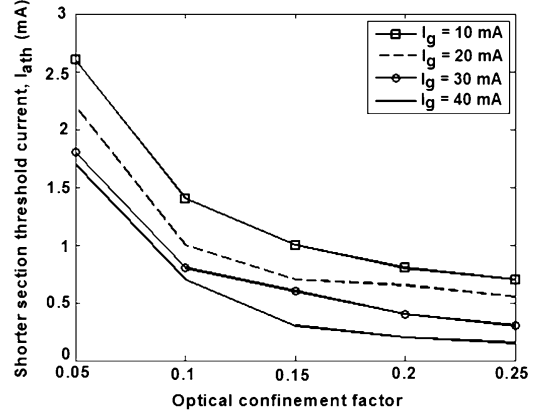


Fig. 6. Shorter section threshold current variation with optical confinement factor.

current leads to light emission even in the absence of shorter section current.

AM efficiency enhancement (gain lever) depends on the threshold current of the laser diode. In bisection laser diode, RF signal is applied into the shorter section and a constant current is injected to the longer section. The shorter section threshold current variation with optical confinement factor are plotted and shown in Fig. 6. The longer section currents (I_g) are fixed as 10 mA, 20 mA, 30 mA and 40 mA, respectively. The shorter section threshold current is found as decrease exponentially for an increase in optical confinement factor and also with longer section current. A shorter section threshold current of 2.6 mA is obtained for an optical

confinement factor of 0.05, at 10 mA current injection at longer section. At 40 mA current injection to the longer section, a threshold current of 0.15 mA is obtained for the optical confinement factor of 0.25.

4. Effect of optical confinement factor on gain lever

The frequency response of the two section laser diode is analyzed for various optical confinement factors. The shorter section bias currents are fixed as $7 I_{\text{ath}}$, $10 I_{\text{ath}}$ and $12 I_{\text{ath}}$. A 20 mA current is provided to the longer section of the laser diode. The shorter section bias current is fixed as 15.4 mA ($7 I_{\text{ath}}$). A shorter section threshold current of 2.2 mA is obtained for optical confinement factor 0.05 (Fig. 6). The RF current magnitude is fixed as 3 mA. The frequency is varied from 100 kHz to 50 GHz. For unlevered case, a dc current of 17.7 mA with 1.5 mA RF current is injected into both longer and shorter section ($I_a = I_g$) which represents the condition, where both sections are shorted. The frequency response corresponding to optical confinement factors of 0.05 and 0.1 are provided in the Figs. 7 and 8, respectively. The peak resonant frequency are calculated for gain lever and unlevered case under these optical confinement factors.

The effect of optical confinement factor on gain lever is evaluated at 900 MHz, 1.8 GHz and 2.4 GHz RF modulation. These frequencies are used for commercial GSM cellular communication and WLAN (IEEE 802.11b/g) interface, hence used in the simulation. The shorter section bias currents are fixed as $7 I_{\text{ath}}$, $10 I_{\text{ath}}$ and $12 I_{\text{ath}}$. To evaluate the gain lever performance at 900 MHz, a 3 mA RF signal is provided along with the DC current (I_a) to the short section. The gain lever are evaluated for different values of optical

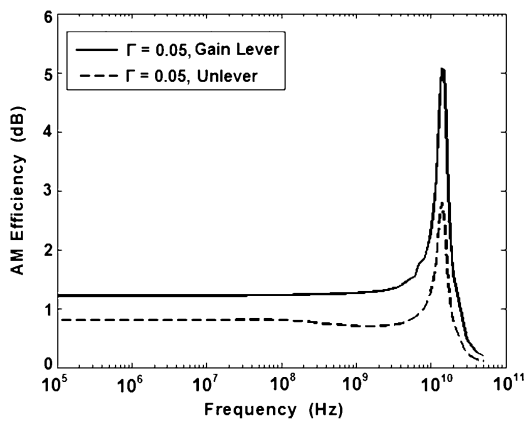


Fig. 7. Frequency response of the gain lever laser diode ($\Gamma = 0.05$).

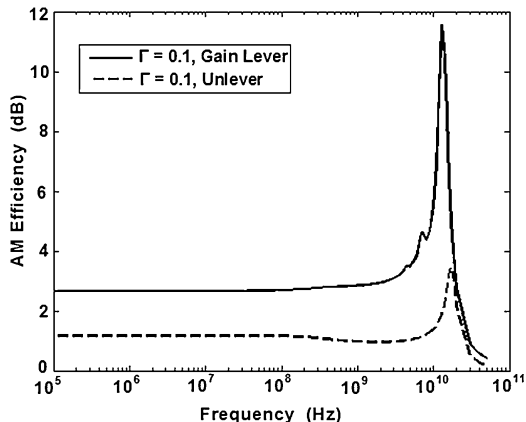


Fig. 8. Frequency response of the gain lever laser diode ($\Gamma = 0.1$).

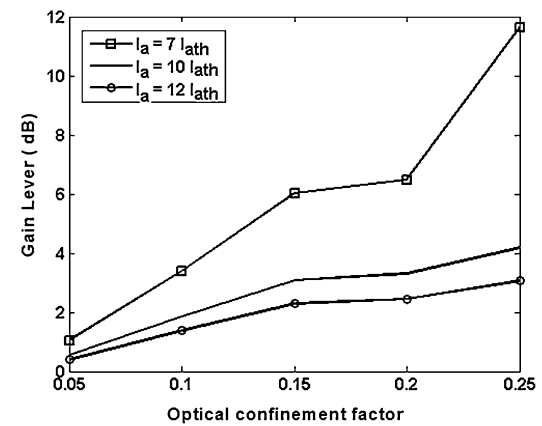


Fig. 9. Gain lever variation with optical confinement factor at 900 MHz ($I_g = 20$ mA).

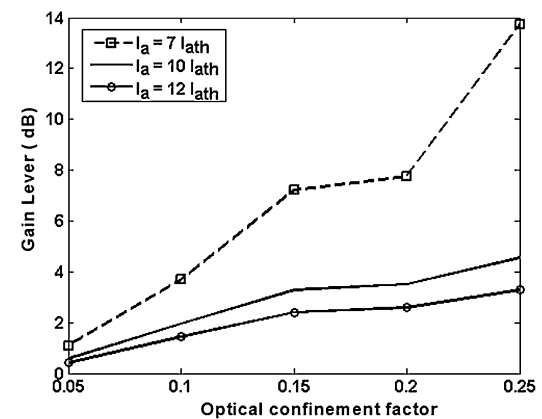


Fig. 10. Gain lever variation with optical confinement factor at 1.8 GHz ($I_g = 20$ mA).

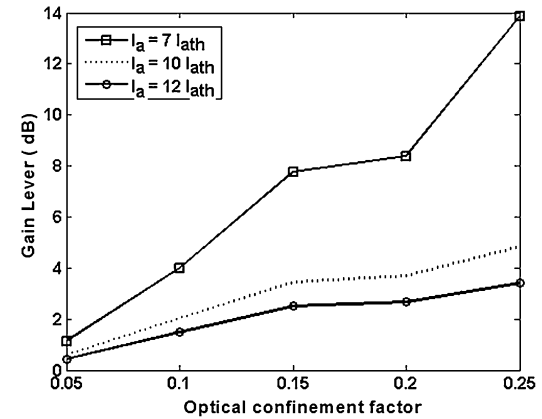


Fig. 11. Gain lever variation with optical confinement factor at 2.4 GHz ($I_g = 20$ mA).

confinement factor and plotted in Figs. 9–11 for 900 MHz, 1.8 GHz and 2.4 GHz, respectively. A constant current of 20 mA is provided to the longer section in this analysis. For the calculation of AM efficiency in unlevered laser diode, a 900 MHz RF current at 1.5 mA is applied to shorted section ($I_a = I_g$). Gain lever or AM enhancement (gain lever) is calculated as the ratio of AM efficiency for RF signal in two section laser diode to the same as in unlevered laser diode. A similar analysis is repeated for 1.8 GHz and 2.4 GHz frequencies under same optical confinement factors. The gain lever is found to be low for optical confinement factor of 0.05 at $12 I_{\text{ath}}$. The shorter section bias current is high for this optical confinement factor. A maximum gain lever is obtained for optical confinement factor of

0.25 with shorter section bias current of $7 I_{\text{ath}}$. This effect is mainly due to the low shorter section bias current. A 0.55 mA threshold current is obtained for this condition. As the bias current is fixed well above the threshold current, the gain lever is found to reduce. This is in accordance with the theory that gain lever is maximum around threshold current and reduces beyond threshold current [11].

5. Analysis of intermodulation distortion

The effect of optical confinement factor on third and fifth order intermodulation distortion are analyzed in this section. The IMD3 and IMD5 components fall within the main signal band and it is difficult to remove. The main focus of this analysis is to find the magnitudes of intermodulation products with the variation of optical confinement factor. The magnitudes of the third and fifth order intermodulation distortion are evaluated for 900 MHz, 1.8 GHz and 2.4 GHz as center frequencies. The spacing between two carriers are fixed as 20 MHz. The optical confinement factor is varied from 0.05 to 0.25. The bias currents used for this simulation is similar to the gain lever analysis presented in Section 4. The two tone frequencies are 890 MHz (f_1) and 910 MHz (f_2) for the 900 MHz case. These two tone currents are applied in to the rate equations and output RF spectrum is plotted in Fig. 12. The output consists of the primary frequency components, third order intermodulation tones (IMD3) and fifth order intermodulation components (IMD5). The third order intermodulation frequencies are 870 MHz ($2f_1 - f_2$) and 930 MHz ($2f_2 - f_1$), respectively. Similarly, the fifth order intermodulation frequencies are 850 MHz ($3f_1 - 2f_2$) and 950 MHz ($3f_2 - 2f_1$). The shorter section bias currents are fixed as $7 I_{\text{ath}}$, $10 I_{\text{ath}}$ and $12 I_{\text{ath}}$. The longer section bias current is fixed as 20 mA. The magnitude of IMD3 products are -35.54 dBc and -34.96 dBc for the shorter section bias current of 15.4 mA ($7 I_{\text{ath}}$) under the optical confinement factor of 0.05. Similarly, the IMD5 component magnitudes are obtained as -37.15 dBc and -37.97 dBc under the similar operating conditions. The analyses are repeated for other optical confinement factors and bias currents.

The fundamental frequencies of 1.79 GHz (f_1) and 1.81 GHz (f_2) are chosen for the analysis in the case of 1.8 GHz center frequency. Similarly, 2.39 GHz (f_1) and 2.41 GHz (f_2) are used for the carrier frequency of 2.4 GHz. RF spectrum of the optical output with two tone input are shown in the Figs. 12–14, for the center frequencies 900 MHz, 1.8 GHz and 2.4 GHz, respectively. The value of optical confinement factor is fixed as 0.1 for this analysis.

The RF spectrum of the optical output with two tone input are shown in the Fig. 15 (900 MHz), Fig. 16 (1.8 GHz) and Fig. 17 (2.4 GHz), respectively, for the optical confinement factor of 0.25.

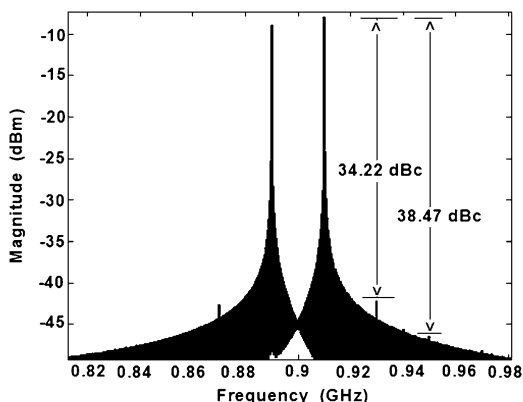


Fig. 12. RF spectrum of the optical output with two tone frequencies at 890 MHz and 910 MHz ($\Gamma = 0.1$).

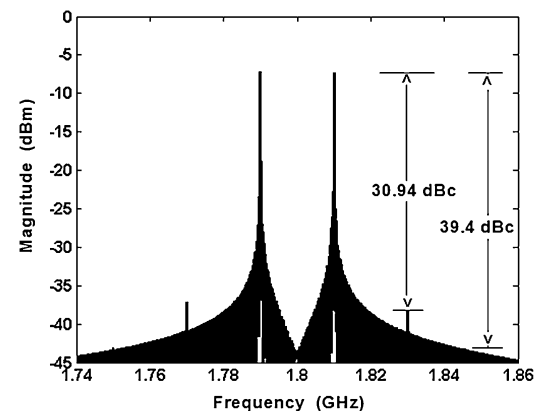


Fig. 13. RF spectrum of the optical output with two tone frequencies at 1.79 GHz and 1.81 GHz ($\Gamma = 0.1$).

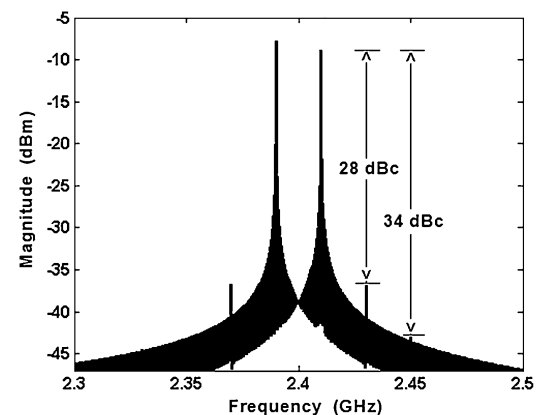


Fig. 14. RF spectrum of the optical output with two tone frequencies at 2.39 GHz and 2.41 GHz ($\Gamma = 0.1$).

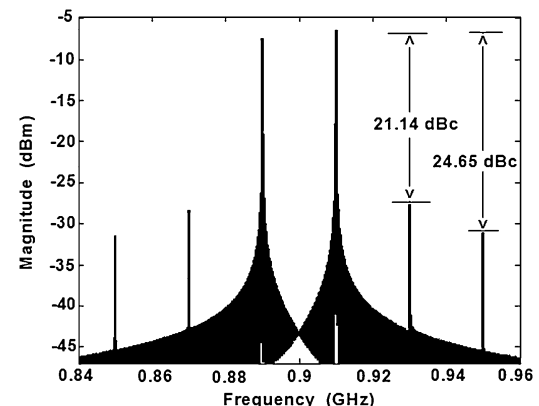


Fig. 15. RF spectrum of the optical output with two tone frequencies at 890 MHz and 910 MHz ($\Gamma = 0.25$).

The longer section bias current is fixed as 20 mA. A threshold current of 5.5 mA is obtained for shorter section under this longer section biasing condition at an optical confinement factor of 0.25. The shorter section bias currents is fixed as 3.85 mA ($7 I_{\text{ath}}$). The magnitude of RF current provided to the shorter section is 3 mA. The magnitude of IMD3 products are obtained as -20.96 dBc and -21.14 dBc, respectively, for the two tone input frequencies 890 MHz (f_1) and 910 MHz (f_2). Similarly, the output for fifth order intermodulation components are -24.06 dBc and -24.64 dBc. This analysis is repeated for other RF carrier frequencies of 1.8 GHz and 2.4 GHz and corresponding output are plotted (Figs. 16 and 17).

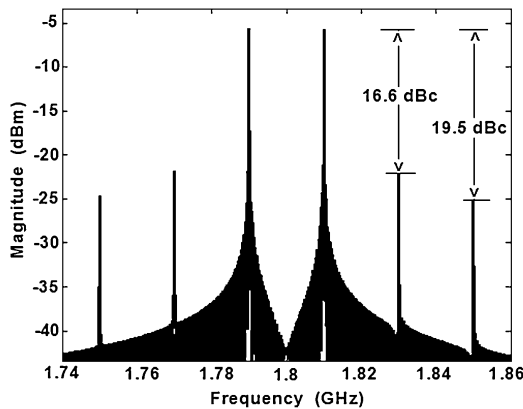


Fig. 16. RF spectrum of the optical output with two tone frequencies at 1.79 GHz and 1.81 GHz ($\Gamma = 0.25$).

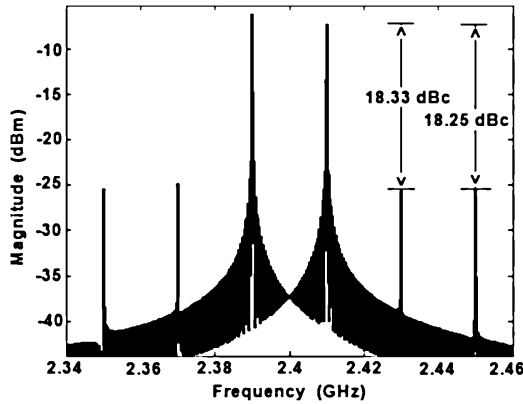


Fig. 17. RF spectrum of the optical output with two tone frequencies at 2.39 GHz and 2.41 GHz ($\Gamma = 0.25$).

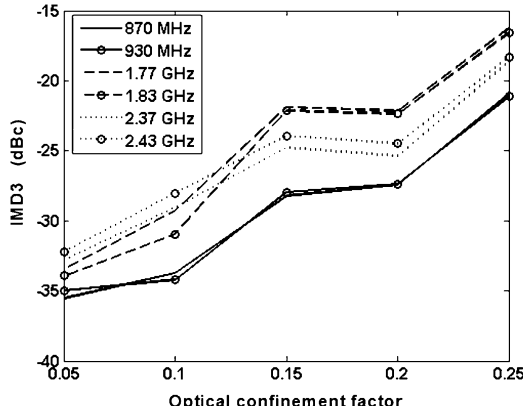


Fig. 18. Third order intermodulation distortion variation with optical confinement factor.

The magnitudes of third and fifth order intermodulation components are evaluated with optical confinement factor variation and plotted in the Figs. 18 and 19. The longer and shorter section bias currents are 20 mA and 7 I_{ath} for this analysis. The IMD3 components are 870 MHz and 930 MHz for the center carrier frequency of 900 MHz. At the center carrier frequency of 1.8 GHz, the IMD3 products are 1.77 GHz and 1.83 GHz. Similarly, for the carrier frequency of 2.4 GHz, the third order intermodulation terms at 2.37 GHz and 2.43 GHz are obtained. The magnitudes of IMD3 and IMD5 components are obtained as -35.54 dBc and -37.97 dBc for the optical confinement factor of 0.05 at 900 MHz. Similarly, for the same

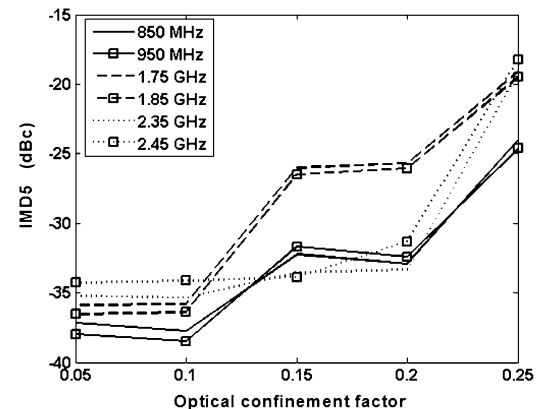


Fig. 19. Fifth order intermodulation distortion variation with optical confinement factor.

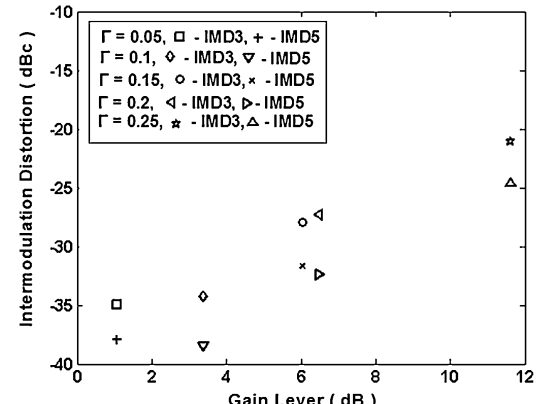


Fig. 20. Gain lever and intermodulation distortion variation with optical confinement factor ($f = 900$ MHz).

optical confinement factor -33.48 dBc (IMD3) and -35.88 dBc (IMD5) components are obtained for the center frequency of 1.8 GHz. At 2.4 GHz, the evaluated magnitudes of IMD3 and IMD5 are -32.81 dBc and -35.23 dBc, respectively. Similarly, for 0.25 optical confinement factor, the calculated magnitudes of IMD3 components are -20.96 dBc, -16.26 dBc and -18.63 dBc at 900 MHz, 1.8 GHz and 2.4 GHz, respectively. The magnitudes of IMD3 and IMD5 components are found to increase with optical confinement factor.

6. Optimum conditions for gain lever and intermodulation distortion

Gain lever, IMD3 and IMD5 are evaluated for different optical confinement factors (0.05 – 0.25) for the frequencies of 900 MHz, 1.8 GHz and 2.4 GHz. The bias currents are chosen based on the optical confinement factor. The results of these analyses are consolidated and plotted. Intermodulation distortion (IMD3, IMD5), gain lever variation with optical confinement factors are shown in Fig. 20 (900 MHz), Fig. 21 (1.8 GHz) and Fig. 22 (2.4 GHz), respectively. The bias currents are 20 mA (I_g) and 7 I_{ath} are used for this analysis. A minimum gain lever (1 dB) and minimum intermodulation distortion are obtained for the optical confinement factor of 0.05 ($f = 900$ MHz). This result is mainly due to the higher shorter section current than other optical confinement factors. The optical power magnitude is also higher for this condition. At the same time, if the optical confinement factor is increased to 0.25, gain lever and distortion are found to increase. Similar behavior is obtained for 1.8 GHz and 2.4 GHz carrier frequencies. It is favored to have

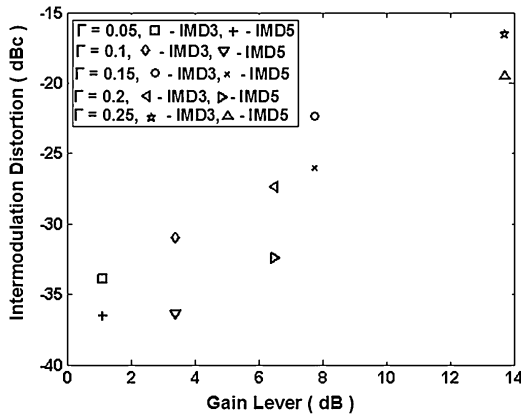


Fig. 21. Gain lever and intermodulation distortion variation with optical confinement factor ($f=1.8 \text{ GHz}$).

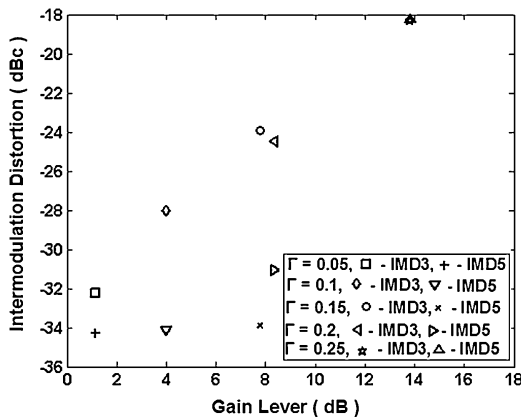


Fig. 22. Gain lever and intermodulation distortion variation with optical confinement factor (2.4 GHz).

the bisection laser diode with maximum gain lever and minimum intermodulation distortion. A gain lever of 6 dB, IMD3 of -28 dBc and IMD5 of -32 dBc are obtained for the optical confinement factor of 0.15 at 900 MHz. A similar trend is observed with other RF carrier frequencies. An optical confinement factor of 0.15 is predicted as optimum value for gain lever, third and fifth order intermodulation distortions.

7. Conclusion

The effect of optical confinement factor on gain lever and intermodulation distortion are analyzed in bisection, Multiple Quantum Well (MQW) laser diode. Rate equations for two section laser diode are numerically solved to analyze this effect. The optical confinement factor is varied from 0.05 to 0.25. The variation of gain lever, IMD3 and IMD5 magnitudes with optical confinement factor are analyzed at 900 MHz, 1.8 GHz and 2.4 GHz RF modulation. A gain lever of 13.85 dB is obtained for the optical confinement factor of 0.25 at the bias point of $7 I_{\text{ath}}$ and $I_g = 20 \text{ mA}$ at 2.4 GHz. The magnitudes of IMD3 and IMD5 are observed as -35.54 dBc and

-37.97 dBc , respectively, at 900 MHz for an optical confinement factor of 0.05. Gain lever and intermodulation distortion are found to increase with increase in optical confinement factor. A optimum value of optical confinement factor is predicted to get reasonable gain lever and minimum intermodulation distortion.

References

- [1] Hamed A.-R., Shozo K., Radio over fiber technologies for mobile communications networks, Norwood, MA, 2002.
- [2] C.H. Cox, E.I. Ackerman, G.E. Betts, J.L. Prince, Limits on the performance of RF over fiber links and their impact on device design, *IEEE Trans. Microw. Theory Tech.* 54 (2006) 906–920.
- [3] H. Ueno, R. Takahashi, Y. Kawamura, H. Iwamura, Static and dynamic response of multiple quantum well voltage controlled bistable laser diodes, *IEEE J. Quantum Electron.* 32 (1996) 873–883.
- [4] M.G. Madhan, P.R. Vaya, N. Gunasekaran, Effect of source and load resistance on the performance of bistable lasers, *IEEE Photonics Technol. Lett.* 12 (2000) 380–382.
- [5] M.G. Madhan, P.R. Vaya, N. Gunasekaran, Circuit modeling of multimode bistable laser diodes, *IEEE Photonics Technol. Lett.* 11 (1999) 27–29.
- [6] M.G. Madhan, P.R. Vaya, N. Gunasekaran, A new bistable laser diode configuration for all optical switching, *IEEE Photonics Technol. Lett.* 11 (1999) 644–646.
- [7] K.J. Vahala, M.A. Newkirk, The optical gain lever: a novel gain mechanism in the direct modulation of quantum well semiconductor lasers, *Appl. Phys. Lett.* 54 (1989) 2506–2508.
- [8] N. Moore, K.Y. Lau, Ultrahigh efficiency microwave signal transmission using tandem-contact single quantum well GaAlAs lasers, *Appl. Phys. Lett.* 55 (1989) 936–938.
- [9] L.D. Westbrook, C.P. Seltzer, Reduced intermodulation free dynamic range in gain levered lasers, *Electron. Lett.* 29 (1993) 488–499.
- [10] C.P. Seltzer, L.D. Westbrook, H.J. Wicks, The “gain lever” effect in InGaAs/InP multiple quantum well lasers, *J. Light. Technol.* 13 (1995) 283–289.
- [11] M.D. Pocha, L.L. Goddard, T.C. Bond, R.J. Nikolic, S.P. Vernon, J.S. Kallman, E.M. Behymer, Electrical and optical gain lever effects in InGaAs double quantum-well diode lasers, *IEEE J. Quantum Electron.* 43 (2007) 860–868.
- [12] H.-K. Sung, M.C. Wu, Amplitude modulation response and linearity improvement of directly modulated laser using ultra strong injection locked gain lever distributed Bragg reflector lasers, *J. Opt. Soc. Korea* 12 (2008) 303–308.
- [13] F. Rana, C. Monolatou, M.F. Schubert, Tapered cavities for high modulation efficiency and low distortion semiconductor lasers, *IEEE J. Quantum Electron.* 43 (2007) 1083–1087.
- [14] S. Piramasubramanian, M.G. Madhan, A novel distortion reduction scheme for multiple quantum well gain lever laser diodes, *J. Opt.* 15 (2013) 055501.
- [15] S. Piramasubramanian, M.G. Madhan, Simultaneous reduction of IMD3 and IMD5 in bisection laser diode by feedback second harmonic injection, *Opt. Commun.* 328 (2014) 151–160.
- [16] G. Monthier, F. Libbrecht, K. David, P. Vankwikelberge, R.G. Baets, Theoretical Investigation of the second-order harmonic distortion in the AM response of 1.55 μm F-P and DFB lasers, *IEEE J. Quantum Electron.* 27 (1991) 1990–2002.
- [17] J. Chen, R.J. Ram, R. Helkey, Linearity and third-order intermodulation distortion in DFB semiconductor lasers, *IEEE J. Quantum Electron.* 35 (1999) 1231–1237.
- [18] Fernando X.N., Sesay A.B., Nonlinear distortion compensation of microwave fiber optic links with asymmetric adaptive filter, *Proceedings of the International Microwave Symposium (IMS 2000)* 3/3 (2000) 1821–1824.
- [19] I.-H. Choi, S.-H. Lee, H.-C. Kwon, Y.-W. Choi, S.-K. Han, Compensation of intermodulation distortion of laser diode by using optoelectronically predistorted signals, *Microw. Opt. Technol. Lett.* 48 (2006) 1144–1147.
- [20] S.-H. Lee, D.-G. Lim, W.-K. Sung, H.-J. Lim, S.-K. Han, Feedback harmonic injection technique for reduction of third order intermodulation distortion in radio over fiber link, *Microw. Opt. Technol. Lett.* 48 (2006) 2072–2074.
- [21] C.S. Aitchison, M. Mbabele, M.R. Moazzam, D. Budimir, F. Ali, Improvement of third order intermodulation product of RF and microwave amplifiers by injection, *IEEE Trans. Microw. Theory Tech.* 49 (2001) 1148–1154.
- [22] T.-K. Lee, Y.-T. Moon, H.-S. Kim, Y.-W. Choi, Theoretical analysis and realization of optoelectrical predistortion optical transmitter for the simultaneous suppression of IM3 and IM5 signal, *Opt. Commun.* 285 (2012) 2697–2701.
- [23] R.S. Tucker, High speed modulation of semiconductor lasers, *J. Lightwave Technol.* 3 (1985) 1180–1182.
- [24] H. Olesen, J.-I. Shim, M. Yamaguchi, M. Kitamura, Proposal of novel gain-levered MQW DFB lasers with high and red-shifted FM response, *IEEE Photonics Technol. Lett.* 5 (1993) 599–602.